Biophysical Studies of the Lpt Pathway

Biophysical studies of the Lpt pathway

A dissertation presented

by

Alexander Hall George

to

The Committee on Higher Degrees in Chemical Biology

in partial fulfillment of the requirements

for the degree of

Doctor of Philosophy

in the subject of

Chemical Biology

Harvard University

Cambridge, Massachusetts

June 2017

Dissertation Advisor: Professor Daniel Kahne Alexander Hall George

Biophysical studies of the Lpt pathway

Abstract

The outer membrane (OM) of Gram-negative bacteria is impermeable to many antibiotics because its outer leaflet is composed entirely of lipopolysaccharide (LPS), a large glycolipid with an extracellular saccharide that is between a dozen and hundreds of sugars long. LPS forms tight associations, preventing entry of many small molecules. LPS is synthesized at the inner membrane (IM), and is transported to the OM by the seven-protein Lipopolysaccharide transport (Lpt) pathway. While the Lpt proteins of the IM are readily identified as an ABC transporter, and the ATP dependence of the early steps of LPS transport are well characterized, the mechanism of the OM components of the Lpt pathway remains unclear.

This thesis describes efforts towards improving our model of the mechanism of LptD/E, the translocon in the OM responsible for flipping and inserting LPS across and into the OM. LptE is a lipoprotein that sits within the membrane-integral β-barrel of LptD. LptE had previously been shown to function as a chaperone for LptD folding, but had no known function in LPS transport. We used surface plasmon resonance (SPR) to show that LptE not only binds LPS, but disrupts and solubilizes LPS aggregates, and that mutants of LptE that lead to a compromised OM are also deficient in their ability to disaggregate LPS. We also used SPR to measure dissociation constants between LptE and six different soluble fragments of LPS, showing that LptE binds LPS by the di-glucosamine-di-phosphate, with neither the core oligosaccharide nor the acyl chains making notable contributions to binding. This, combined

with the structural work of others, suggests a model for LptE function in which, by binding the charged headgroup, it disrupts LPS-LPS interactions and guides the sugars of LPS through the hydrophilic lumen of LptD while the lipids transfer directly from a periplasmic aggregate to the interior of the OM. A desire to understand the energy requirements of this transfer led us to build on a reconstitution of LPS transport between liposomes. We used a combination of fluorescent flow cytometry and confocal microscopy to show that two populations of liposomes, each containing either the IM or OM complex, associate only in the presence of LptA, indicating that LPS transport occurs via a bridge of Lpt proteins that could transduce energy from the IM ATPase LptB to the OM. This reconstitution will allow for future studies of how different Lpt pathway mutants and differently modified forms of LPS alter LPS transport efficiency.

Table of Contents

Acknowledgements

"A scientist is *always* fine"

-Carlos, *Welcome to Night vale*

I owe credit to a great many people for sustaining me throughout graduate school and allowing me to reach this season. Due to limitations of both space and my own memory, I have undoubtedly forgotten some names below, so thank you to all of the friends, family, co-workers, and mentors who helped to get me here.

I am deeply indebted to my advisor, Professor Daniel Kahne. I could not have hoped for an advisor better suited to my particular quirks and needs. Dan always encouraged me to speak my mind, and was exceptionally patient with me on occasions that I neglected to be tactful in doing so. He always offered much needed optimism in the face of failed experiments and helpful advice and constructive criticism in the planning and interpretation of my research. I appreciate that, unlike some in his position, he cares for his students as people, and not only as workers. His help and support in my transition from research to other pursuits has been essential.

I am grateful for the advice and help of all of the current and former members of my dissertation advisory committee. Professors Rachelle Gaudet, Vlad Denic, and Richard Losick all provided essential support, feedback, and guidance. Professor Suzanne Walker, in addition to serving on my DAC at various points, served as a fantastic unofficial second advisor, and I thank her for her generosity at the Kahne/Walker lab holiday parties.

Many contemporary researchers made the work in this dissertation possible and the time conducting it enjoyable. I thank David Sherman, Suguru Okuda, and Lisa Freinkman for their excellent training and for their tireless labor in establishing many of the techniques that I relied

on. Ran Xie, Becca Taylor, Carolin Doering, and Goran Malojčić have been peerless collaborators, and my work has greatly benefitted from being done alongside them, as well as their advice. Particular thanks go to Dorothee Andres, who originated the SPR work discussed below, trained me in all of the associated methods, was never anything but a pleasure to work with, and, along with her charming family, generously hosted me on my visit to Germany. Peter Foster of the Needleman lab was essential to all of the optical microscopy described, and offered an essential new point of view to troubleshooting and interpreting the reconstitution of LPS transport. Away from the bench, I must thank Helen Corriero and Mike Quinn, who have kept the lab running smoothly in spite of the best efforts of its members and leader, and helped me to negotiate Harvard's bureaucracy and Dan's complicated schedule on countless occasions.

Many lab members that I did not directly collaborate with made the lab a pleasant and welcoming work environment, and offered invaluable feedback and discussion throughout the last six years. In no particular order, it would be between difficult and impossible to imagine my time in lab without John Janetzko, James Lee, Joseph Wzorek, David Westwood, Tristan Owens, and everyone who ever went out for trivia night. Special thanks are due to Michael Mandler, who has been exceptionally patient with the high-entropy environment I have created in our shared cubicle and helped to transform said cubicle into a sukkah, Janine May, whose assistance in preparing for job interviews was immensely helpful, Aaron Garner, who was very generous in guiding me through his collection of single malt scotch and other potable distillates, and Katie Schaefer and Sara Schwanger Martin for enjoyable discussions of, respectively, *Hannibal* and *The Americans*. Thank to all of the friends outside of lab who have provided many well-timed hugs, cups of tea, pints of beer, rambling conversations, so-bad-it's-good movie viewings, and games of Power Grid through graduate school and the time before.

I owe much to many past teachers and mentors for providing the education and guidance that got me to graduate school, and the list here is far from exhaustive. I thank professor Kathleen Howard of Swarthmore College for first getting me interested in membranes and Neil Hackett, my supervisor when I was a technician at Weill Cornell, for his support in my graduate school application, and for providing some necessary grounding when we were engaged in what was essentially mad science. I am eternally grateful to Rebecca Jackman of the Commonwealth School. No subsequent chemistry instructor has lived up to the high bar she set, and she has continued to provide invaluable advice and support long after I ceased to be her student.

My family has never been anything but supportive and loving. It is challenging to find words of thanks sufficient for those who have been there for me since before my memory begins. Mom and Dad, thank you for a loving home, an appreciation of the value of education, that slide rule, and so much more. B., thank you for being the best older sibling a kid could hope for. You truly embiggened the role with your cromulent performance.

Last, but by no means least, I thank my wife, Miriam Newman. No matter how doomed my graduate career felt, you responded with love, support, and encouragement. Thank you for your patience with me on this strange journey, and for your fantastic editorial services in the writing of this dissertation; any sections that are clearly written are almost certainly due to your influence and advice, and sections that are a mess are so because I either ignored or failed to seek your advice. It has been a delight and a privilege to have known you for the past 12 years and be married to you for the last five, and I look forward to writing the next chapter in our life together. Because of you, life is light, bright, and sparkling, and I am happier than I could have been without you. Others only smile, I laugh.

Chapter 1: Introduction

1.1: Introduction

Gram negative bacteria such as *Escherichia coli* are surrounded by not just an inner phospholipid bilayer membrane and peptidoglycan cell wall, as is the case for Gram positive bacteria, but also by a second outer membrane[1]. This outer membrane, rather than being a phospholipid bilayer, has its outer leaflet composed entirely of lipopolysaccharide (LPS), a large glycolipid. The outer membrane serves as a barrier to many hydrophobic drugs, in large part due to the hydrophilic layer created by the many sugars of LPS[2,3]. LPS is made in the inner membrane, and then transported to the outer membrane by the seven protein Lpt pathway[4-8]. This thesis is concerned with how different proteins of the Lpt pathway interact with LPS, and with developing tools to better be able to study how perturbations of the Lpt pathway effect LPS transport. The first chapter provides an introduction to the biology of the outer membrane and LPS transport. The second discusses work deciphering the function of the protein LptE in disaggregating LPS prior to insertion into the outer membrane. The third focuses on work that characterizes how LptE binds the LPS molecule to facilitate its disaggregation and transposition through the outer membrane. The fourth describes the use of an *in vitro* reconstitution to test the hypothesis that LPS transport to the outer membrane occurs via a membrane-to-membrane protein bridge.

1.2: The Gram-negative cell envelope as a barrier

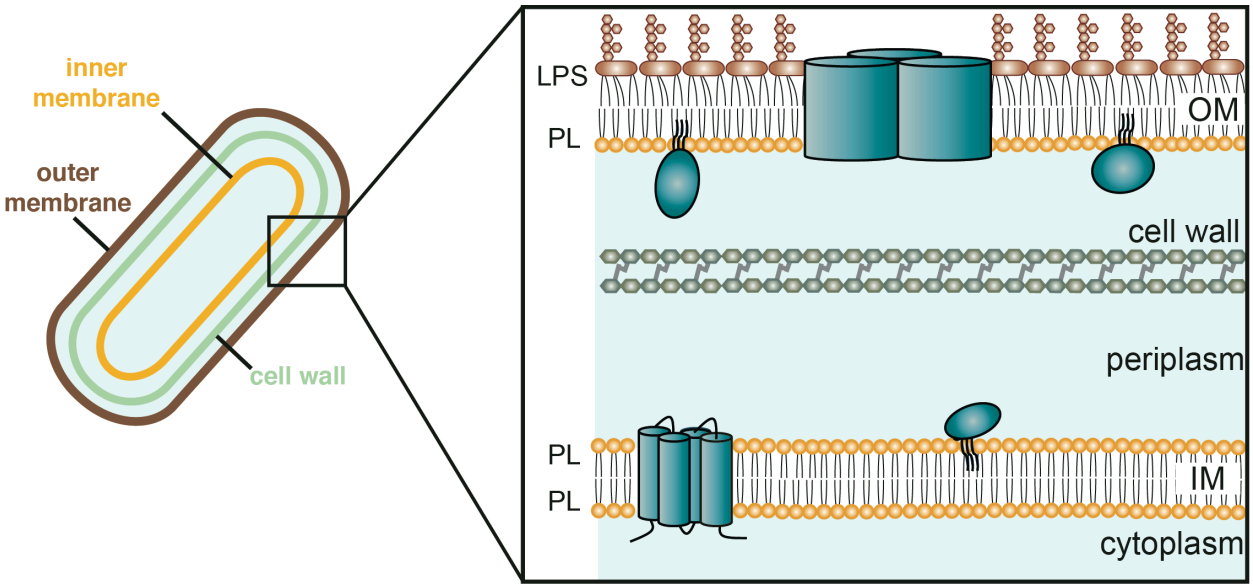

Figure 1.1: The cell envelope of Gram-negative bacteria. Cells are bound by a phospholipid bilayer inner membrane, which is in turn surrounded by a thin peptidoglycan cell wall, and an outer membrane. The space between the two membranes is known as the periplasm. The outer membrane's outer leaflet is composed of lipopolysaccharide, a large glycolipid. Outer membrane proteins are either □-barrels or periplasm-facing lipoproteins.

1.2.1: Gram-negative bacteria have a unique cell envelope

Gram-negative bacteria have an outer membrane (OM) that wraps around the cell of Gram-negative bacteria, outside of the peptidoglycan cell wall, defining a space between the inner membrane (IM) and OM known as the periplasm (Figure 1.1). The Gram-negative cell wall is thin when compared to that of Gram-positive species, but still provides enough rigidity to shape the cell and prevent lysis in conditions of high osmolarity. Braun's lipoprotein, embedded in the inner leaflet of the OM, binds the cell wall to the outer membrane[1]. The periplasm is between 10 and 50 nm across, holding 30% of the cell's volume, and lacks ATP or any equivalent energy source[9,10]. The OM is distinct from the IM and other cell membranes in a number of ways. Rather than a phospholipid bilayer, its out leaflet lacks phospholipid, instead

consisting entirely of LPS, transported to the OM by the Lpt pathway[6]. The means of phospholipid transport to the OM remains unknown, but retrograde transport of excess phospholipid from the OM to the IM is done by the Mla pathway[11,12]. The membrane proteins of the OM come in two forms. Lipoproteins are soluble proteins that are anchored in the inner leaflet of the OM by a tri-acylated lipid tail, transported by the Lol pathway[13]. □-barrels are integral membrane proteins folded into the OM by the Bam pathway[14].

1.2.2: Antibiotic resistance shows the importance of the OM

The OM of Gram negative bacteria serves as a barrier between the cell and its environment. This is of great clinical importance, as it is impermeable to many antibiotics. Antibiotic resistance is a huge problem[15,16]: in the United States alone, there are two million antibiotic resistant infections leading to 23,000 deaths every year[17]. Many antibiotics used to treat Gram-positive pathogens, such as vancomycin, have never been effective against Gram-negative bacteria due to the OM's role as a barrier. While recent novel antibiotics such as daptomycin have provided relief against Gram positive pathogens[18,19], they cannot cross the OM. By contrast, no new class of antibiotics that can treat Gram negative bacteria has been discovered since the development of the quinolones in 1962[20], rendering antibiotic resistance especially dire for Gram negative pathogens[21,22]. Two of the three pathogens deemed "urgent" by the CDC are Gram negative. Drug resistant *Neisseria Gonorrhoeae* leads to 246,000 resistant infections every year. Carbapenem-resistant enterobacteriaceae cause a smaller 9,000 infections every year, but have become resistant to virtually all available antibiotics[17]. The situation is sufficiently dire that clinicians have been prescribing colistin, an antimicrobial polypeptide that had been known but

not used for decades due to nephrotoxicity[23], but resistance to colistin has recently been identified in the clinic[24-26].

1.2.3: The OM's unique lipid composition

The OM is such an effective barrier to antibiotics due to its unique composition. In contrast to the phospholipid bilayer preferred by most biological membrane, the OM displays complete asymmetry between its leaflets, with the inner leaflet being made of phospholipids and the outer leaflet composed entirely of lipopolysaccharide (LPS). This was first suggested by electron microscopy studies where isolated OM exposed to ferritin conjugated to antibodies raised against the sugars of LPS only showed ferritin labeling on its external side[27]. This was confirmed by several biochemical assays. Exposure of ^{32}P-labeled *Salmonella typhimurium* cells to phospholipase C, which liberates the phosphate from available phospholipids, showed no liberated phosphate unless the experiment was performed with strains that produced severely truncated LPS. Phosphoethanolamine is the primary phospholipid component of the OM, but tritium-labeled cells exposed to CNBr-dextran, which binds PE but cannot cross the OM, similarly failed to show any dextran-PE conjugates except in strains with truncated LPS[28]. These data suggest that, in healthy cells, the phospholipids of the OM are almost completely localized to the inner leaflet. Experiments in which cells were exposed to galactose oxidase, which can act on the galactose present in the LPS saccharide, shows that the LPS in cells experiences the same rate and degree of conversion as LPS in solution, suggesting that all of the LPS in the cell is at the outside of the cell[29]. Combined, the above experiments confirmed the model of a completely asymmetrical OM.

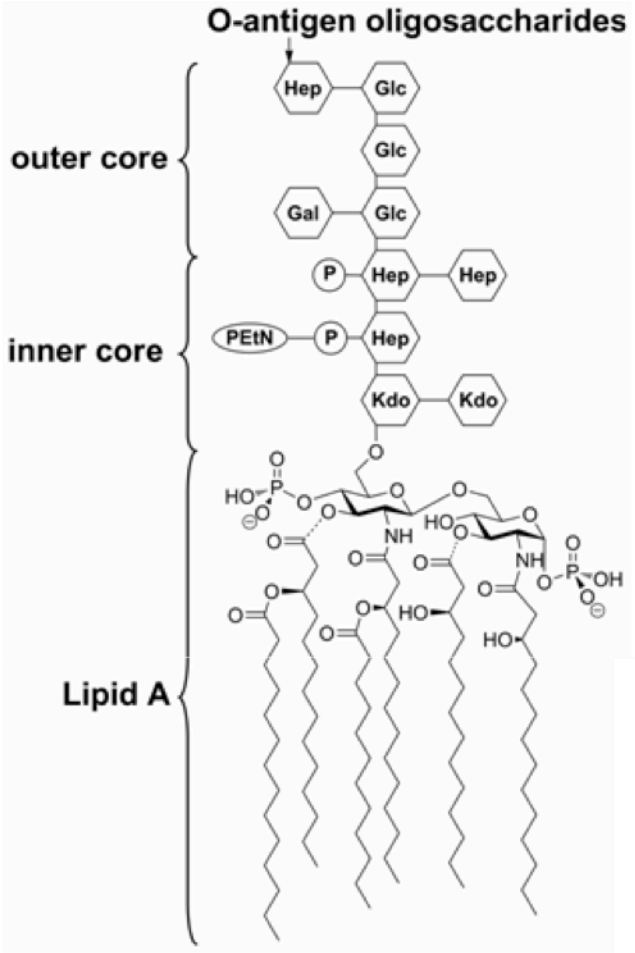

Figure 1.2: The structure of *E. coli* K-12 LPS. A short core oligosaccharide is attached to the di-glucosamine-di-phosphate of the hexa-acylated lipid A. In strains other than K-12, a repeating O-antigen saccharide is attached to the core oligosaccharide.

LPS itself is a large glycolipid composed of several parts (Figure 1.2). At its base is lipid A, a large lipid with between five and seven (six is typical for *E. coli*) acyl chains attached to a di-glucosamine-di-phosphate headgroup. These acyl chains make up the hydrophobic core of the outer leaflet of the OM. Attached to the headgroup is the core oligosaccharide, made of 10 sugars in *E. coli* K-12 and further subdivided into the inner and outer core, and attached to that is the O-antigen oligosaccharide, a short oligomer that varies greatly between species and strains and can repeat dozens of times[4]. LPS including the O-antigen is often referred to as S-LPS. The K-12 strain of *E. coli* used in most laboratory experiments lacks the O-antigen, leading to a so-called

"rough" phenotype[30]. Such LPS, containing the whole core oligosaccharide but lacking the O-antigen is referred to as Ra-LPS; LPS lacking the outer core is referred to as Re-LPS.

1.2.4: LPS lateral associations make the OM less permeable

The structural features described above make LPS largely responsible for the increased impermeability of the OM. This was initially shown by measuring the diffusion rates of very hydrophobic molecules such cholesterol as across different membranes. Membranes made of a phospholipid bilayer allowed steroids to diffuse across them at a rate two orders of magnitude higher than OM's from strains that produce S-LPS. OM from strains producing the truncated Re-LPS are 16-25 times more permeable to steroids as S-LPS containing OM, and [31,32], and Δ*lpxA* and Δ*lpxD* strains, each producing under-acylated LPS , show a similar increased permeability to steroids[33]. Strains producing Re-LPS and those producing LPS with fewer acyl chains are much more sensitive to antibiotics[34]. All of this shows that full LPS molecule are required for the OM to properly serve as a barrier to hydrophobic molecules and antibiotics. There are several mechanisms contributing to this effect. Removing the outer core saccharides from LPS makes it more difficult to insert proteins into the OM[35,36], leading phospholipid filling the space that would be filled with proteins, creating a more permeable phospholipid bilayer in patches of the OM[2,28]. LPS having between five and seven acyl chains, as opposed to the two found on most phospholipids, leads to a more rigid, less fluid membrane with a higher melting temperature, making it less permeable[3,31]. These lipid-lipid interactions contribute to exceptionally tight LPS-LPS interactions: LPS self-associates readily, and when mixed into phospholipid membranes will self-segregate into patches[37]. Also essential to the tight LPS-LPS interactions are the ionic interactions between the anionic phosphates of LPS and divalent cationic metals such as Ca^{2+}

and Mg^{2+}. Purified LPS inevitably contains a molar excess of such divalent cations, even if it has been thoroughly dialyzed[38]. LPS requires such small divalent cations to form aggregates *in vitro*[39], and molecular dynamics simulations indicate that LPS molecules cannot form lateral interactions with each other without divalent cations[40]. Chelators that remove Ca^{2+} and Mg^{2+}, such as EDTA, also liberate large quantities of LPS from the membrane, permeabilizing it, and further stressing the primacy of the polyelectrolyte web in stabilizing LPS-LPS lateral interactions, and thus the OM[2]. Modifications to LPS can further improve the OM's impermeability, leading to increased antibiotic resistance[41].

The OM's asymmetry and the tight self-association of LPS immediately lead to questions about the energy required to maintain this topology. While the asymmetry of the OM is now accepted by all in the field, Nikaido and coworkers' research establishing this was initially rejected because reviewers believed that it was "thermodynamically impossible"[3]. The entropic costs of this strict asymmetry are obvious, and it is unclear how much the favorable LPS-LPS interactions described above can balance that out. Purified OM allowed to incubate briefly at 37° C loses its asymmetry, as judged by EM images after immune-ferritin labeling[27], suggesting that the asymmetry is unfavorable, and thus requires energy to establish. Once established, the difficulty of flipping LPS, with its dozens to hundreds of sugars, through the hydrophobic core of the OM, likely helps to maintain the asymmetry of the OM. This kinetic barrier also makes establishing the asymmetric topology more difficult, especially as the periplasm lacks an energy source[10], and all of the LPS must be moved from the IM across the periplasm and then flipped through the OM (vide infra).

1.3: Lipopolysaccharide biosynthesis and modifications

1.3.1: LPS biosynthesis in the IM

While LPS is all moved to the OM, it has been known for decades that it is synthesized in the IM for decades[42]. The biosynthesis of lipid A all takes place on the inner leaflet of the IM and has been established by Raetz and others and is reviewed in detail elsewhere[4,7,12,43]. In brief, LpxA acylates UDP-GlcNac, and LptC removes the UDP in the committing step of lipid A biosynthesis. It is then acylated again. One bi-acylated GlcNac is then joined to another which has already been phosphorylated, and the new molecule is phosphorylated again, leading to Lipid IV_A, a tetra-acylated di-glucosamine-di-phosphate that serves as the minimal viable LPS fragment for transport to the OM[44]. Two Kdo monomers are ligated to the di-glucosamine headgroup, before LpxL and LpxM add the fifth and sixth acyl chain, leading to Kdo_2-Lipid A. The rest of the core oligosaccharide is then attached, piecewise, to the Kdo's, prior to Ra-LPS being flipped across the IM by MsbA. The O-antigen, not present in K-12 derived *E. coli* strains, is produced on a separate undecaprenyl carrier on the inner leaflet of the IM and flipped across to the periplasm by one of three different pathways, depending on the strain and species, before being ligated to Ra-LPS before its transport to the OM.

1.3.2: Modifications of LPS

There are a variety of modifications that cells make to their LPS in response to specific environmental stresses and stimuli. These occur at both the IM and the OM, and help to protect the cell from assorted antimicrobial peptides and other environmental stresses. As such, they can serve as biomarkers for both the health of the OM, and for where LPS transport has bottlenecked

under certain conditions. These modifications are reviewed in detail elsewhere[41]. Those most important to *E. coli* are reviewed briefly here.

Lipid A can have its di-glucosamine-di-phosphate group modified via attachment of different moieties to the phosphate while in the periplasmic leaflet of the IM (Figure 1.3). ArnT attaches L-Ara4N, and EptA attaches phosphoethanolamine. Expression of both proteins is regulated by PmrA/B, a two-component regulator that responds to changes in pH, as well as concentration of Mg^{2+}, Fe^{3+}, and the presence of polymyxins. These modifications help protect the cell from polymyxin, L-Ara4N by removing the charge polymyxins require to bind LPS, and phosphoethanolamine by an as of yet unknown mechanism[45,46]. The L-Ara4N modification is also seen in *Pseudomonas aeruginosa* response to the novel antibiotic L27-11, thought to target the LptD/E complex[47].

At the OM, PagP adds removes a palmitate from a phospholipid to attach it to LPS[41]. PagP expression is controlled by the PhoP/Q system, which is responsive to Mg^{2+} concentration, as well as the presence of amphipathic □-helical antimicrobial peptides[48], and □*pagP* cells are more susceptible to some non-polymyxin antimicrobial peptides[49]. PagP also modified LPS in response to an excess of phospholipid in the OM, helping to restore balance to the LPS: phospholipid ratio[3].

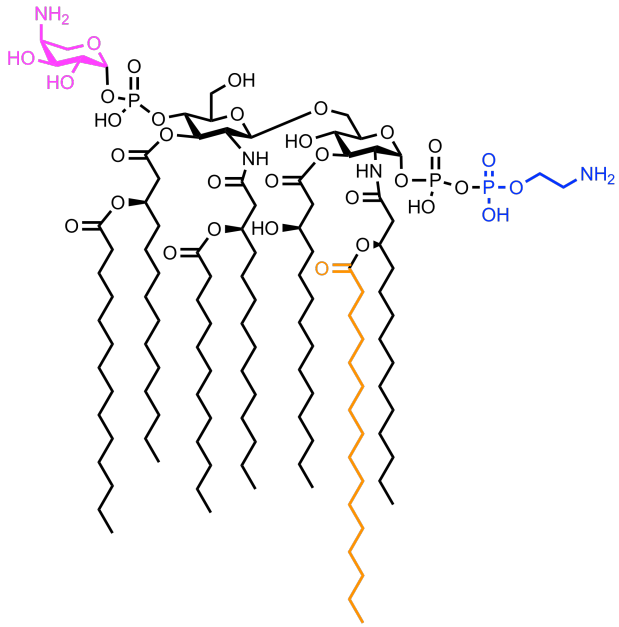

Figure 1.3: Modifications that *E. coli* makes to lipid A. In the periplasmic leaflet of the IM, the phosphates can be modified via either addition of L-Ara4N by ArnT (magenta) or addition of phosphoethanolamine by EptA (blue). At the OM, PagP can attach a palmitate (orange).

1.4: The Lpt pathway

1.4.1: Early work on LPS transport

Decades before the Lpt pathway was identified, it was known that LPS was made in the IM and transported to the outer leaflet of the OM. Shortly after others identified sucrose density ultracentrifugation as a means of separately purifying the IM and OM[50], Mary Jane Osborn and coworkers used this technique to analyze the components of the two membranes, showing that LPS is located almost entirely in the OM[51]. They were also able to combine this with pulse chase studies to show that LPS is moved from the IM to the OM but not vice versa[42], and thus that LPS is made in the IM. Nikaido and coworkers, as mentioned above (Section 1.2.3), showed that LPS is entirely within the outer leaflet of the OM, establishing the final resting place of LPS[3]. Only after Raetz and coworkers began deciphering the lipid A biosynthetic pathway in the cytoplasmic leaflet of the IM were any proteins involved in LPS transport identified. MsbA, the flippase

responsible for translocating LPS from the inner to the outer leaflet of the IM, had been identified as a multicopy suppressor of a temperature-sensitive mutant of *htrB*, and had been assumed to be a transporter of some sort due to its being an ATP-binding cassette (ABC) transporter. Raetz's discovery that *htrB* (then renamed *lpxL*) produced an acyltransferase in the LPS biosynthetic pathway led to the hypothesis that lipid A was the substrate of MsbA[7]. MsbA's role in LPS transport was confirmed by temperature sensitive mutants of MsbA leading to buildup of LPS precursors in the IM at the non-permissive temperature[52], and MsbA was confirmed as the lipid A flippase by showing that these mutants, at the non-permissive temperature, caused a buildup of LPS with modifications localized to the inner leaflet of the IM[53]. Prior to the discovery of the Lpt pathway, it was thus known where LPS originated, where it wound up, and how the first step of this process occurred, but how it was extracted from the IM, moved across the periplasm to the OM, and then flipped through the OM to the outer leaflet remained a mystery.

1.4.2: Identification of the components of the Lpt pathway

Work over the last two decades has identified seven essential proteins responsible for moving LPS from the IM to the OM, which collectively make up the lipopolysaccharide transport (Lpt) pathway, with components in the IM, periplasm, and OM. Four Lpt proteins (LptB/F/G/C) form an ABC transporter complex in the IM, while LptA is a soluble periplasmic domain, and LptD/E form a plug and barrel structure in the OM. LptB, A, and C were identified as essential genes in a transposon screen[54], and depletion of any of these was found to lead to a buildup of LPS at the inner membrane, confirming their role in LPS transport[55,56]. LptF and LptG were identified via a reductionist bioinformatics search for Lpt proteins: Ruiz and coworkers

searched for predicted membrane proteins in *E. coli* that could also be found in LPS-producing endosymbionts with much smaller proteomes. Their role in LPS transport was confirmed by depletion strains showing compromised, permeable OMs, and a buildup of LPS with modifications that can only take place in the IM[57].

The discovery of the OM components of LPS transport was a longer process. LptD was initially identified as a source of suppressor mutations for strains deficient in maltodextrin import[58]. The gene was initially labeled *imp* (for increased membrane permeability), and *imp* mutants were found to render *E. coli* more sensitive to antibiotics, and later to organic solvents, leading to the conclusion that it had an as-yet unknown role in membrane integrity biogenesis and giving it the new name *ostA* (organic solvent tolerance)[59]. The Silhavy lab soon showed that *imp/ostA* was essential, and that deletion of *imp/ostA* led to a novel fraction in purified *E. coli* membranes containing phospholipids and OM proteins, confirming the role of the Imp/OstA protein in OM biogenesis[60]. Imp/OstA's role in LPS transport specifically was confirmed when Tommassen and coworkers took advantage of the fact that LPS is not essential in *Neisseria memingitidis*[61,62] and deleted *imp/ostA*. The resulting strain produced much less LPS than wild type strains, and what LPS it contained was modified by neither LPS-modifying enzymes contained in the OM nor those researchers added to the surrounding environment, confirming Imp/OstA's involvement in LPS transport[63].

The final Lpt protein to be identified, LptE, had previously been known to exist, but its function was sufficiently mysterious that it was named RlpB for rare lipoprotein. The Kahne and Silhavy lab, curious if there were OM proteins involved in LPS transport beyond Imp/OstA, found that RlpB pulled down with polyhistidine-tagged Imp/OstA on nickel resin, and showed RlpB to be essential. Depletion of RlpB led to an increased density in the OM similar to that seen

with depletion of Imp/OstA. Electron microscopy revealed an abnormal membrane structure under RlpB depletion, and depletion led to lipid A being hepta-acylated[64]. This last point indicates that the OM contains excess phospholipid relative to LPS, as *E. coli* cells respond to such stress by using the OM enzyme PagP to remove acyl chains from phospholipid and attach them to Lipid A[65]. Soon thereafter, Imp/OstA and RlpB were renamed LptD and LptE, respectively[56].

1.4.3: The LptB/F/G/C complex is an ABC transporter in the IM

Shortly after identifying the components of the Lpt pathway, researchers began to characterize their structure and function. The inner-membrane associated proteins, LptB, F, G, and C, proved to form an ABC transporter. As it was the only cytoplasmic protein, LptB was long hypothesized to be the ATPase powering LPS transport, and this was supported by sequence analysis showing LptB closely resembled the nucleotide binding domains of ABC transporters[7,55]. Sequence analysis led to the prediction that LptF and LptG were the transmembrane components of an ABC transported complex associated with LptB, and the association was soon confirmed by the fact that co-expression of LptF and LptG stabilized LptB, and they co-purify as a complex, which could also contain LptC at a stoichiometry of 2:1:1:1 LptB:F:G:C[66]. As the first step for LPS transport to the OM must be its removal from the IM, it was hypothesized that this was the function of the IM LptB/F/G/C complex. The complex was confirmed to show ATPase activity[67], and LptB mutants that prevent either ATPase activity or interaction with LptF and LptG both proved fatal[68]. Furthermore, crystal structure of LptB, in complex with both ATP and post-hydrolysis ADP, reveal that ATP hydrolysis leads to a

conformational change in LptB where it interacts with LptF and LptG[68], suggesting a means by which the energy from ATP hydrolysis is translated into extraction of LPS from the membrane.

1.4.4: LptE is needed to fold LptD, and forms a plug to the LptD barrel in the OM.

The LptD/E complex forms a plug and barrel, with the β-barrel of LptD wrapping around LptE, which is almost completely buried within LptD and which is essential to its proper folding. LptE's discovery via pull-down, and the impossibility of overexpressing LptD without simultaneously overexpressing LptE suggested it was associated with LptD, and this was confirmed when moved as a single band in semi-native SDS-PAGE, and quantitative amino acid analysis confirmed the complex contained the two proteins at equimolar quantities[69]. Sequence analysis indicated that LptD was split between a small N-terminal periplasmic domain and a large C-terminal β-barrel[70,71], and this was confirmed by expressing LptD constructs consisting of only one or the other domain. Proteolytic analysis showed that LptE and the C-terminal domain of LptD formed a tight complex, protected from proteolytic degradation, suggesting that LptE might sit within LptD[69]. Freinkman and coworkers made use of amber-codon suppression, developed by the Schultz lab[72,73], to incorporate the photocrosslinkable artificial amino acid *p*-benzoyl-L-phenylalanine[74] into LptE at 27 positions, and identified six locations leading to an LptE-LptD crosslink. The crosslinking sites were predicted to be on all sides of LptE, and one site crosslinks to an extracellular loop of LptD, showing that LptE is surrounded by LptD and is inserted deep into the LptD β-barrel, confirming the plug and barrel model[75].

Beyond just serving as a plug for LptD, LptE is also essential to the proper folding of LptD. Like all periplasmic and OM proteins, LptD and LptE are expressed in the cytoplasm and secreted into the periplasm, unfolded, by the SEC machinery[76]. LptE receives its lipid anchor and

folds in the IM, before being transported to the inner leaflet of the OM by the Lol pathway[13]. The chaperone SurA shuttles LptD across the periplasm in an unfolded state, and the BamA/B/C/D/E complex folds LptD into the OM[14,77,78]. Folding of LptD is complicated by its four cysteine residues: these must form the correct pair of disulfide bonds in order to function, and LptE is essential to proper oxidation[79]. A mutant form of LptE, LptE6, shows reduced association with LptD, and leads to misfolded LptD, but is suppressed by mutants to BamA, implying that LptE's association with LptD is used by the Bam machinery to correctly fold LptD[80]. This was confirmed by a painstaking mapping of the intermediate oxidation states of LptD[81], and by using site-specific photocrosslinking to trap an intermediate state in which LptD is wrapped around LptE but does not form a complete barrel, with both LptD and LptE interacting with components of the Bam complex[82].

1.4.5: The Lpt pathway forms an LptA-mediated bridge across the periplasm

With the discovery of the Lpt pathway, there soon emerged two models for LPS transport[5] (Figure 1.4A): one in which the Lpt proteins formed a continuous bridge that LPS traveled along, and one in which LptA served as a soluble shuttle, ferrying individual LPS molecules from the IM complex to the OM translocon, similarly to how the Lol pathway transports lipoproteins[13,83,84]. Early biochemical data were consistent with a bridge model. When periplasmic extract is added to spheroplasts, it extracts lipoproteins, but not LPS. Concurrent pulse-chase experiments showed that LPS continues to move from the IM to the OM in spheroplasts devoid of the periplasm, suggesting that LPS cannot even leave the IM without the OM components of the Lpt pathway, but that LPS transport does not require anything in the periplasmic solution[85]. Crystal structure of LptC and LptA revealed them to share a β-jellyroll

structure, with a distinct hydrophobic groove, and sequence similarity (and later structural biology) showed the N-terminus of LptD to share the fold[86-88]. Of particular note was that when crystalized in the presence of LPS, LptA formed a tetramer, stacking end over end, leading to a long, continuous hydrophobic groove down the whole tetramer[89]. LptA was also found to form oligomers in a concentration-dependent fashion in solution[90], suggesting that LptA might not exist as a free monomer in the periplasm. All of this was consistent with the bridge model, but there was still no direct evidence of a bridge in cells.

Researchers in the Kahne lab soon confirmed that the Lpt proteins could form a continuous bridge across the periplasm. Fractionation of *E. coli* membranes via density ultracentrifugation had previously revealed two OM fractions, dubbed OM_H and OM_L due to their respective densities, with OM_L also containing part of the IM, suggesting regions of IM-OM association[91]. All Lpt proteins are found in the OM_L fraction, including those embedded in or associated with the IM (LptB/F/G/C). LptA, a soluble protein localized to the periplasm, also fractionates in the OM_L, and was found exclusively in the OM fractions when expressed at native levels, unlike other soluble periplasmic proteins such as the maltose binding protein MalE, suggesting that LptA does not exist as a free soluble protein, as might be expected in the periplasmic shuttle model of LPS transport. An LptA-His construct, however, associated with the IM rather than the OM, suggesting that LptA does interact with both membranes, and that the polyhistidine tag disrupts interactions between LptA and the OM. Pull-down experiments were consistent with the co-fractionation data. When polyhistidine-tagged constructs of any of LptB, LptC, or LptF are purified from cell lysate via nickel affinity chromatography, all of the Lpt proteins, including the components of the OM translocon, are co-purified[92]. This indicated direct physical interaction between all seven of the Lpt proteins, as opposed to colocalization in the

same membrane fraction, especially as other OM proteins, such as BamA, did not co-purify with components of the Lpt IM complex. The co-fractionation and co-purification of all of the Lpt proteins, in concurrence with the lack of LptA as a free protein in periplasmic fractions, support the bridge model for LPS transport, in which all seven Lpt proteins form a continuous trans-periplasm complex inserted into both IM and OM.

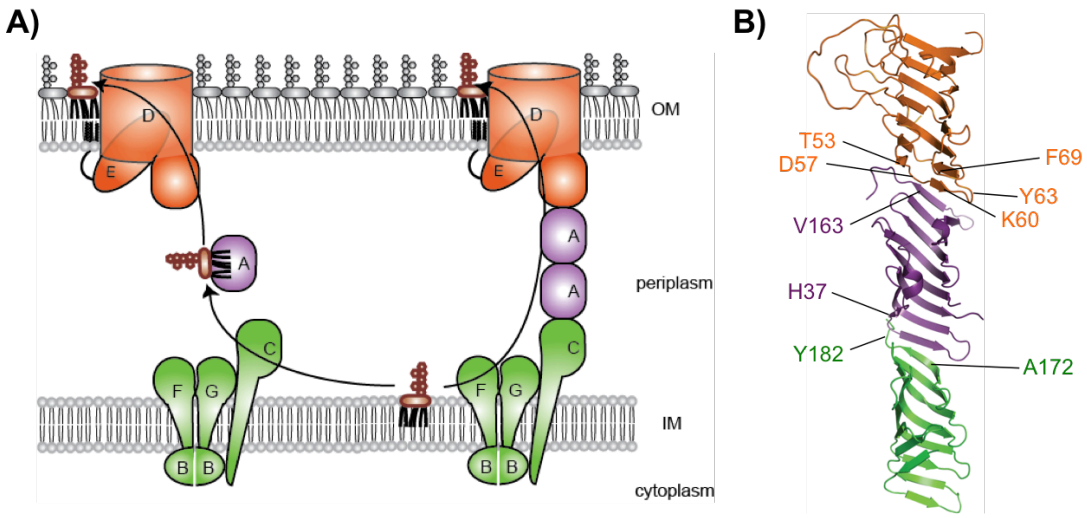

Figure 1.4: A) The Lpt pathway could transport LPS via a periplasmic shuttle (left) or a bridge containing an unknown number of LptA monomers (right). B) Sites of crosslinking between LptC (green) and LptA (purple), and between LptA and the N-terminal domain of LptD (orange).

Crosslinking studies in the Kahne lab also showed association between LptA and both LptC and LptD. Using the same *in vivo* site-specific photocrosslinking technique described above, pBPA was inserted at sites throughout LptA, LptC, and the N-terminus of LptD, and strains expressing these mutants were exposed to UV light to crosslink. LptC and LptA were found to crosslink each other, but only when pBPA was placed along the C-terminal edge of the LptC □-jellyroll or along the N-terminal edge of the LptB □-jellyroll. Similarly, LptA and LptD

crosslinked to each other, but only via pBPA placed on the C-terminal edge of LptA or the N-terminal edge of LptD[93]. The location of these crosslinks suggests that LptC interacts with LptA and LptA with LptD in the fashion seen in the tetrametic crystal structure of LptA, with the C-terminal edge of one β-jellyroll lining up with the N-terminal edge of the next to form a continuous β-jellyroll across the two proteins (Figure 1.4B). This leads to an obvious model of the structure of the proposed bridge, in which LptC, LptA, and LptD all interact in this fashion to form continuous hydrophobic channel across the periplasm. In this model, there could be multiple LptA monomers between LptC and LptD. In addition, only properly oxidized LptD could crosslink or be crosslinked by LptA, showing that proper folding of LptD is a pre-requisite. In addition, only properly oxidized LptD could crosslink or be crosslinked by LptA, showing that proper folding of LptD is a pre-requisite for LptA-LptD association, and thus for formation of the proposed bridge[93].

1.4.6: The Lpt pathway transports LPS in a continuous chain: the PEZ model

Having shown the Lpt pathway to be essential for LPS transport and established a model for the structure and assembly of the Lpt pathway, researchers in the Kahne lab began to study the mechanism by which the Lpt pathway transported LPS to the OM. Using the same amber-codon mutants used for identification of protein-protein contacts in the bridge, they searched for sites where the Lpt pathway crosslinked LPS, finding crosslinking sites exclusively along the inside of the hydrophobic groove of LptC, LptA[94], and LptD[95]. Overexpression of the LptB/F/G/C complex led to a buildup of LPS crosslinked by LptC, and co-overexpression of LptA with the IM complex led to a buildup of LPS crosslinked by LptA. This shows that the crosslinks are on-pathway, indicates that LPS transport can begin without a complete Lpt bridge,

but that LPS cannot move past LptC without LptA to receive it, and likewise cannot move past LptA without the OM translocon present. The LptC and LptA crosslinks to LPS were repeated in an *in vitro* system using right-side-out (RSO) vesicles. This granted an extra measure of control, allowing researchers to show that crosslinking is ATP-dependent for both LptC and LptA.

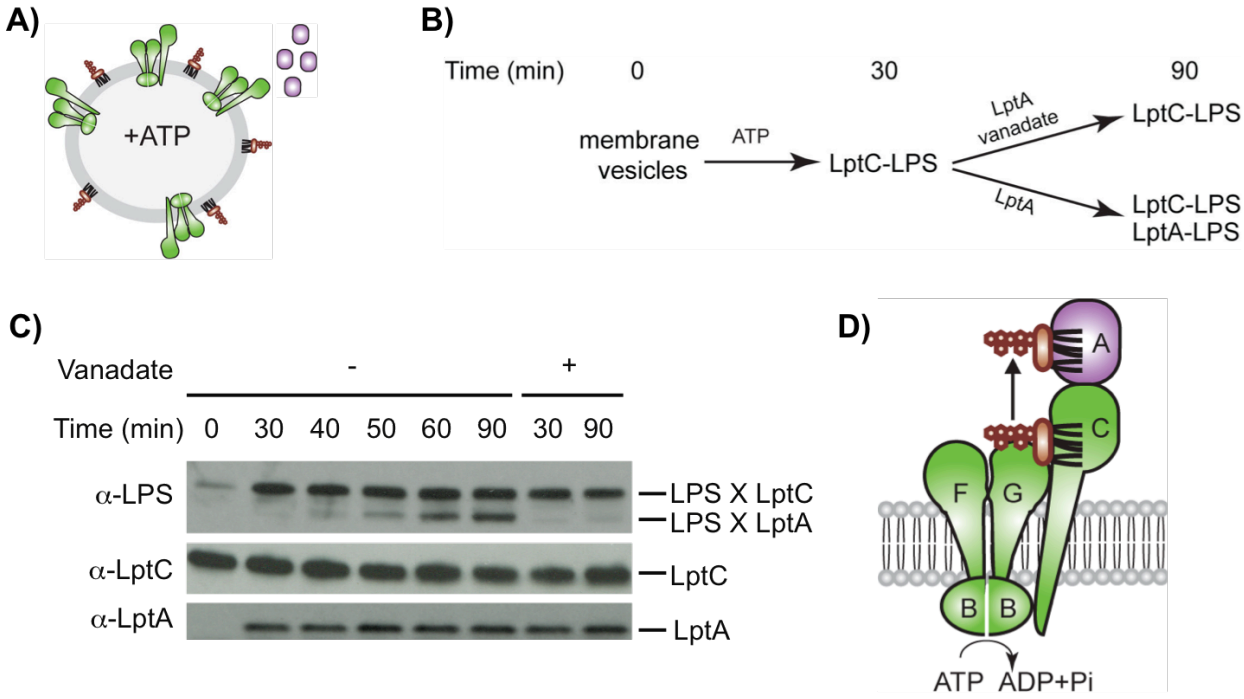

Figure 1.5: Handoff of LPS from LptC to LptA is ATP dependent. A) LptA-I36Am and right side out vesicles made from the IM of a strain expressing LptC-T47Am were used. B) Vesicles were incubated with ATP for 30 minutes to pre-load LptC with LPS. At 30 minutes, LptA was added, with or without vanadate. Vesicles were exposed to UV light for crosslinking at 0, 30, 40, 50, 60, and 90 minutes. C) Western blots of crosslinked samples. LptC crosslinks LPS under all circumstances, but LptA fails to crosslink LPS when vanadate halts ATPase activity. D) LptC can only transfer LPS to LptA when ATPase activity is possible, suggesting a model in which LptB powers LPS transport at steps beyond LptC.

Researchers were then able to show that handoff of LPS by LptC to LptA is ATP-dependent (Figure 1.5), by adding LptA only after RSO vesicles had been pre-incubated with ATP to ensure LPS-loading of LptC. Crosslinking can be seen in in LptA in the presence of ATP, but not when vanadate, which inhibits ATPase function, is added simultaneous to LptA[94].

This led to the PEZ model (Figure 1.6) for LPS transport, a combination of the above data with the bridge model for the structure of the Lpt pathway. According to the PEZ model, each instance of ATP hydrolysis by LptB is coupled to extracting a single LPS molecule from the IM and passing it to LptC. LPS forms a continuous chain on the bridge, bound by LptC, LptA, and LptD, from the IM to the OM. Each molecule of LPS added to the bottom of the protein bridge pushes all of those ahead of it one step further down the bridge, with the LPS at the end pushing through the translocon into the outer leaflet of the OM.

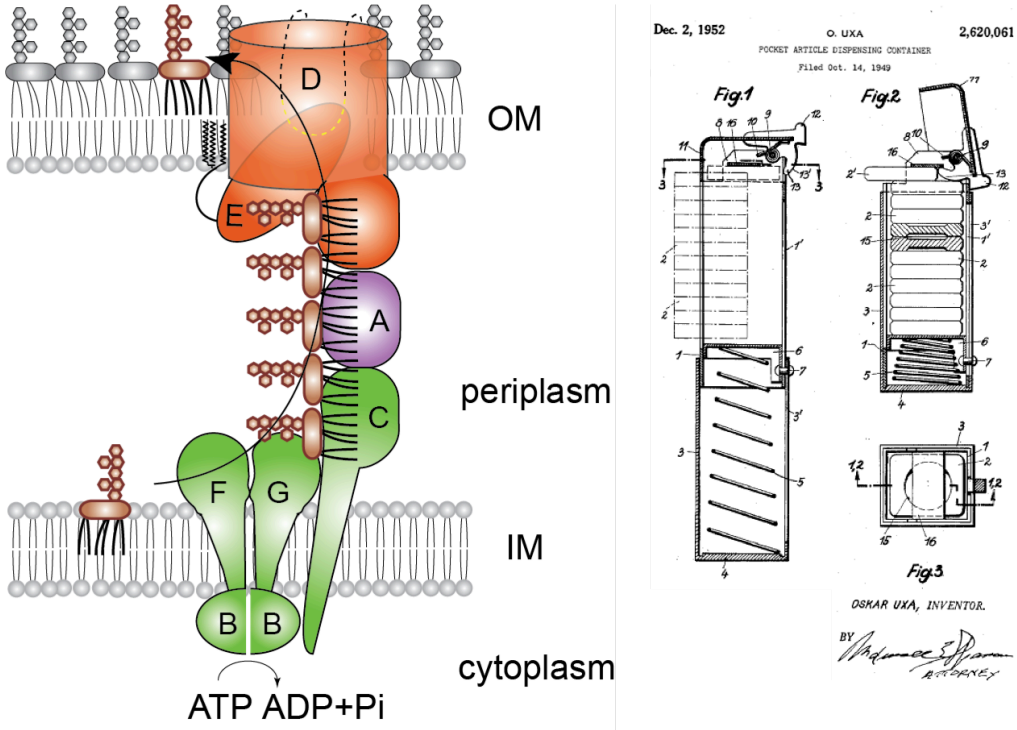

Figure 1.6: The PEZ model for LPS transport (Left). LPS forms a continuous chain along the Lpt bridge, with each ATP-powered addition of a new LPS molecule at LptC pushing all LPS already on the bridge closer to the OM, and the LPS at the end of the bridge out into the OM through an unknown mechanism. This resembles the mechanism at work in a PEZ dispenser, in which a spring at the bottom pushes all individual PEZ up for every PEZ removed at the top. Figures on the left are from US patent #2,620,061[96].

1.4.7: Unresolved questions about LPS transport

Our knowledge about LPS transport has grown greatly in the last 15 years, but many questions remain unanswered. We lack an understanding of the mechanism of the LptD/E translocon. How does it move a large, amphipathic molecule like LPS through the middle of a

membrane, against a concentration gradient, to the outer leaflet of the OM? Of particular interest is the role of LptE. LptE is known to serve as a plug for the LptD barrel, preventing leakage through the barrel[75], and LptE is required to properly fold LptD, and thus form interactions with LptA[69,80-82,93]. What is unknown is if LptE serves a direct role in LPS transport, helping LptD to bind LPS and move it from LptA to the OM, or if is purely a chaperone for LptD assembly and a plug for the LptD β-barrel. Chapter two addresses this question, showing LptE acts on LPS, and chapter 3 characterizes how LptE binds LPS, and confirms LptE binding of LPS *in vivo*.

Many of the remaining mysteries in LPS transport can be better understood via a complete *in vitro* reconstitution of LPS transport from pure components. A reconstitution would allow for comparison of the efficiency of transport of different Lpt pathway mutants. The energy dependence of the later steps of LPS transport are unclear, and a complete reconstitution would help to understand this. Developing such a reconstitution has been an active focus of research in the Kahne lab for years, and Suguru Okuda and David Sherman have developed one in which LPS in transported from LptB/F/G/C liposomes to liposomes containing LptD/E. This reconstitution, while a triumph of biochemistry, remains incomplete, because it is still unknown how the liposomes are arranged, and there is no conclusive proof of if the reconstitution forms a bridge between the liposomes as predicted. If the LptD/E translocon requires energy to flip LPS across the OM, this would mandate a bridge to transfer energy from the IM, so determining if LPS transport is reconstituted via a bridge would both help to finally resolve the bridge vs. chaperone question and shed light on the energy requirements of the final step of LPS transport. Chapter 4 is dedicated to determining if the Okuda-Sherman reconstitution transports LPS via a bridge between liposomes.

Chapter 2: LptE binds to and disrupts LPS aggregates

This chapter is adapted from Malojčić, Andres, *et al*., 2014[97].

Collaborators: Goran Malojcic, Dorothee Andres, Marcin Grabowicz, Natividad Ruiz, Tom Silhavy, Daniel Kahne

Explanation of contributions: I was heavily involved in interpretation of all data and the writing of the paper. I was also involved in the planning of the EM experiments, and performed the LptE-immobilization experiments with Dorothee Andres.

2.1: Introduction

2.1.1: LptE serves as a plug for the LptD β-barrel and as a chaperone for LptD folding

While the function of much of the Lpt machinery is known, the role played by LptE remains unclear. What is known is that LptE is essential in *E. coli* and many Gram-negative bacteria, plays a role in LPS biogenesis, and serves several functional roles. It has been clear since it was shown to interact with LptD that LptE serves a role in LPS biogenesis. LptE depletion strains show a similar phenotype to LptD depletion strains: they show a buildup of excess membrane material, deformed excess membrane is visible in electron micrographs of cells, and an increase in hepta-acylation of LPS by PagP, and OM localized enzyme that removes acyl chains from phospholipid to attach them to LPS, and that's activity serves as an indication of excess phospholipid in the OM. In addition, autoradiography shows that LPS is not transported to the OM without LptE, as LPS synthesized after depletion of LptE[64], showing that LptE is required for LPS transport to the OM, and in its absence the OM becomes deformed.

LptE serves as a plug for the LptD β-barrel, preventing LptD from being an open membrane pore. LptD and LptE protect each other from proteolysis, suggesting a tight interaction[69]. Site-specific photocrosslinking studies of LptE found multiple sides of LptE interacted with LptD, indicating it is enveloped by the β-barrel of LptD, and showed it to interact with a large extracellular loop of LptD[75]. Crystallographic studies of the LptD/E complex have confirmed this[88,98]. Strains expressing a mutant LptD lacking in this loop are viable, but have a compromised OM, showing LptE's role as a plug for LptD is needed to maintain OM integrity.

LptE also serves as a chaperone for the folding of LptD into the OM. LptD has four cysteines that form two disulfide bonds between the first and third cysteines and the second and fourth cysteines, passing through an intermediate state where the first and second form a disulfide bond as it folds. LptD cannot fold properly and achieve the correct oxidation state without LptE[79], and is stuck at the intermediate folding stage when LptE is depleted[81]. Crosslinking studies show that LptD will only interact with LptA when it has a achieved its proper oxidation state[93]. LptE is thus needed for LptD to fold properly, and thus to be able to form the Lpt bridge needed for LPS transport.

2.1.2: Structure of LptE suggests a direct interaction with LPS

While LptE plays an essential structural role in the Lpt pathway, it remains unclear if it is directly involved in LPS transport, or serves as just a chaperone and plug for LptD. LptE is not required for LPS transport in *Neisseria meningitidis*[99], suggesting that any such role it may play is not conserved. The first evidence for LptE having a direct role in LPS transport was the finding that LPS bound to resin-immobilized LptE. This binding saturates, shows competition between different forms of LPS, and is specific to LPS rather than other lipids[69]. That LptE binds

LPS is consistent with a function in transport beyond plugging LptD.

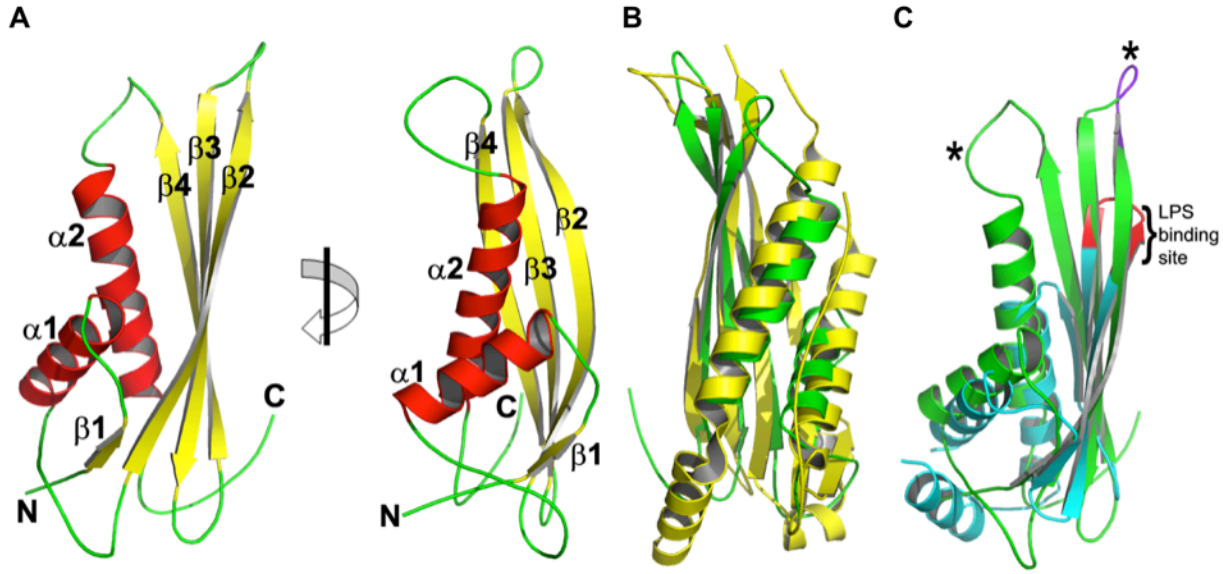

Fig. 2.1 The structure of LptE is homologous with proteins which bind negatively charged oligosaccharides, including LPS. (**A**) LptE exhibits a two-layer sandwich architecture composed of a four-stranded b-sheet (labeled as b1-b4) and two a-helices (labeled as a1 and a2) packed against one surface of the sheet. (**B**) Overlay of LptE (green) with HpaA (yellow), a protein from *H. pylori* that binds neuraminyllactose (PDB ID 3BHG; RMSD of C_a atoms 3.16 Å). (**C**) LptE (green) exhibits structural similarity to the horshoe crab anti-LPS factor, LALF (cyan), an LPS binding protein from the hemocytes of *Limulus* (RMSD of C_a atoms 2.74 Å). The amphipathic loop (AL) in LALF, connecting its strands b2-b3 is highlighted in red and labeled, as is the structurally analogous loop connecting b2-b3 in LptE (purple). The positions of basic residues R91 (in the loop connecting b2 and b3, highlighted in purple) and K136 (in the loop connecting strands b4 and a2) is indicated by asterisks.

The solution of the crystal structure of LptE provided strong evidence that LptE binds LPS and allowed for the development of a hypothesis of how it would do so. LptE has an elongated structure, consisting of two □-helices (□1 and □2) and four □-strands, with the first (□1) being significantly shorter than □2-□4. The helices are packed against each other and against one face of the four-stranded □-sheet, as in LptE homologs from other organisms (fig. 2.1A).

A search for structural homologs revealed the closest matches to be proteins that bind negatively charged sugars. One was a putative neuraminyllactose-binding hemagglutinin homolog, the *Helicobacter pylori* adhesion A (HpaA), whose ligand is a negatively charged

trisaccharide 3-siallyllactose (Figure 2.1B) [100,101]. Another was the black tiger shrimp (*Penaeus monodon*) and Atlantic horseshoe crab (*Limulus polyphemus*) anti-LPS factor (LALF) (fig. 2.1C)[102]. This protein, found in the hemolymph of arthropods, is part of a primitive host defense system against microbial invasion[103,104]. It has been proposed that these anti-LPS factors bind LPS through interactions between negatively charged phosphates attached to the di-glucosamine-di-phosphate headgroup of the lipid A of individual LPS molecules and a region corresponding to the exposed loop connecting β strands 2 and 3 (highlighted in red in the structure of LALF and in violet in the corresponding location in LptE in fig. 2.1C)[105]. Synthetic peptides derived from the corresponding loop in LALF also demonstrate LPS binding[106] . These similarities suggest that LptE binds the sugars of LPS, and implicate the β2-β3 loop of LptE as a putative LPS binding site. Bioinformatics highlights the importance to LPS binding of the loop connecting the β4 strand with the α2 helix, proximal to the other putative binding site, as it is among the most highly conserved segments for LptE homologs in Proteobacteria (Figure 2.2).

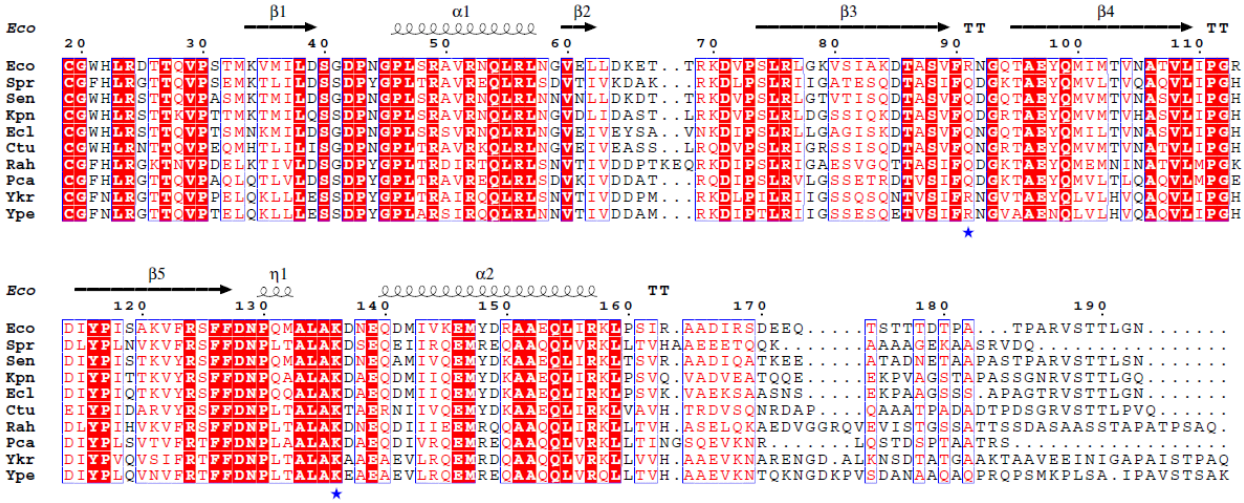

Figure 2.2: Structure-based sequence alignment of LptE homologs constructed by selecting representative homologs in descending sequence identity. Escherichia coli (Eco), Serratia proteamaculans (Spr) (84%), Salmonella enterica (Sen) (78%), Klebsiella pneumoniae (Kpn) (70%), Enterobacter cloacae (Ecl) (69%), Cronobacter turicensis (Ctu) (62%), Rahnella (Rah) (58%), Pectobacterium carotovorum (Pca) (54%), Yersinia kristensenii (Ykr) (51%),

and Yersinia pestis (Ype) (47%). Percent identity with E. coli protein is indicated in parentheses. Blue stars indicate the position of conserved basic residues whose mutation causes a phenotype.

2.1.3: Charge-swapping mutations to the putative binding sites compromise OM integrity

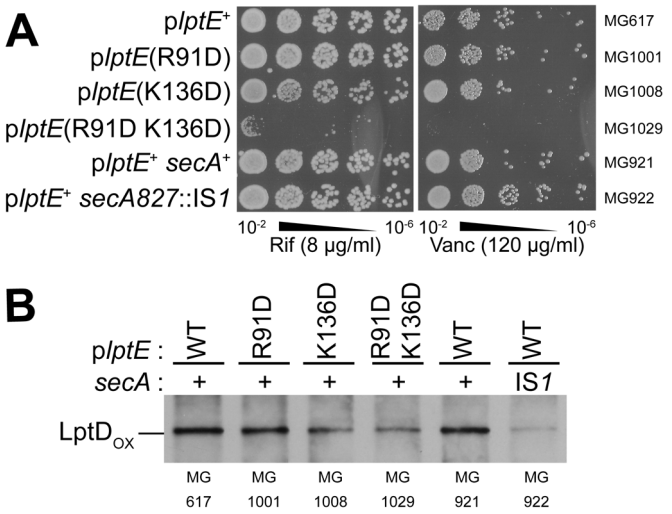

Figure 2.3: Changing both R91 and K136 in LptE perturbs the OM barrier. Sensitivity to rifampin and vancomycin was determined for each strain by plating serial dilutions of cultures (**A**). Level of OM-assembled $LptD_{OX}$ were determined in *lptE* haploid strains expressing the denoted plasmid-borne *lptE* alleles (**B**). *secA* alleles linked to *leuA*::Tn*10* were introduced in the p*lptE*$^{+}$ expressing strain.

This leads to the attractive hypothesis that residues in these two loops are involved in LPS binding. Basic residues are crucial to LALF's binding of LPS, and both LALF and HpaA bind negatively charged saccharides, suggesting that basic residues on the putative binding loops of LptE bind LPS by the negatively charged phosphates attached to the di-glucosamine headgroup of lipid A. Mutants replacing a basic residue in each of the putative binding sites (marked with asterisks in figure 2.1C) with acidic residues (R91D and K136D) do not individually show significant OM permeability defects against several antibiotics, but cells expressing only the dual mutant LptE(R91D,K136D) became sensitive to rifampin and vancomycin (Figure 2.3A). As the OM is usually impermeable to vancomycin and rifampin, this phenotype is characteristic of defective OM biogenesis[77,78,107]. In theory this could be because LptE(R91D,K136D) is deficient as a chaperone of LptD, but this is disproven by the mutant

secA827::IS*1*, which causes a greater defect in LptD assembly than LptE(R91D,K136D) (Figure 2.3B) without inducing sensitivity to rifampin or vancomycin (fig. 2.1.3.3A). LptE(R91D,K136D) is thus deficient in LptD/E translocon function.

2.1.4: Biophysical tools can confirm and characterize the LptE-LPS interaction

The combination of structural and genetic evidence led us to hypothesize that LptE interacts with LPS at the R91 and K136 residues, likely with the negatively charged phosphates of LPS, as a requirement for translocation to the cell surface. Toward this end, we sought a method by which we could characterize LptE's binding of LPS, and determine the R91D and K136D mutants were deficient in LPS binding as hypothesized. Solubilized LPS has the propensity to form aggregates, making biochemical characterization challenging[108]. Surface plasmon resonance (SPR) techniques offer a way around this. By immobilizing LPS aggregates on the surface of an SPR biosensor chip, binding of different proteins or peptides can be measured, without the need to keep LPS in solution. This has been used to study binding of LPS by antimicrobial peptides[109] and the tailspike proteins of the 9NA and P22 bacteriophages[110]. I worked with Dorothee Andres to use technique to measure the binding of different LptE variants to LPS, to allow for confirmation or modification of our hypothesis.

2.2: Results & Discussion

2.2.1: LptE strips LPS aggregates from a surface

To measure LPS binding by LptE, LPS first had to be immobilized onto an SPR chip. We injected poly-L-lysine over a gold SPR chip with a carboxymethylated dextran layer to create a

positively charged surface that the negatively charged LPS could lay down on. A chip (CM3) with a short carboxymethylated dextran layer over the gold surface was used to minimize the distance between the LPS and the gold base of the surface and maximize sensitivity, as signal strength falls off with distance from the surface. LPS was extruded to create uniform, smaller, temporarily soluble aggregates, and passed over the chip, leading to stable deposition of LPS that does not wash off under normal buffer flow (figure 2.4). The surface was stripped clean with detergent following testing of each potential LPS binder, and regenerated with PLL and LPS for the next. LptE and other potential LPS binders can thus be passed over to measure their affinity for LPS.

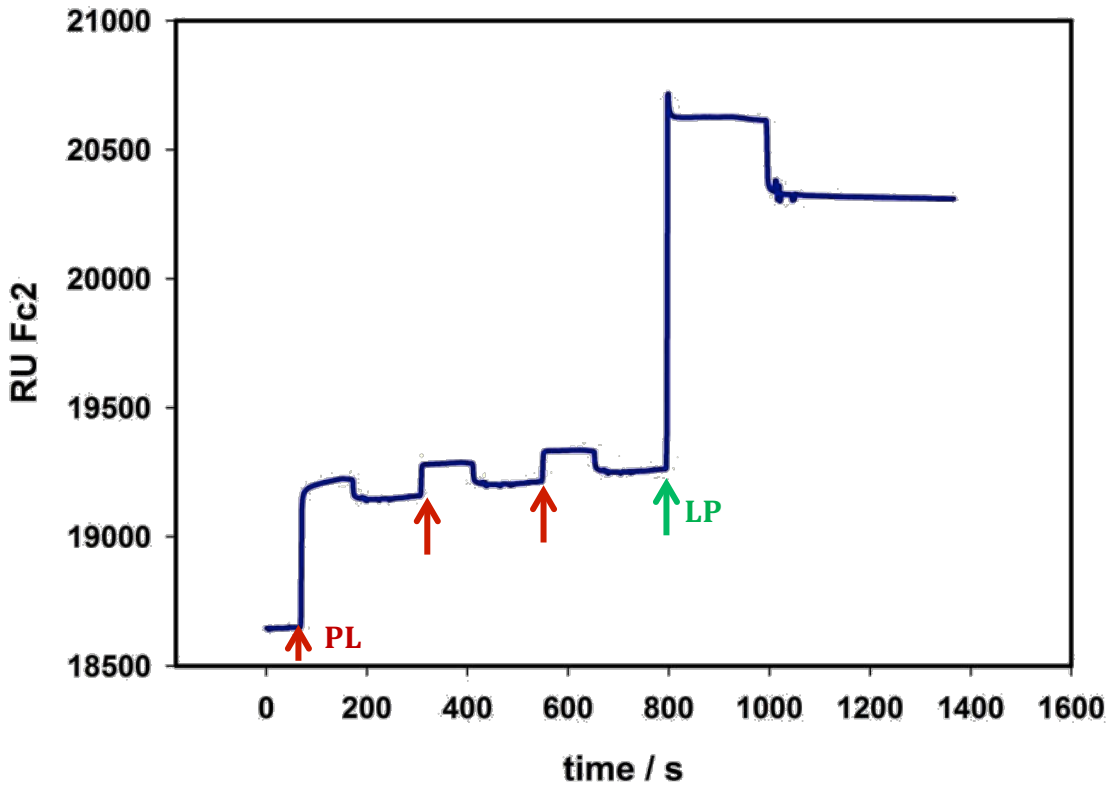

Figure 2.4: Preparation of a stable LPS surface for SPR binding studies. A gold chip with a shallow layer of carboxymethylated dextran (CM3) is first saturated with PLL (injections marked with red arrows) to create a positively charged surface. Freshly extruded LPS is then deposited on the surface (green arrow). LPS remains stably bound to the surface after injection of addition LPS has stopped (blue star).

Polymyxin B and RNase A were used as positive and negative controls for measurement of LPS binding. When chips derivatized with LPS are subjected to injections of polymyxin B, a cyclic cationic antimicrobial polypeptide that binds LPS[111], it remains on the surface after the injection has ceased, as indicated by the change in mass adhered to the chip (measured in resonance units) (Figure 2.5, orange), whereas RNase A, a protein known to recognize other negatively charged sugars, is not retained by LPS (Figure 2.5, cyan). The square-shaped signal observed for RNase A arises from mass entering and leaving the flow cell without interacting with the surface. Both positive (polymyxin B) and negative (RNase A) controls thus behave as expected, confirming the validity of the system for measuring LPS binding behavior.

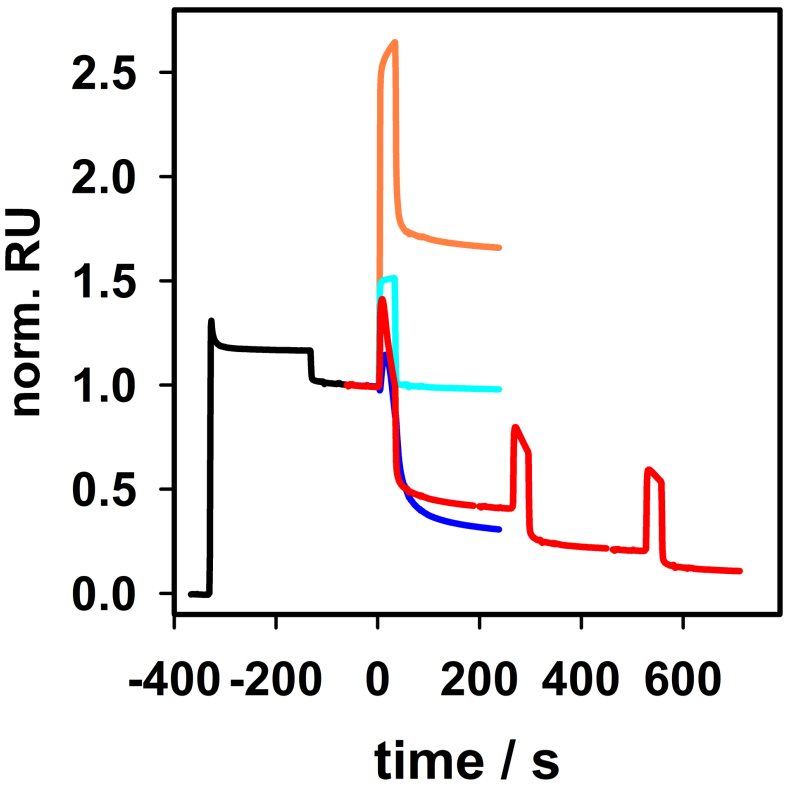

Figure 2.5: LptE binds and solubilizes surface bound LPS. 0.1 mM LPS was loaded onto CM3 SPR chips saturated with polylysine for 200 s (black). Multiple, consecutive injections of 60 µM LptE remove LPS from the surface (red). 40 µM polymyxin B (orange) binds to LPS, whereas the same concentration of RNase A (cyan) is not retained. The LptE structural homolog LALF extracts LPS (4 µM, blue).

LptE, in contradiction to our initial hypothesis, does not mimic polymyxin B's binding behavior. Upon injection of LptE, the sensorgram shows an initial increase followed by rapid decrease of signal below the level achieved by LPS deposition prior to injection of LptE, rather than the enduring increase in signal seen with polymyxin B. Multiple injections of the same concentration of LptE converge on a signal intensity corresponding to the level before the application of LPS, indicating that LptE removes LPS from the chip surface (Figure 2.5, red). Therefor, LptE solubilizes LPS adhered to the PLL on a CM3 chip. Because the structure of LptE shows homology to the eukaryotic protein LALF, which binds and transports LPS[102,112], we wondered whether LALF would show similar aggregate-removing properties with LPS in our SPR assay. In fact, LALF was able to extract LPS from the chip surface in the same fashion as LptE (Figure 2.5, blue). Thus, while LptE is not simply an LPS binding protein, it clearly interacts with LPS in a more interesting fashion, similar to that of its homolog LALF.

2.2.2: LptE must bind LPS first in order to solubilize LPS aggregates

We analyzed the concentration dependence of LptE's interaction with LPS-coated surfaces. Both the degree and rate of LPS removal are dose dependent. Two discrete interaction steps that are responsible for the removal of LPS become visible (Figure 2.6). At lower concentrations, LptE is first retained on the surface before extraction of LPS commences, whereas at higher concentrations the binding and extraction steps are of comparable kinetics and are thus indistinguishable. Hence, LPS solubilization is a two-step process, where LptE molecules bind to the LPS aggregate until a critical concentration of LptE is achieved, at which point the second step of LPS extraction begins.

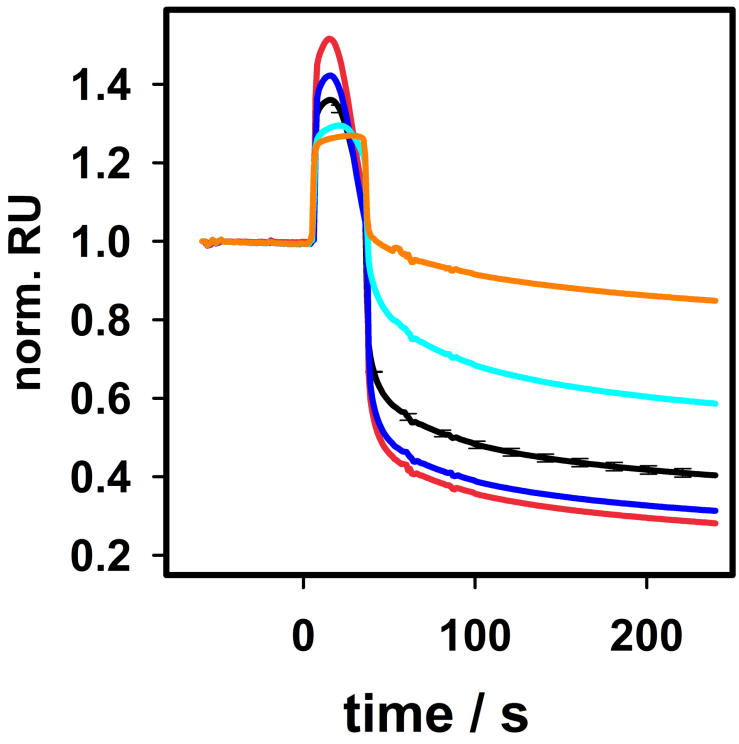

Figure 2.6: Concentration dependence of LptE binding and extraction activity. 20µM LptE (orange), 40µM LptE (cyan), 60 µM LptE (black) with standard deviation for every 20 measurement points, 80 µM LptE (blue), 100 µM LptE (red).

2.2.3: LptE's LPS disaggregation capability is dependent on basic residues in the putative binding sites and essential for proper OM biogenesis

Our next question was if LptE's binding and disaggregation of LPS is mediated by the predicted R91 and K136 residues of the putative binding sites. We repeated our assay with both single mutants (R91D and K136D) and the double mutant LptE, and found that the single and double mutant LptE proteins exhibit defects in their ability to solubilize LPS. LptE(K136D) extracts LPS from the surface less efficiently that wild-type LptE (wtLptE), whereas LptE(R91D) is even less efficient and the double mutant LptE(R91D,K136D) extracts no LPS from the surface (Figure 2.7). Increasing the concentration of either LptE(R91D) or LptE(K136D) does allow some extraction, whereas the double mutant is still incapable of

extracting LPS (Figure 2.8). These observations are consistent with the fact that only the double mutant shows a phenotype *in vivo*. That LptE(R91D,K136D) is deficient in LPS disaggregation capability *in vitro* and leads to a compromised OM *in vivo* strongly suggests that LptE's ability to interact with LPS is not just a quirk of our *in vitro* system, but is key to its function in LPS biogenesis in the cell.

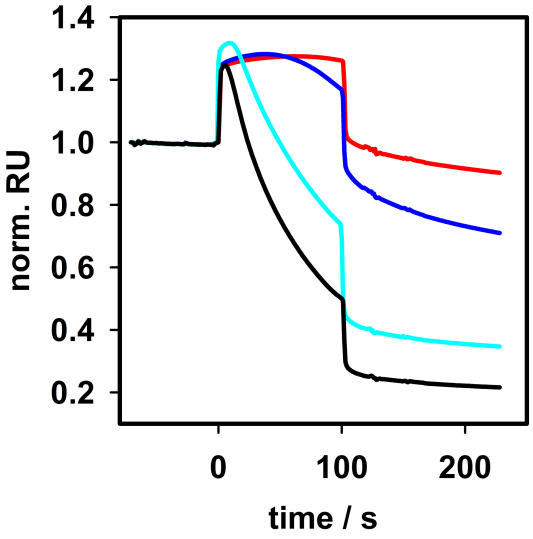

Figure 2.7: 100 s injections of 60 µM wt LptE (black) rapidly removes LPS from the chip, while 60 µM LptE (R91D, K136D) (red) does not. Single amino-acid substitutions show their contribution to the effect, with 60 µM LptE (R91D) in blue and 60 µM LptE (K136D) in cyan.

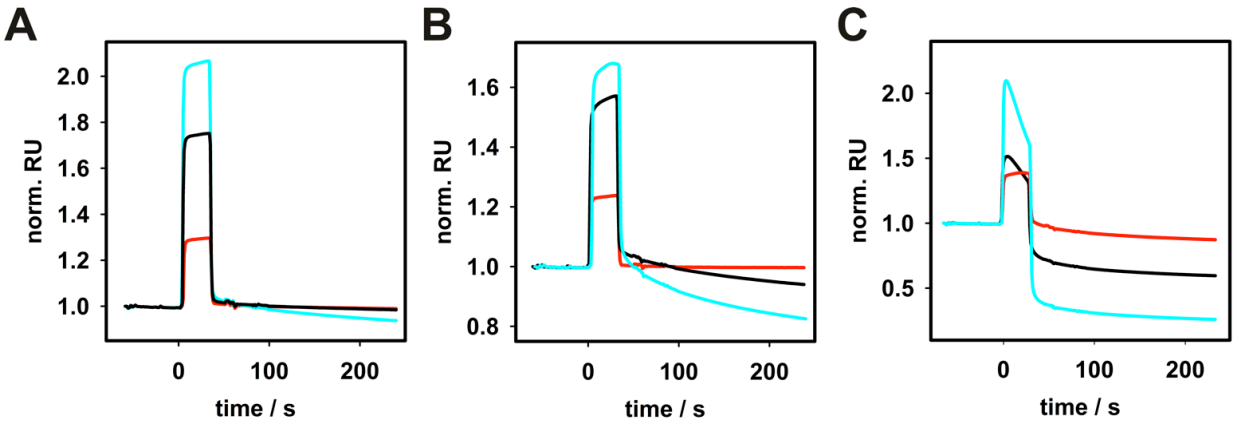

Figure 2.8: Concentration dependence of LPS disaggregation activity for different LptE mutants. (**A**) LptE (R91D/K136D) at 20 µM (red), 80 µM (black) and 150 µM (cyan) (**B**) LptE R91D at 10µM (red), 80 µM (black) and 100 µM (cyan) (**C**) LptE K136D at 10 µM (red), 60 µM (black) and 150 µM (cyan). All LptE variants were injected for 30 s over Ra-LPS covered chip at 25°C.

To determine whether LptE(R91D,K136D) is deficient in binding, or only in its ability to extract LPS, we immobilized LptE, both wild type and the double mutant, on an SPR chip and passed the same concentration of freshly extruded LPS over the surface. Ra-LPS binds both irreversibly, but saturates in neither case, and binds the double mutant less well than it binds wtLptE (Figure 2.9). This suggests that LptE(R91D,K136D) has diminished LPS binding capability, but that it can still bind LPS at all while it is incapable of stripping LPS aggregates supports our interpretation that binding and aggregation are separate processes and that the *lptE(R91D,K136D)* mutations primarily effects the latter. Taken together, these data suggest that amino acids R91 and K136D are part of an LPS-interaction site on LptE that acts to solubilize LPS by altering LPS-LPS interactions.

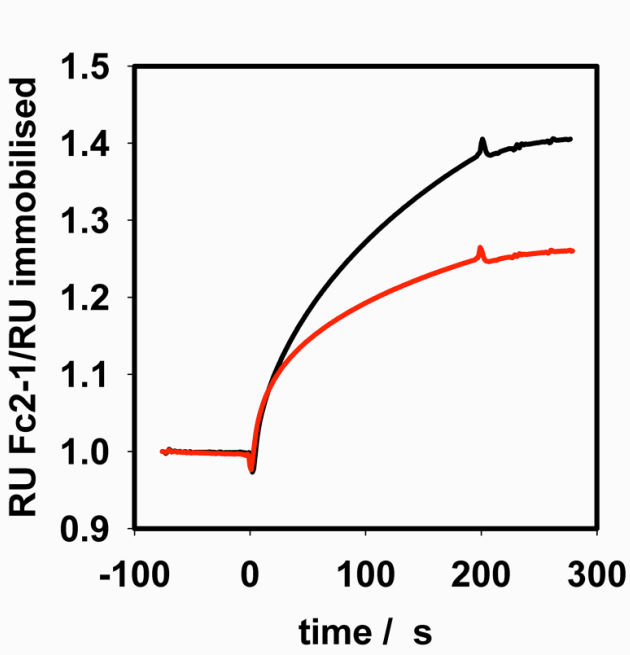

Figure 2.9: SPR measurements with LptE immobilised with LPS analyte. LptE wt (black) and LptE (R91D/K136D) was immobilised at pH 5.5 and 100 µM RaLPS was passed over in TBS pH 8 at 25°C. RaLPS binds both irreversible, and RU is similar when compared to immobilisation level. For wt, the standard deviation does not exceed 1%.

2.2.4: LptE disrupts LPS aggregates at a sub-equimolar level

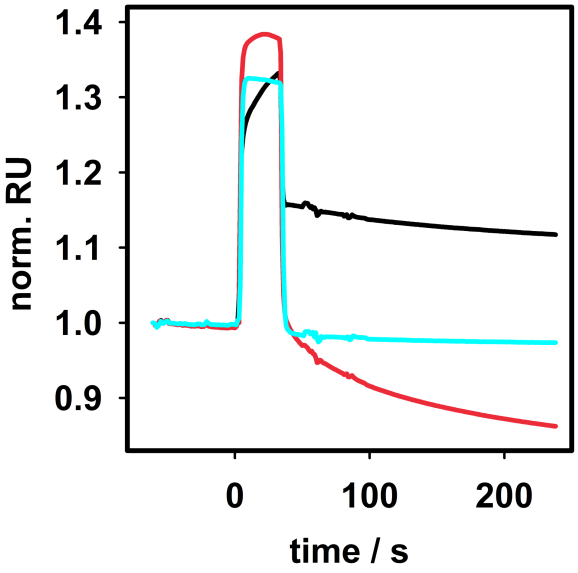

Figure 2.10: Pre-incubation of LptE with exces LPS. 10 μM LptE without (red) and with (cyan) incubation of 1 mM LPS prior to injection over LPS chip. Black line represents injected 1mM LPS over an existing LPS surface.

The fact that LptE can facilitate LPS extraction from the surface of the chip implies that interactions between LptE and LPS are more favorable than intermolecular interactions between LPS molecules, and LptE removes LPS from the surface by disrupting these LPS-LPS interactions. An alternate interpretation that must first be discounted is that LptE could simply be disrupting the interactions between LPS and the surface, not disrupting the aggregates themselves. It is not surprising that LPS-binding proteins would bind LPS so tightly given the extreme sensitivity of the limulus amebocyte lysate endotoxin detection assay[113]. Given that LptE can extract LPS from the chip surface, we wondered whether the reverse was also true (i.e., whether it can prevent LPS from sticking to the surface). Consistent with expectation, if a high concentration (1 mM) of LPS in solution is passed over an LPS-coated chip, an increase in signal is seen, suggesting that additional LPS molecules can adhere to the LPS surface. If 10 μM LptE is preincubated with 1 mM LPS before injection, no solubilization of LPS from the surface by

LptE happens. Remarkably, we also see no increase in LPS binding to the surface, even though it is present in a 100-fold excess relative to LptE (Figure 2.10). Sub-stoichiometric amounts of LptE are capable of preventing the interaction of LPS with LPS. One interpretation of these results is that LptE's disruption of LPS-LPS interactions alters the structure of the LPS aggregates, even at low concentration.

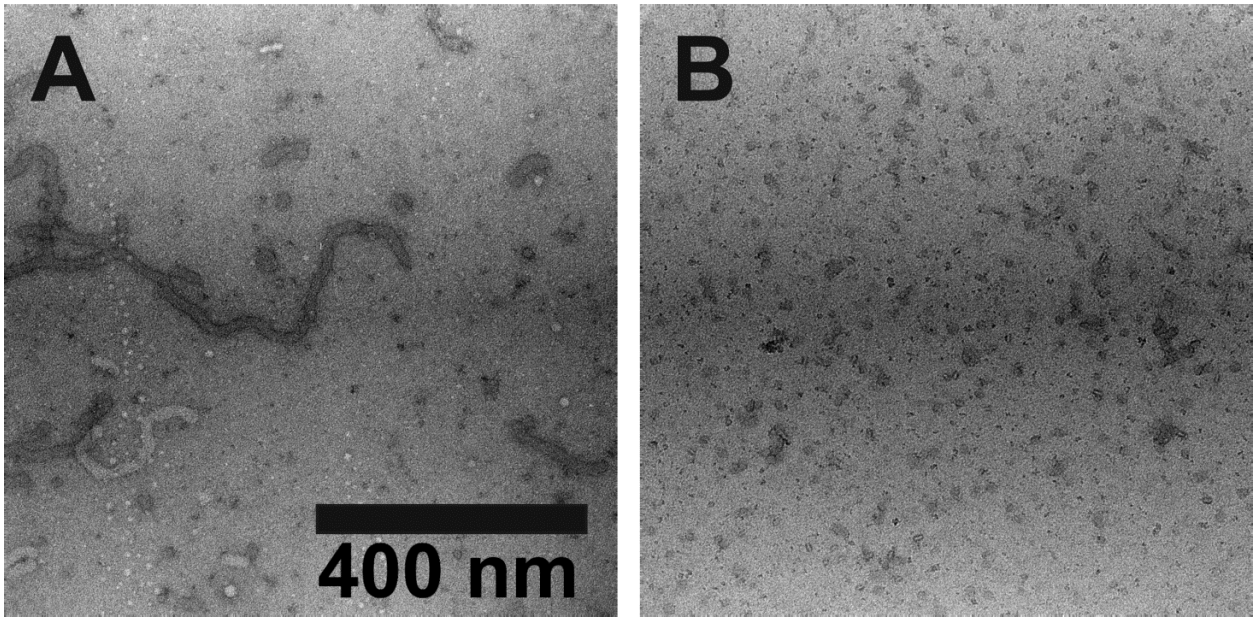

Figure 2.11: TEM images of LPS aggregates before and after LptE incubation. (**A**): 100μM LPS or (**B**): 100μM LPS with 10μM LptE were stained with 2% uranyl acetate and imaged on carbon covered grids at 49 000 fold magnification.

We used transmission electron microscopy (TEM), with the help of Vu Nguyen of the Leschziner lab, to test this hypothesis. While TEM provides only a static snapshot of the LptE-LPS interaction, it can elaborate the structure of the LPS aggregates used as a way of complementing our SPR data. On a carbon-covered grid, pure LPS forms extended tubular filaments that are about 17 nm wide. Compared with E. coli OM that have a diameter of 13 nm, these filaments could represent a bilayer structure[114]. LPS has a distinctly low critical micelle

concentration (CMC) (sub-picomolar) compared with other glycolipids, which are often in the millimolar range, and therefore aggregates readily (Figure 2.11A). Imaging the solutions of LPS:LptE (at a 10:1 ratio) reveals that the filaments disappear for wild-type LptE (Figure 2.11B), confirming that LptE disassembles LPS aggregates rather than just separating them from the PLL surface.

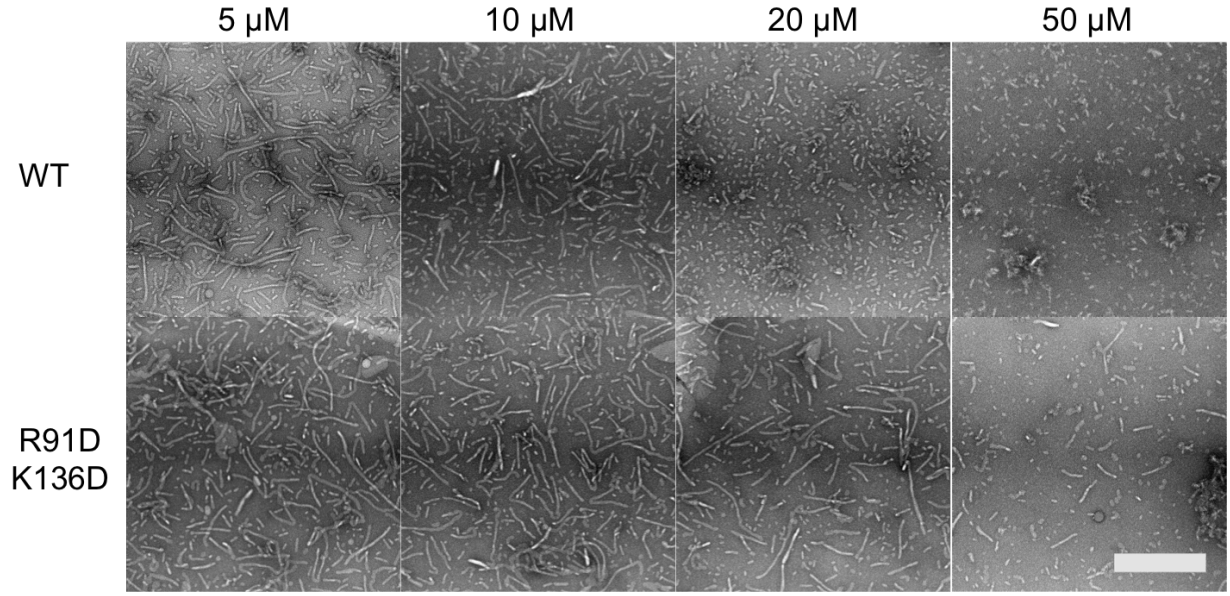

Figure 2.12: The R91D-K136D mutant of LptE is less effective as disrupting LPS aggregates. Varied concentrations of WT-LptE were incubated with 200 μM of LPS prior to TEM imaging (top). LPS aggregates get increasingly smaller as the concentration of LptE increases. The same effect is seen with LptE-R91D-K136D, LPS aggregates maintain their size until a higher concentration of the mutant. Scale bar represents 300 nm.

We wanted to see if this disaggregation activity was concentration dependent, and if it relied on the R91 and K136 residues, so we pre-incubated a fixed concentration of LPS with increasing concentrations of both wtLptE and LptE(R91D,K136D) (Figure 2.12). Both wtLptE and LptE(R91D,K136D) disaggregate LPS at high concentrations, but it is much more pronounced and is visible at lower concentrations for wtLptE. LptE therefore disrupts strong LPS–LPS interactions and affects its aggregation propensity. Free LPS is not able to spontaneously insert into phospholipid vesicles[115,116]. Because of its low CMC, there is a barrier

to insertion into phospholipids that presumably involves monomerization. The disaggregation of LPS by LptE observed in TEM and surface plasmon resonance could help to insert LPS into the OM.

2.2.5: LptE's disaggregation allows for a model of LptE function

Our results establish that LptE binds LPS specifically and that this is crucial to LptE's function *in vivo*. Despite the relatively low conservation of its amino acid sequence, LptE homologs are widespread among Gram-negative organisms and are predicted to fold into the same 3D structure. The striking resemblance of the structures of LptE and the anti-LPS factors from arthropods, known to bind LPS through the loop connecting β strands 2 and 3, enabled us to probe LPS binding in that region. *In vitro* binding experiments established that LptE binds LPS, is able to interfere with LPS–LPS interactions, and affects LPS's aggregation state. Rationally designed mutant LptE proteins that lack exposed positive charges of the R91 and K136 residues in the putative binding site, previously shown *in vivo* to have a compromised OM indicative of a compromised LPS assembly pathway, mirror this effect in SPR and TEM experiments, where they exhibited significantly diminished ability to extract and disaggregate LPS. As such, LptE's ability to alter the aggregation state of LPS is key to proper OM biogenesis. The architecture and substrate-binding sites of LptE and LPS-binding proteins from the hemolymph of arthropods point to a convergent evolution of this fold for LPS binding.

The crystal structure of E. coli LptE, combined with homology structural models and synteny analyses, had revealed that the loops containing basic residues, are conserved across LptE homologs. These conserved loops resemble a region of the OM β-barrel protein FhuA; its crystal structure of FhuA bound to LPS reveals that binding is mediated by a loop bearing

positive charges[105,117]. These authors point to the fact that the FhuA LPS-binding motif bears significant resemblance to eukaryotic LPS-binding proteins. We think it is noteworthy that many of these proteins, in particular LALF, bactericidal permeability increasing protein (BPI) [118], and LPS-binding protein (LBP) [119], possess functions that extend beyond the mere binding of LPS. It has been hypothesized that the eukaryotic structural homolog LALF participates in not only the binding of LPS but also in its transport to and insertion into phospholipids membranes as part of the Limulus host immune response[102,112]. LBP and BPI are elongated in shape and contain a duplicated fold similar to that of LptE. They bind LPS through an analogous exposed loop at a tip that connects β-strands and exhibits conserved stretches of alternating cationic and hydrophobic residues[105]. LBP monomerizes LPS aggregates either to present it to CD14 or, at high LPS concentrations, to insert it into membranes to activate cells independent of CD14[120,121]. Our SPR data reveal that LptE not only binds LPS but also is capable of disrupting the interactions between LPS molecules. The ability to remove immobilized LPS off the surface of the SPR chip has been observed before in SPR experiments involving lipid transfer proteins in an analogous experimental setup[122,123]. These proteins transfer glycolipids between lipid membranes. Accordingly, LptE might be able to disaggregate and transfer LPS into the OM in vivo.

Our observations of the unusual LPS-disaggregation behavior of LptE in vitro may help explain many of the phenomena that the OM translocon facilitates. We have previously proposed that LPS is transported in a continuous stream from the outer leaflet of the IM to the cell surface along the periplasmic bridge formed by LptC, LptA, and LptD and that ATP hydrolysis in the cytoplasm provides energy to drive this string of LPS molecules in a unidirectional fashion against a concentration gradient[94]. The OM translocon must take individual LPS molecules from

this 1D stream and facilitate their passage into the 2D LPS assembly in the outer leaflet. The major barrier (bottleneck) in this process is clearly the transport of the amphipathic LPS molecule through the hydrophobic interior of the OM. We have shown that LptE's interactions with LPS are sufficient to facilitate removal of LPS from an LPS aggregate on an SPR chip. We have also shown the converse; in the absence of LptE, added LPS will insert into LPS aggregates on an SPR chip (Figure 2.10). Taken together, these experiments imply that LptE–LPS interactions are more stable than LPS–LPS interactions on the surface of an SPR chip. We have also shown that LptE can alter the aggregate state of LPS in solution (Figures 2.11-12), apparently disrupting LPS–LPS interactions. In the OM translocon, a substoichiometric amount of LptE must facilitate LPS transfer through a narrow pore into the outer leaflet while preventing its insertion into the inner leaflet of the OM. We propose a model wherein LptE acts as a transfer protein to facilitate LPS movement into the OM by providing more favorable interactions between itself and LPS than between aggregated LPS molecules in the periplasm. Eventually, LptE must release LPS into the outer leaflet. LptE's strong interactions with LptD could be responsible for this final step of LPS transport; by engulfing LptE, LptD facilitates the release of LPS from LptE. If this is so, then LptE is a catalyst for LPS assembly into an asymmetric LPS membrane. Localizing LptE to the inner leaflet away from the cell surface prevents this catalyst in prokaryotic systems from degrading the outer leaflet as similar proteins, such as LALF, are presumed to do in eukaryotic immune systems.

2.3: Materials and Methods

Protein expression and purification for biophysical experiments and TEM

C-terminally deca-histidine tagged LptE(C19M) and the corresponding (R91D, K136D)

double mutant was overexpressed and purified according to previously established protocol[69]. LptE was overexpressed using BL21(λDE3) cells containing the plasmid pCDF-*lptE-his*. All cells were grown in LB with 50 mg/ml streptomycin and 0.2% glucose. A starter culture was grown to mid-log at 37° C, diluted 1:150 into 1.5L of fresh culture, and grown at 26° C until OD600 ≈ 0.6, at which point overexpression was induced via addition of 0.1 mM IPTG and cells were grown for an additional 20 hours. Following pelleting by centrifugation, cells were resuspended in 30 ml TBS (20mM Tris-HCl, 150 mM NaCl, pH 8.0) containing 1mM PMSF (Sigma) and 50 μg/ml DNase I (Sigma), before lysis via three passes through a cell disruptor (Avestin) between 15-20,000 psi. Ten minutes of centrifugation at 5,000 *g* removed unlysed cells, and ultracentrifugation (Model XL-90, Beckman) at 100,000 g for 30 minutes led to a membrane pellet. 18 ml of TBS-B (20 mM tris-HCl, 300 mM NaCl, 20 mM imidazole, pH 8.0) supplemented with 1% Anzergent 3-14 (Anatrace) and 0.1 mg/ml lysozyme from chicken egg white (Sigma), and left to rock at 4° C for two to three hours to extract and solubilize the membrane proteins. The solution was ultracentrifuged as above, and the supernatant was mixed with 3 ml of Ni-NTA resin (Qiagen) that had been pre-equilibrated in TBS-B, before rocking at 4° C for another 30 minutes. The solution was applied to a column and drained by gravity, and the filtrate was passed over the resin again before washing the resin with four washes of 15 ml of TBS-B supplemented with 0.02% Anzergent 3-14, and finally being eluted with 12 mL of TBS supplemented with 1% octyl-glucoside (Anatrace) and 200 mM imidazole. The eluate was concentrated to a final volume of 500 μl with a 10 kDa cutoff spin concentrator (Millipore). Final purification occurred via size exclusion chromatography on a Superdex 200 column (GE healthcare) in TBS with 1% octyl-glucoside. For TEM experiments, in order to remove any LPS that may have co-purified with LptE during this procedure, LptE solution in TBS was

additionally passed over the polymyxin containing Detoxi-Gel Endotoxin Removal Column (1 mL resin, Pierce, USA).

Surface plasmon resonance

E. coli EH100 Ra-LPS (LPS) was obtained from Sigma Aldrich and contained less that 3% of protein contamination. It was dissolved to 5 mg/ml in water and solubilized with repeated freeze thawing cycles. After adjusting the buffer to 20 mM Tris-HCl pH 8.0, 150 mM NaCl and diluting Ra-LPS to 0.5 mg/ml, it was extruded 21 times at 70 °C through a 100 nm pore size filter.

All experiments were performed using a Biacore X100 at 25 °C in the same buffer at a flow rate of 10 µl/min. LPS was immobilized according to[109]. Briefly, 60 µg/ml poly-L-lysine was injected 3 times for 100 s over a clean CM3 chip surface to generate a positively charged surface. A 200 s injection of negatively charged LPS saturated the surface. LptE wt, LptE(R91D/K136D), LptE(R91D), LptE(K136D), RNase A or polymyxin B were injected for 30 s and response was followed for 1000 s after injection. After each protein injection, the CM3 chip was stripped clean with detergent and loaded from the beginning. Response units were normalized to loaded LPS for each individual run. Standard deviation in response units for LptE wt was not more than 3.5%. A CM5 chip with immobilized LptE in the active channel was established by injecting 400 µg/ml LptE (R91D/K136D) or LptE wt for 300 and 1000 s respectively on an EDC/NHS activated Biacore CM5 chip in 20 mM Na-Acetate pH 5.5. After ethanolamine deactivation of excess reactive groups, about 5000 RU were immobilized. The reference channel was blank immobilized with ethanolamine. For interaction measurements, 100

μM extruded LPS was passed for 200 s in TBS pH 8, 25 °C. LPS was removed with 0.03% DDM in TBS pH 8 in between runs.

Electron microscopy

In identical TBS pH 8 buffer, 200 μM LPS with varying concentrations of wild type LptE or LptE (R91D/K136D), were incubated for 3 hours at 25°C . 50 μM LptE without LPS or 200 μM LPS without LptE underwent the same incubation as controls. Samples were then applied to carbon films on 400 square-mesh copper grids (Electron Microscopy Sciences, CF-400-Cu) and allowed to absorb for 5 minutes at room temperature. The samples were stained with 2% uranyl formate solution and dried under a stream of nitrogen. Images were collected under low-dose conditions (~20 electrons/Å2) on a Tecnai G2 Spirit microscope (FEI, Hillsboro, OR) operating at 120 keV and equipped with a US4000 4K x 4K CCD camera (Gatan, Inc., Pleasanton, CA). The samples were imaged at a nominal magnification of 49,000. The pixel size at the sample level was 2.3 Å.

Chapter 3: LptE and LptC bind LPS by the di-glucosamine-di-phosphate headgroup of lipid A

Collaborators: Dorothee Andres, Carolin Doering, Daniel Kahne

Explanation of Contributions: With Dorothee Andres, I planned, executed, and analyzed all of the LptE fragment binding experiments, as well as the LptC binding experiments with lipidated LPS fragments. I planned and executed the LptE-LPS crosslinking experiment independently.

3.1: Introduction

As we have shown, LptE binds and disaggregates LPS *in vitro*. However, the nature of the binding remains an open question. We hypothesize ionic bonds between two positively charged loops of LptE and the negatively charged di-glucosamine-di-phosphate headgroup of lipid A; this is well-supported by comparison to other LPS-binding proteins, but we lack direct evidence. The hydrophobic portions of lipid A must presumably remain isolated from aqueous solution for disaggregation to be favorable; this suggests that LptE could interact with other portions of the LPS molecule, especially the acyl chains of lipid A.

Similarly, the mechanism by which proteins of the Lpt bridge bind LPS is also unknown. LptC and the other proteins of the Lpt bridge share a β-jellyroll structure with a hydrophobic groove[86-88]; we believe that commonality indicates an important role of LPS acyl chains for binding. The β-jellyroll proteins, unlike LptE, have been confirmed to bind LPS *in vivo*[94,95,124]; the work outlined in this chapter confirms that LptE binds LPS *in vivo* as well as *in vitro* and maps the binding of LPS by LptE and LptC.

A comparison of LptE to proteins known to bind LPS suggests two possible mechanisms by which LptE could bind LPS, singly or in combination: via the di-glucosamine-di-phosphate headgroup of lipid A—as indicated by the mutations described in the last chapter—or via the hydrophobic acyl chains. Other prokaryotic and eukaryotic LPS-binding proteins frequently bind LPS by similar mechanisms[105,125]: the crystal structure of FhuA reveals a cluster of 4 positively charged amino acids that form ionic bonds with the phosphates of LPS[117]; the crystal structure of the TLR4-MD-2-LPS complex shows that both proteins form ionic bonds with the phosphates of LPS[126]; mutants of lipopolysaccharide-binding protein (LBP) lacking a group of cationic amino acids cannot bind LPS[127]; and mutations of CD14 lacking conserved cationic residues are likewise unable to bind LPS[125]. Our assumption that LptE binds LPS by a similar mechanism is supported by LptE's close structural homology to LALF; LALF binds LPS via a loop containing a tetrad of cationic residues, arranged much like those required for FhuA to bind LPS[105,106,128]. The R91D mutation—which hampers LptE's ability to disaggregate LPS, as discussed in chapter 2—is located at the equivalent β2- β3 loop on LptE; the R91D-K136 double mutant, which has additionally mutates a second cationic residue on a proximal loop into an acidic residue, shows no disaggregation activity. Despite this previous work on LptE and other LPS binding proteins, there are no data confirming that LptE specifically binds the phosphates of LPS.

It is certainly possible that LptE could interact with other components of the LPS molecule as well. Both LptE it and the bridge proteins of the Lpt pathway—LptC, LptA, and the N-terminus of Lpt—seem likely to bind LPS by its hydrophobic lipid chains. The previously noted structural research also shows an important role for the acyl chains of lipid A in several protein-LPS interactions. The FhuA crystal structure includes an LPS molecule associated with the side of the □-barrel, roughly parallel to the major axis of the barrel; the acyl chains form

extensive Van der Waals contacts with the β-barrel, holding the acyl chains in ordered conformations[105,117]. The TLR4-MD-2 complex buries the lipids of LPS in a hydrophobic pocket of MD-2[126,129], while CD-14 binds LPS both via a hydrophobic pocket for the lipids and ionic residues for the di-glucosamine-di-phosphates[125]. By extension, it would not be unusual for LptE to bind the lipids of LPS. If binding occurs between the putative binding site of LptE and the di-glucosamine-di-phosphate of LPS, this could easily align the lipids along the length of LptE.

There exist only limited experimental data analyzing LptE's binding of LPS, leaving the moieties of LPS bound by LptE a mystery. Resin-immobilized LptE can be used to capture LPS; this is true for Ra-LPS, Re-LPS, and lipid A[69], indicating that the core oligosaccharide is not essential and highlighting the potential importance of the lipids. As LPS interacts strongly with itself, LptE must disrupt the tight LPS-LPS interactions; TEM images confirm that LptE solubilizes LPS aggregates by breaking them apart. LPS-LPS interactions are mediated both by the polyelectrolyte network formed by its charged phosphates and divalent metal cations and by lipid-lipid interactions[3]; to replace these interactions with a more favorable LptE-LPS interaction, LptE would presumably need to bind the lipid chains in order to isolate them from the surrounding aqueous environment. An alternate, but not mutually exclusive, model for LptE's disruption of LPS aggregates posits that by binding the lipid A headgroup, LptE increases the functional headgroup size of LPS, increasing membrane curvature and resulting in smaller LPS aggregates.

Similarly, the nature of the interactions of LptC, LptA, and nLptD with LPS remain unclear. The Lpt pathway would also need to keep the acyl chains isolated while LPS is transported across the periplasm via the putative bridge; all of the bridge proteins share the same β-jellyroll conformation featuring a hydrophobic groove that is a probable home for the acyl

chains of LPS. This model is supported by the crystal structure of LptD, which shows the hydrophobic portion of a detergent molecule buried within the groove of LptD[88]; this evidence is suggestive of the interactions between other Lpt proteins and LPS, but it is indirect at best.

The SPR techniques describe in chapter 2 can be modified to give more insight into which components of LPS are essential for binding by LptE and LptC, as has already been demonstrated with LptC. By anchoring LptC to the surface of the SPR chip and exposing it to different fragments of delipidated LPS (Figure 3.1), previous researchers in the Kahne lab were able to measure the dissociation constants for each of the fragments tested[130]In addition, this technique can also be expanded: by using soluble, partially-lipidated LPS fragments, we can determine if the lipids contribute to LPS binding for either LptC or LptE.

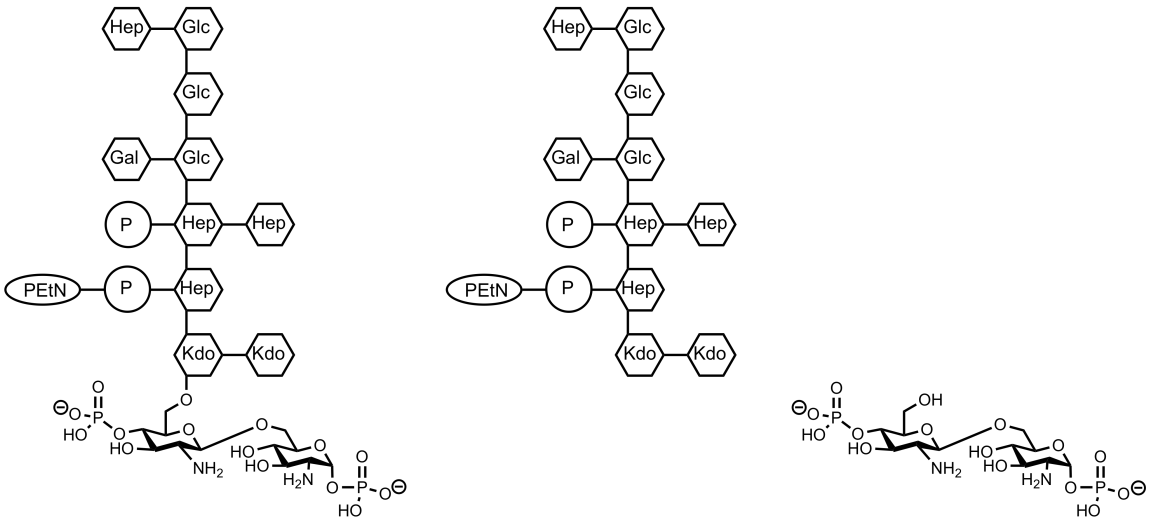

Figure 3.1: LPS saccharide fragments used for SPR studies. Left, the core oligosaccharide with the lipid A di-glucosamine-di-phosphate headgroup. Center, the core oligosaccharide without modification. Right, the di-glucosamine-di-phosphate alone.

Previous work has shown that LPS can be captured by LptE-affinity chromatography[69] and that LptE disaggregation of LPS shows two-step kinetics[97], which indicates that LptE binds LPS. However, this work was done with *in vitro* purified systems; *in vivo* interactions between

LptE and LPS are suggested but have yet to be confirmed. *E. coli* strains expressing only the R91D/K136D mutant of LptE have been shown to be deficient in *in vitro* LPS disaggregation activity and are sensitive to vancomycin, which demonstrates a compromised outer membrane and suggests that LptE's disaggregative function is needed for proper OM biogenesis. This is all consistent with a model in which LptE binds and disaggregates LPS in the last steps of its transport to the OM, but the model requires confirmation that LptE binds LPS in the cell.

Others in the Kahne lab have used site-specific photocrosslinking via amber codon suppression[72-74] to identify *in vivo* LPS binding sites along the inside of the hydrophobic grooves of LptA, LptC, and LptD[94,95], confirming the groove as a site of LPS binding during transport. The same *in vivo* photocrosslinking technique can be used to confirm that LptE binds LPS inside of the cell and, in combination with fragment binding studies, confirm our model for LptE's role in LPS transport and OM biogenesis.

3.2: Results & Discussion

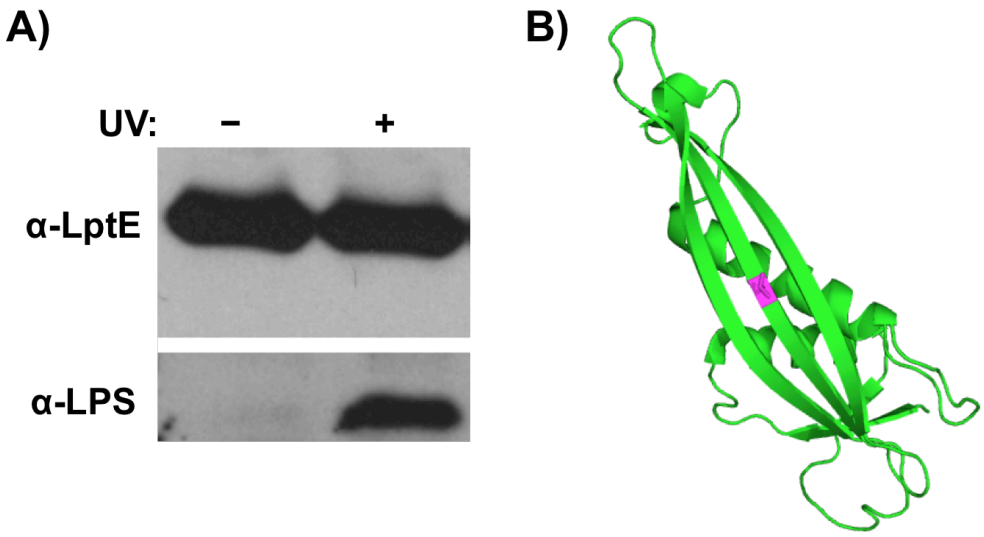

Fig. 3.2.1.1 LptE binds LPS *in vivo*. A) □-LptE and □-LPS western blots show that LptE(T103Am) crosslinks LPS in cells in a UV-dependent fashion. B) The T103 residue, highlighted in magenta on the LptE crystal structure.

3.2.1: LptE crosslinks LPS *in vivo*

Site specific *in vivo* photocrosslinking confirms that LptE binds LPS in the cell. Previous researchers have used site-specific *in vivo* photocrosslinking to identify LPS binding sites in the Lpt proteins LptC, LptA, and LptD. While the same technique had been used to show that LptE sits within the β-barrel of LptD, it had not been used to identify *in vivo* sites of interaction between LptE and LPS. We repeated the same crosslinking experiments used to study the structure of LptE and LptD, growing the same 12 amber-codon suppression mutant LptE strains to midlog phase, exposing them to UV to induce crosslinking, and purifying the LptE via nickel-affinity chromatography and TCA precipitation. Crosslinks were identified via □-LptE and □-LPS western blot. LptE was found to crosslink LPS at the T103Am position (Figure 3.2). This crosslink was repeatable, though it required a larger culture and crosslinking time than *in vivo* crosslinks between LptC, LptA, or LptD and LPS. That LptE repeatably crosslinks LPS *in vivo* indicates that LptE interacts with LPS in cells, and not just in the reductionist *in vitro* conditions used to study LptE-LPS interactions. The interaction between LptE and LPS at the T103 position appears to be fleeting when compared to the interactions seen between the Lpt bridge proteins and LPS along the bridge's hydrophobic groove, as judged by the need for longer crosslinking time with more cells to reliably capture it. The T103 residue is not in either of the loops of LptE predicted to be LPS binding sites, indicating that while those loops may be responsible for the specific interaction with the phosphates attached to the di-glucosamine headgroup of Lipid A, other parts of LptE also interact with LPS. Two models for this readily present themselves. In one, LptE binds the headgroup as predicted, and this aligns LPS with LPS such that the lipids are pressed against the □-sheet of LptE. Alternately, LPS could transition swiftly from being bound by the hydrophobic groove of the periplasmic domain of LptD to being bound by LptE, and the

benzophenone at T103 could crosslink the sugars as they pass by the β-sheet while the LPS transitions between two bound states. While this crosslinking data help to confirm the validity of our *in vitro* methods, it does not resolve the question of how LptE binds LPS. A more detailed understanding of which components of LPS bind LptE will help distinguish between and refine these models.

3.2.2: LptE specifically binds the charged lipid A headgroup, and not the core oligosaccharide, of LPS

LptE has an entirely different structure from LptC, and so its binding behavior cannot be assumed from direct comparison to LptC. The data obtained for LptC can only be used to make inferences about LPS binding in its homologs LptA and nLptD. In order to better characterize LptE's interactions with the sugars of LPS, and to understand how it might compare and contrast to binding of LPS by the proteins of the Lpt bridge, I continued to work with Dorothee Andres to adapt a method that had previously been to study LptC's binding of different sugar fragments of LPS[130]. In short, an LPS-binding protein is anchored to the surface of an SPR chip and different fragments of LPS are passed over at different concentrations, allowing for calculation of dissociation constants. Different LPS oligosaccharide fragments can be produced by purification and selective degradation of LPS from different mutant strains. LptC was found to bind the oligosaccharide of LPS without any of the lipids, and to bind the di-glucosamine-di-phosphate much more tightly than the core oligosaccharide.

LptE was anchored to a CM5 SPR chip via amine coupling via the protocol determined in the last chapter. Three LPS sugar fragments were passed over LptE (Figure 3.1): the core oligosaccharide with the di-glucosamine-di-phosphate lipid A head group, the same core

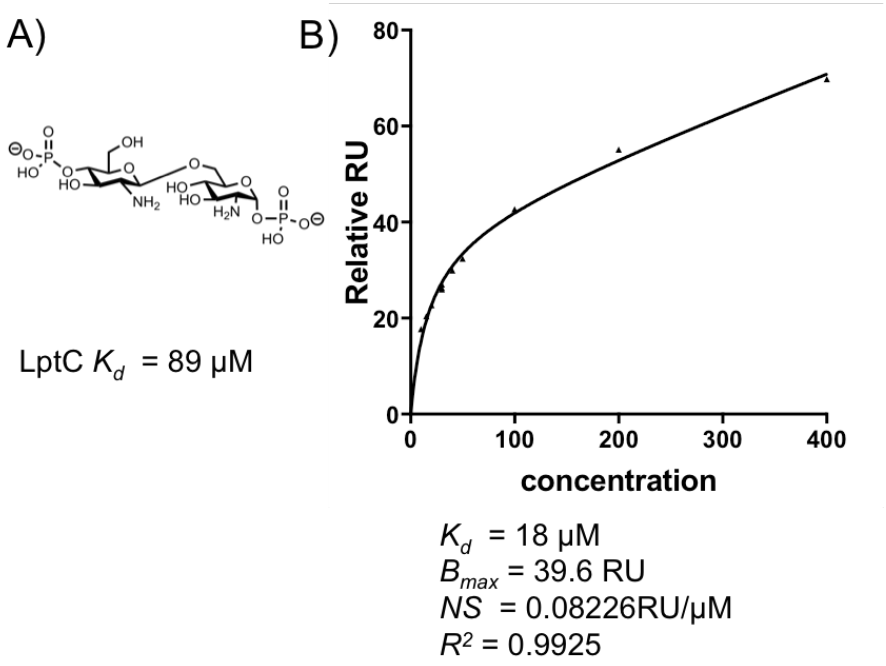

Figure 3.3: Binding of the di-glucosamine-di-phosphate headgroup of lipid A. A) Structure of di-glucosamine-di-phosphate with K_d for its binding by LptC. B) RU relative to baseline at different concentrations of di-glucosamine-di-phosphate with curve fit and calculated K_d for LptE.

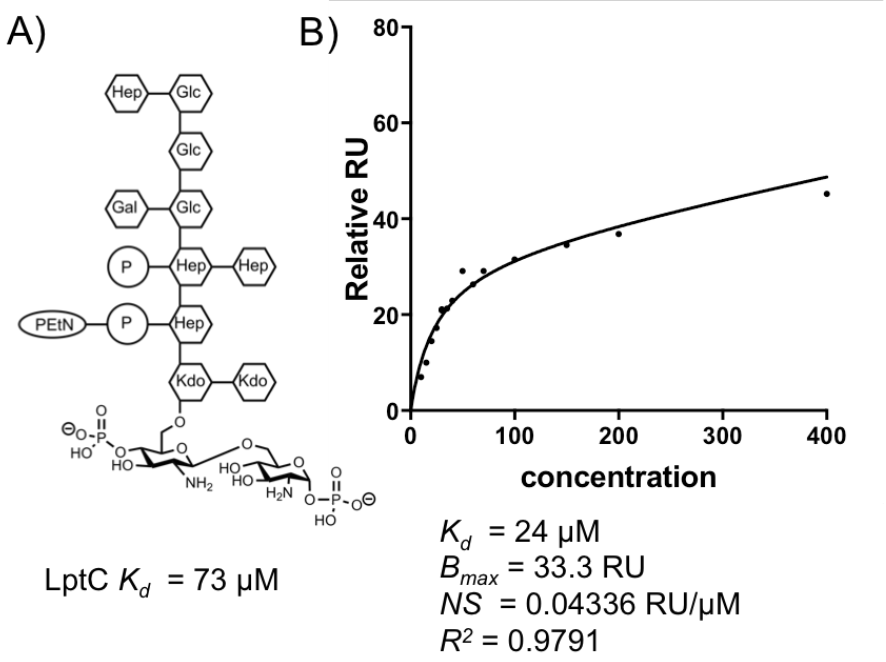

Figure 3.4: Binding of the core oligosaccharide of LPS with the di-glucosamine-di-phosphate headgroup of lipid A attached. A) Structure of the saccharide with K_d for its binding by LptC. B) RU relative to baseline at different concentrations of di-glucosamine-di-phosphate with curve fit and calculated K_d for LptE.

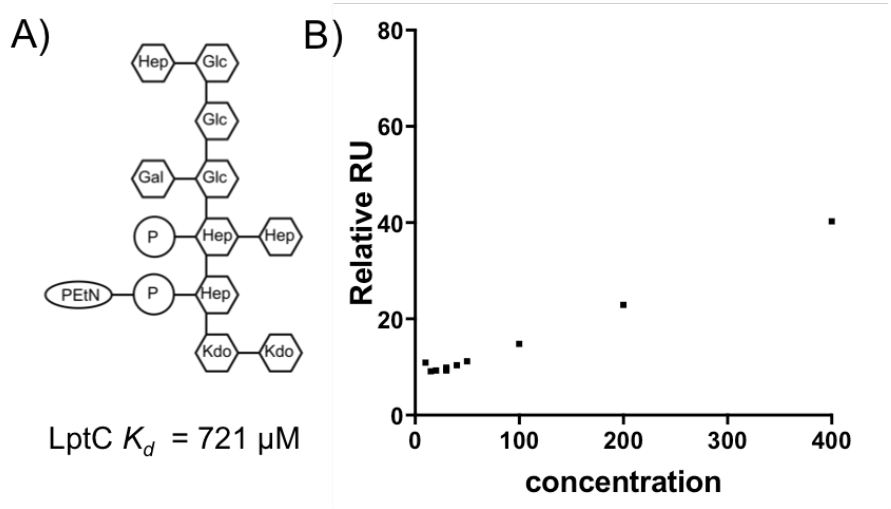

Figure 3.5: Binding of the core oligosaccharide of LPS A) Structure of the core saccharide with K_d for its binding by LptC. B) RU relative to baseline at different concentrations of di-glucosamine-di-phosphate passed over LptE. Data could not be fit to for specific binding.

oligosaccharide without the lipid A head group, and the di-glucosamine-di-phosphate lipid A head group without any further sugars. The complete oligosaccharide and the lone di-glucosamine-di-phosphate both showed reversible saturation binding, whereas the core oligosaccharide without the lipid A headgroup showed no interaction with LptE except at the highest concentration. While the data could not be fit with a standard specific binding curve, they could be fit when a non-specific linear binding component was incorporated , allowing for calculation of dissociation constants and comparison with those obtained for LptC . LptE binds the di-glucosamine-di-phosphate with a K_d of 18 μM (Figure 3.3), which is comparable to its affinity for the complete oligosaccharide (K_d = 24 μM, Figure. 3.4). Both of these values suggest slightly tighter binding than LptC showed for either the di-glucosamine-di-phosphate (K_d = 89 μM) or the complete oligosaccharide (K_d = 73 μM). The core oligosaccharide did not show any specific binding to LptE (Figure 3.5), in contrast to its weak but measurable binding (K_d = 721 μM) by LptC.

Based on the above data, LptE can be said to bind LPS by the di-glucosamine-di-phosphate. LptE does not specifically bind the core oligosaccharide at all, whereas the di-glucosamine-di-phosphate is essential to LptE binding of LPS. This also shows that the acyl chains of lipid A are not essential to LptE's ability to bind LPS. LptE's binding of LPS is similar to LptC's, in that the lipids are not essential and the charged phosphates are of the greatest import. LptE differs from LptC in that it does not bind the core oligosaccharide at all; indeed, the core oligosaccharide appears to hinder LptE's ability to bind the di-glucosamine-di-phosphate. LptC, on the other hand, binds the lipid A headgroup and the complete oligosaccharide comparably, and binds the core oligosaccharide less tightly, indicating that while it interacts most strongly with the di-glucosamine-di-phosphate, it also interacts more faintly with the core oligosaccharide. The lipids of LPS are not essential to either LptC or LptE's ability to bind LPS, but we cannot know if they contribute to binding without looking at the interaction between the Lpt proteins and lipidated LPS fragments.

3.2.3: The acyl chains of lipid A do not lead to an increase in affinity for LptC or LptE

To determine if the lipids of LPS contribute to its binding by LptC or LptE, the existing techniques had to be adapted to allow for study of lipidated species. As was shown in chapter 2, complete LPS cannot be used to measure dissociation constants via SPR, as it never achieves saturation (Figure 2.9). The methods used to produce different LPS sugar fragments, however, can be adapted to produce partially de-lipidated LPS species with the same variety of oligosaccharide composition leading to three different soluble bi-acylated LPS fragments for study[130].

LptC and LptE were anchored to a CM5 chip prepared as above. When either was exposed to any of the bi-acylated LPS species described above, the fragments bound reversibly, but did not completely wash away after injection ceased. This prevented repeated measurements with the same surface preparation. We began washing between runs with 0.03% DDM until the SPR signal had returned to pre-LPS injection baseline levels. Both LptC and LptE were stable to DDM washes, confirming that this would allow for measurement of binding data for the partially lipidated fragments.

Using the above modification of the SPR technique used to measure binding to LPS sugar fragments, dissociation constants were obtained for each of the above lipidated LPS fragments with LptC and LptE (Figures 3.6-8). LptC binding is consistent with a model in which both lipids and the core oligosaccharide are of little importance for binding. While there is some variation, LptC bound each of the lipidated LPS fragments comparably to binding the de-lipidated Ra-LPS oligosaccharide (K_d = 73 μM) or just the di-glucosamine-di-phosphate lipid A headgroup (K_d = 89 μM). LptC even bound the de-N-acylated Δ*lpxM* LPS (Figure 3.8, K_d = 181 μM) with slightly reduced affinity, suggesting that the acyl chains attached to LPS via esters may even slightly hinder LPS binding by LptC. That the two de-O-acylated LPS fragments, produced from Ra-LPS (Figure 3.6, K_d = 39 μM), and from LPS from a Δ*rfaC* strain (Figure 3.7, K_d = 32 μM), bound with almost identical affinity despite the latter's lack of most of the core oligosaccharide further supports the theory that LptC interacts only minimally with the core oligosaccharide. The four-fold difference in affinity between the de-O-acylated and de-N-acylated fragments suggests that, insofar as LptC does interact with the lipids, it exhibits a slight preference for those attached via peptide rather than ester couplings.

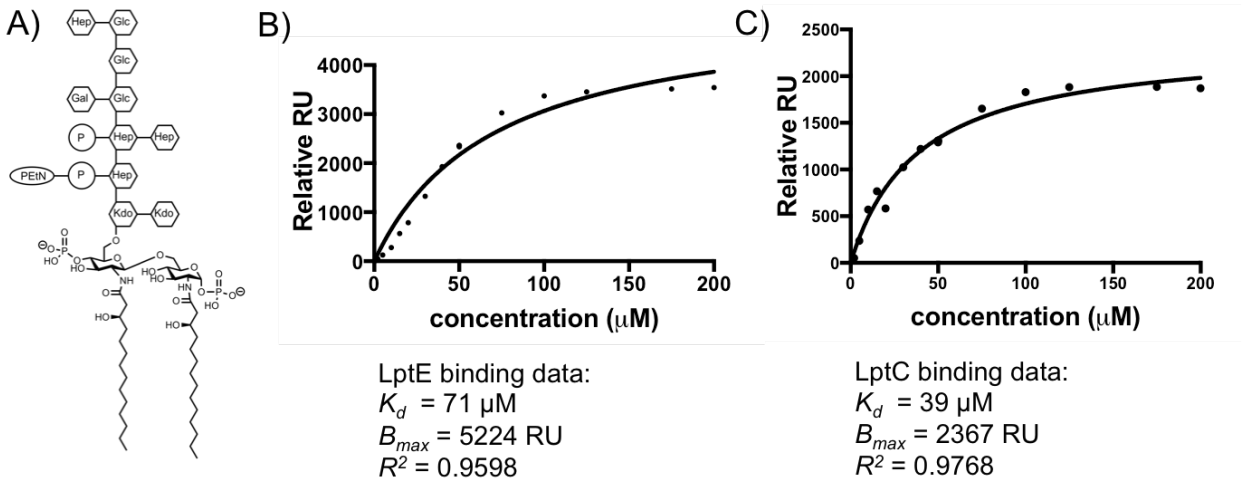

Figure 3.6: A) Structure of Ra-LPS that has been de-O-acylated B) Binding data and curve fit for the ligand with LptE. C) Binding data and curve fir for the ligand with LptC.

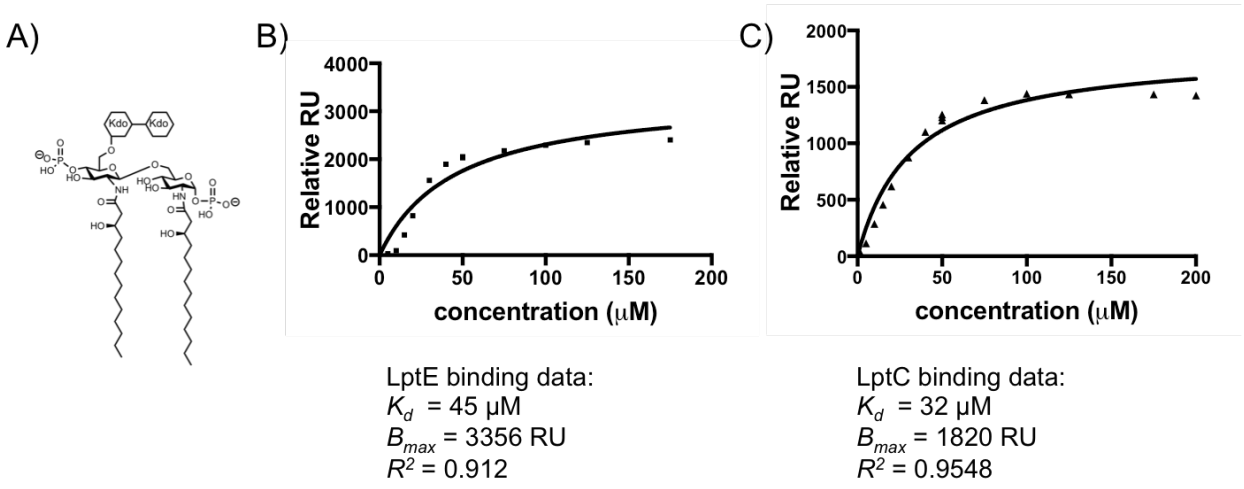

Figure 3.7: A) Structure of LPS from a Δ*rfaC* strain that has been de-O-acylated B) Binding data and curve fit for the ligand with LptE. C) Binding data and curve fit for the ligand with LptC.

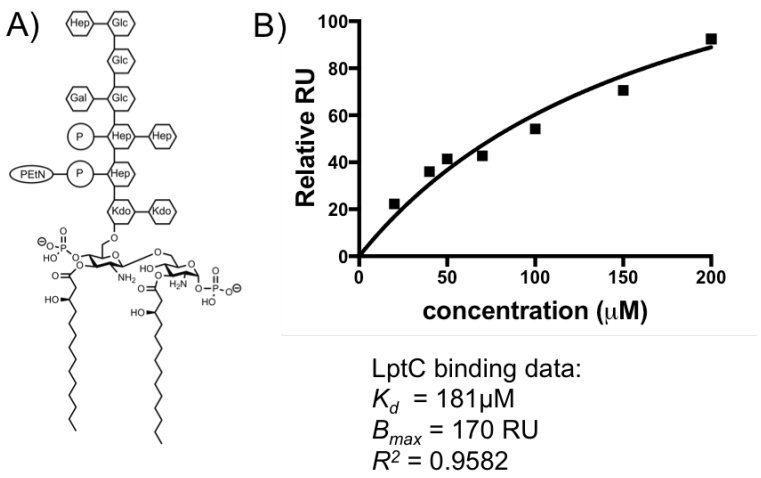

Figure 3.8: A) Structure of LPS from a Δ*lpxM* strain that has been de-N-acylated B) Binding data and curve fit for the ligand with LptC. Binding did not saturate for LptE.

LptE's binding of lipidated fragments suggest that the lipid chains contribute minimally, if at all, to binding. De-O-acylated LPS from both the ΔlpxL and ΔrfaC strains bound reversibly, while the de-N-acylated LPS from the ΔlpxM strain bound but never saturated. This allowed for calculation of dissociation constants of 71 μM and 45 μM for the Δ*lpxL* and Δ*lpxM* fragments, respectively (Figures 3.6-7). As the de-N-acylated fragment never saturated, no dissociation constant could be calculated. That the Δ*rfaC* fragment binds with as great or greater affinity to the Δ*lpxL* fragment that the core oligosaccharide of LPS is not involved in LptE's binding of LPS. This is consistent with how LptE binds the di-glucosamine-di-phosphate as tightly as the whole oligosaccharide, but does not bind the core oligosaccharide without the di-glucosamine-di-phosphate at all. LptE binds both the Δ*lpxL* and Δ*rfaC* fragments with comparable or slightly reduced affinity to completely delipidated LPS, showing that LptE does not bind the N-acyl chains. De-N-acylated LPS's inability to saturate LptE shows that, after any specific binding between LptE and the ligand, it continues to grow aggregates attached to LptE. The readiest

explanation for this is that the O-acyl chains are completely non-interactive with LptE, and are thus free to associate with each other and form aggregates. That LptE does not appear to bind the lipids of LPS at all initially surprised us, as LptE so effectively disaggregates LPS.

3.2.4 : Toward a more complete model of LPS transport

In the Lpt pathway, the LptD/E translocon must extract LPS from an aggregate in the periplasm and pass it through the hydrophobic interior of the OM, whereas LptC need only provide a path that LPS can slide down as part of an aggregate. These differing requirements, along with their different structures, mean that it is not surprising that LptC and LptE bind LPS differently. To disaggregate LPS, LptE need not only bind LPS, but also specifically undo the interactions that contribute to LPS aggregation. While it was surprising to us that neither LptC nor LptE required lipids to bind LPS, this information helps to build a model of LPS transport.

The new binding data for LptC complicate the picture established by other scientists. No individual component of LPS is essential to binding by LptC, but the di-glucosamine-di-phosphate headgroup of lipid A contributes the most to binding. The core oligosaccharide and the lipid A acyl chains contribute minimally to affinity, as none of the partially lipidated fragments, core oligosaccharide containing fragments, or even the complete Ra-LPS display a notably greater affinity for LptC than the lone di-glucosamine-di-phosphate. Sestina and coworkers had previously reported that LptC binds Ra-LPS with a K_d between 28.8 μM and 71.4 μM, comparable to those seen in our SPR experiments for the oligosaccharide without lipids (K_d = 73 μM), suggesting the importance of the sugars over the lipids in binding. They also report that a LPS-mimicking probe, consisting of a bi-acylated sugar monomer without phosphates, binds less well (K_d = 221 μM), consistent with the importance of the di-glucosamine-di-

phosphate seen in SPR studies. At the same time, Sestita and co-workers report that both Ra-LPS and their probe bind LptC irreversibly, suggesting that while the lipids contribute minimally to the affinity of LptC for LPS, they may alter the kinetics of binding. This leads to the question: are the lipids of LPS really in the groove of the bridge? It seems unlikely that the lipids do not interact with LptC at all, as its β-jellyroll structure contains a hydrophobic groove, and the equivalent groove contains hydrophobic detergent in the crystal structure of LptD/E[88]. Our SPR data do not conclusively answer this question, but does complicate the previous model in which the lipids were assumed to be the primary contributor to LptC binding of LPS. LPS forms aggregate structures, with buried lipid chains, readily in solution, and the new data suggest that LPS could form such an aggregate structure along the LptC/A/D bridge.

The LptE binding all supports the initial hypothesis, based on structure and comparison to other LPS binding proteins, that LptE binds LPS by the di-glucosamine-di-phosphate headgroup of lipid A. In contrast, the SPR data shows that LptE appears to bind exclusively to the di-glucosamine-di-phosphate, with the acyl chains and core oligosaccharides contributing nothing. This indicates that the model in which the β-sheet of LptE interacts with the lipids of LPS while the loops at the putative binding site bind the charged headgroup is not accurate, and that LptE really does exclusively bind the di-glucosamine-di-phosphate lipid A headgroup of LPS. It is not entirely surprising that LptE would not independently interact with all of LPS, as LptE sits within the barrel of LptD, and presumably never binds LPS without contributions from LptD and possibly the OM itself.

Lpt proteins binding LPS by the phosphates rather that by the core oligosaccharide supports the pre-existing model that the Kdos of the core oligosaccharide have a roll in LPS recognition by the LPS biosynthesis pathway and in MsbA, but not in later stages of LPS

biogenesis. The minimal viable structure of LPS is lipid IV_A (Figure 3.9), a tetra-acylated LPS precursor lacking the core oligosaccharide[44]. Lipid IV_A can reach the OM, as judged by the presence of OM-localized modifications to lipid IV_A in these strains. Loss of Kdo would usually be fatal, but that can be suppressed by overexpression of either MsbA, the flippase responsible for transposing LPS from the inner to the outer leaflet of the IM, or either LpxL or LpxM, the acyl-transferases responsible for adding the fifth and sixth acyl chains to Kdo_2-lipid IV_A, respectively, showing that the Kdos, is needed only for the pre-Lpt steps in LPS biogenesis[131]. The new data support this model, showing that the Kdos are not only not necessary, but contribute negligibly (in the case of LptC) or not at all (in the case of LptE) to LPS binding by the Lpt machinery.

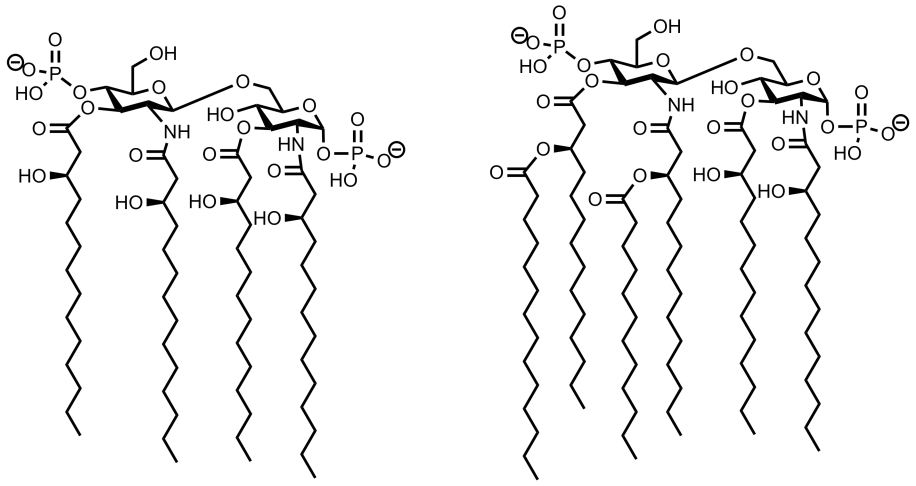

Figure 3.9: Structure of lipid IV_A (left) compared to that of Lipid A (right).

Recent work in other groups has led to a model of LptD/E function. Crystal structures of the LptD/E complex confirmed biochemical evidence[75] that LptE sits within the barrel of LptD, and that confirmed that the n-terminal periplasmic domain of LptD share the β-jellyroll fold of LptC and LptA, with a hydrophobic groove[88,98]. Hydrophobic detergents crystalized within the nLptD hydrophobic groove, suggesting it as a site of LPS lipid binding. More surprisingly,

LptD's unprecedented large β-barrel assumes a two-lobed bean shape. The lobe immediately adjacent to the N-terminus is hollow and hydrophilic, while LptE fills the second lobe, with the external side of the narrow β-sheet formed by LptE's β3-β5 strands facing the hole of the first lobe (Figure 3.10A-B). The β1 and β2 strands of the LptD barrel are exceptionally short, with minimal hydrogen bonds to the adjacent β26 and β3 strands, creating a site of potential barrel opening for release of LPS from the lumen to the outer leaflet of the OM (Figure 3.10C). Molecular dynamics shows that junction of the periplasmic β-jellyroll and the integral β-barrel of LptD sits within the OM, forming an intra-membrane hole[132], and site-specific crosslinking has identified sites of interaction between LptD and LPS at sights along the hydrophobic groove of nLptD, within the lumen of the LptD β-barrel, and at the proposed luminal gate[124], leading to a model in which the acyl chains of lipid A slide directly from the hydrophobic groove of nLptD into the OM, while the sugars pass through the hydrophilic lumen and out into the OM via an opening of the lumenal gate.

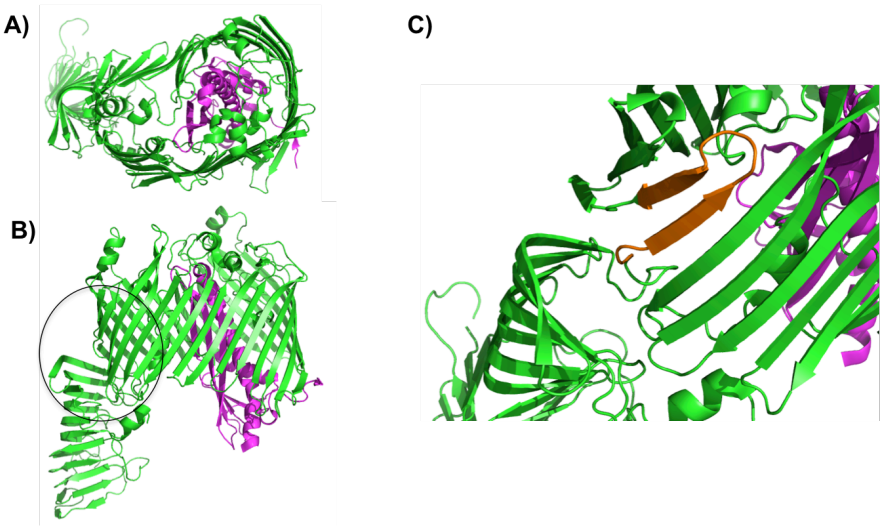

Figure 3.10: A) Top down view from outside of cell of the LptD(green)-LptE(magenta) complex (PDB code 4Q35). LptE fills one lobe of the LptD lumen. B) Side view of the LptD/E complex. The site of the proposed lumenal gate and intramembrane hole is circled. C) Close up of the proposed lumenal gate and hydrophobic hole. The top of the β-jellyroll of the N-terminal opens directly into the membrane. The short β1-β2 hairpin of the barrel is highlighted in orange.

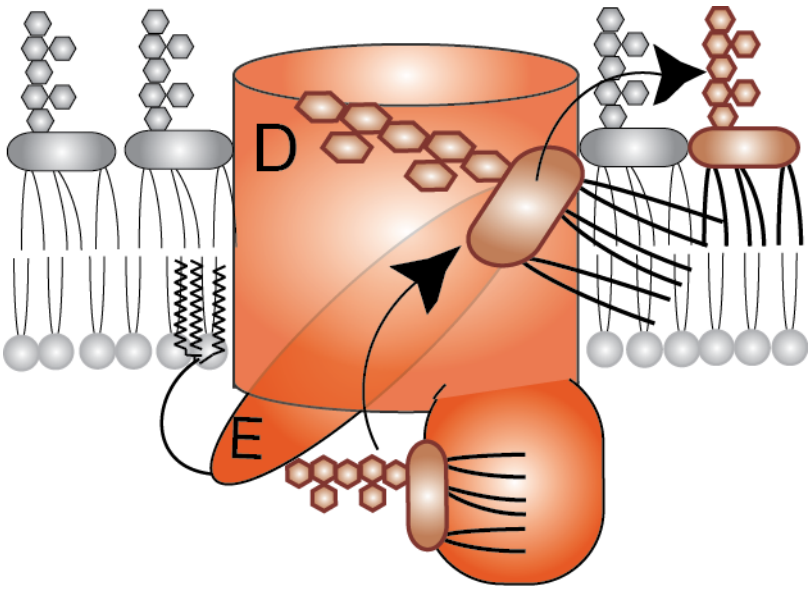

Figure 3.11: A model for the mechanism of translocation of LPS across the OM by the LptD/E complex. LPS reaches the translocon bound by the N-terminus of LptD, in an unknown aggregate state with other LPS (not shown). LptE binds it at the lipid A headgroup, separating it from the aggregate LPS in the periplasm, and guiding the sugars of LPS through the lumen of LptD while the lipids pass directly into the OM. LPS is then released into the outer leaflet via a gate in the side of the LptD β-barrel.

The new LptE-LPS binding data complement these recent structural and biochemical experiments and strengthens the proposed model, showing that in addition to its role as a chaperone for LptD folding and a plug for the LptD β-barrel, LptE stabilizes an intermediate stage of LPS transport, after LPS has left the LptC/A/nD bridge but before it has reached the outer leaflet of the outer membrane (Figure 3.11). The site of LptE-LPS crosslinking is on the lumen-exposed face of LptE that LPS is supposed to pass through. SPR data have shown that LptE interacts only with the sugar-phosphate headgroup of lipid A, rather than its acyl chains, consistent with the model where the sugars of LPS pass through the hydrophilic lumen of the LptD/E complex while the hydrophobic acyl chains pass directly from the hydrophobic groove into the OM. Earlier SPR work showed LptE to have LPS disaggregating activity, despite it not appearing to interact with the lipids of LPS. LPS-LPS interactions in aggregates are stabilized

primarily through a polyelectrolyte chain or web formed by the phosphates of LPS and divalent metal cations such as Magnesium. By binding to the phosphates of LPS, LptE can disrupt LPS-LPS interactions, separating the terminal LPS currently on the bridge from the others on the bridge and stabilizing it in an intermediate state, with its lipids buried within the OM and its sugars stretching through the lumen of the LptD/E complex, on its way to the outer leaflet of the outer membrane of LPS.

This model introduces a new question: if LptE interacts with LPS via ionic interactions with its charged di-glucosamine-di-phosphate, how do modifications to LPS at the phosphates alter LPS transport? Do these modifications, made in response to environmental stresses or to the LPS-binding cationic polypeptide polymyxin, make it more difficult for the LptD/E translocon to extract LPS from its periplasmic aggregate state, reducing LPS transport efficiency? Alternately, do these charge-altering modifications make LPS-LPS interactions weaker, making it easier for the translocon to disrupt them? To answer these questions, and others, we will need to develop a complete reconstitution of LPS transport.

3.3: Materials and Methods

In vivo crosslinking with LptE

Crosslinking experiments followed a modified version of the protocol established by Freinkman[75] and Okuda[94]. MC4100 Δ*lptE::kan* cells containing the pSup-BpaRS-6TRN and pET23/42*lptE-his* (WT or T103Am) plasmids were grown from an overnight starter culture to midlog phase at 37° C with shaking in 100 mL of LB supplemented with 50 μg/ml carbenecillin, 30 μg/ml chloramphenicol, and 900 μM pBPA (Bachem). Their OD_{600}, blanked against LB, was recorded, and the cultures were removed from the shaker and kept at room temperature. Half of

each culture was placed under a UV lamp for 10 minutes. Following this, samples were placed on ice and kept at 4° C for the remainder of the purification. Cells were pelleted, the supernatant discarded, and each pellet was resuspended in 5 ml of TBS-B (20 mM Tris-HCl, pH = 8.0, 300 mM NaCl, 20 mM imidazole) supplemented with 1% Anzergent 3-14 (Anatrace), 0.1 mg/ml chicken egg white lysozyme (Sigma), 5 mM $MgCl_2$, 50 μg/ml DNase I (Sigma) and 1x ProteaseArrest (G-Biosciences). Cells were lysed with a probe sonicator (LOOK UP MANUFACTURER) set to 25% amplitude, with 10 second pulses followed by 10 second rest periods, for a total of three minutes of sonication. Lysed samples were spun at 15,000 G for 30 minutes, and the supernatant immediately decanted and added to a gravity column with 200 μL of Ni-NTA resin (Qiagen) that had been pre-equilibrated with TBS-B supplemented with 0.02% Anzergent 3-14. The sample was allowed to drain, and re-applied to the sample twice. The sample was washed with 2 x 4 ml of TBS-B + 0.02% Anzergent 3-14, before elution with TBS (150 mM NaCl, 20 mM Tris-HCl, pH = 8.0) supplemented with 200 mM imidazole and 0.02% Anzergent 3-14. Samples were TCA precipitated and the pellets resuspended in 10 μl of SDS sample buffer per 0.1 OD_{600} at time of crosslinking. Samples were run on a 4-12% gradient polyacrylamide gel and western blotted using both □-LPS and □-LptE antibodies.

Protein expression and purification for biophysical experiments

C-terminally deca-histidine tagged LptE(C19M) and the corresponding (R91D, K136D) double mutant was overexpressed and purified according to previously established protocol, see section 2.4[69]. LptC was purified as in Doering, 2013[130].

Surface plasmon resonance

All experiments were performed using a Biacore X100 at a flow rate of 10 μl/min at 25° C. For protein immobilization, we used a Biacore CM5 chip (GE healthcare) that had been activated with an amine coupling kit (GE Healthcare). For both LptC and LptE, protein immobilization was done in 20 mM sodium acetate at a pH of 5.5. For LptC, we passed 20 μg/ml of protein over the chip for 420 seconds. For LptE, we passed 400 μg/ml of protein over the chip for 1000 seconds. Following protein immobilization, we passed 1M ethanolamine over the surface for 420 seconds to inactivate free reactive groups. The reference channel did not receive any protein prior to passivation with ethanolamine.

All binding experiments were performed in TBS. Lipidated samples were extruded (see section 2.4) at a concentration of 0.5 mg/ml prior to dilution. LPS fragments were prepared as in Doering, 2013[130].Different concentrations of each LPS fragment were injected for 100 seconds on both channels. The increase in RU at saturation relative to the protein-only baseline was recorded for generation of binding curves. For lipidated samples, the chip was washed with TBS containing 0.03% DDM (Anatrace) until signal had returned to the protein baseline. The chip was washed with TBS between every sample. Data were analyzed using Prism 7 software (GraphPad).

Chapter 4: characterization of the aggregate state of the complete LPS reconstitution.

Collaborators: Peter Foster, Ran Xie, Rebecca Taylor, Carolyn Marks, Dan Needleman, Daniel Kahne

Explanation of contributions: I planned, executed, and interpreted all of the microscopy experiments. In the case of the cryo-TEM experiments, this was done in collaboration with Ran Xie and with the help of Carolyn Marks of the Harvard Center for Nanoscale Systems. For the confocal microscopy, this was done with Peter Foster of the Needleman lab, as well as Ran Xie and Rebecca Taylor. I helped to plan and interpret the flow cytometry experiments, and with Peter performed the associated microscopy for the combined cytometry-microscopy experiments.

4.1: Introduction

Models of the Lpt pathway based on *in vivo* data and techniques have taught us much about LPS transport[64,69,78,79,92-94,133], but they are insufficient to fully understanding the problem. It is impossible to ensure that *in vivo* data are not complicated by extraneous factors in the cell and *in vivo* techniques are furthermore unable to clarify the energetic requirements of LPS transport or confirm that Lpt proteins form a bridge for LPS transport. Similarly, a number of mutants have been identified in Lpt proteins and while it has been established that they compromise the OM[75,97,134], we have yet to establish how many of these mutants alter the Lpt pathway's capacity to transport LPS. In addition, we lack an *in vivo* technique to measure the effect of modifications to LPS phosphates on LPS transport. We believe that an *in vitro*

reconstitution of the Lpt pathway is necessary, in that it will allow further study into the mechanism and inhibition of LPS transport without the limitations of *in vivo* techniques.

Previous researchers in the Kahne lab have developed a liposome-based reconstitution that confirms LPS transport from an initial membrane as far as the N-terminal domain of LptD[95]; while this represents a tremendous accomplishment, it is incomplete in several ways and needs further refinement. First, the extant reconstitution lacks a readout for final release of LPS into the terminal membrane; this is an active area of research by others in the Kahne lab. Second, previous research has left ambiguity in the method of LPS transport within the reconstitution: via a bridge or via a soluble chaperone. The current research, as detailed in this chapter, attempts to address this ambiguity, with particular attention to whether the reconstitution itself takes the form of a bridge—between two liposomes or among a larger aggregate—or if the liposomes do not directly associate. As long as this question remains unresolved, we will be unable to interpret data obtained from the reconstitution and, specifically, unable to determine if the final translocation of LPS across the OM is energy dependent.

As shown in previous chapters, we have determined, first, that LptE can act on LPS and, second, that altering LptE's ability to act on LPS compromises the OM, but without a complete reconstitution we are unable to determine how this occurs or to fully understand LptE's role in the final step of LPS transport. The SPR studies demonstrating that R91D and K136D mutants reduce the ability of LptE to disaggregate LPS *in vitro* analyzed purified LptE, without any of the rest of the Lpt pathway present. As discussed in the introduction to chapter two, related studies suggesting that LptE losing the ability to disaggregate LPS damages the OM by preventing LPS transport[97]: these same mutants, when expressed in lieu of wild type LptE in the *E. coli* cell, render the OM permeable to antibiotics that it cannot usually cross it. In the absence

of a complete reconstitution, however, there have been no data demonstrating that these disaggregation-deficient LptE mutants—or other Lpt pathway mutants—have a diminished ability to transport LPS.

The model for LptD/E function put forward in the third chapter remains incomplete in ways that a reconstitution of LPS transport, and in particular establishing if an Lpt bridge is required, could help to resolve. As previously discussed, in the current model LptE binds the di-glucosamine-di-phosphate of LPS within the β-barrel of LptD, stabilizing LPS in an intermediate state between being bound by the N-terminus of LptD and complete integration into the outer leaflet of the OM, and helps guide the sugars of LPS through the hydrophilic inside of the LptD β-barrel, away from the hydrophobic interior of the OM. However, this working model does not allow us to determine if this step requires additional energy—either to separate LPS from its aggregate state in the periplasm or to finally release LPS from its LptE-bound state—or if LptD/E simply provides a low energy intermediate state for LPS to pass through the interior of the OM, removing the kinetic barrier to its reaching the thermodynamically favorable outer leaflet of the OM. As the periplasm lacks ATP or any comparable energy source[10], any such energy would need to be transduced from the inner membrane through the Lpt bridge; without such a bridge, it would be astonishingly difficult for the cell to transmit the energy to the OM.

We can build on the liposome-based reconstitution developed by previous researchers in the Kahne lab, which transports LPS between proteoliposomes, to assess the existence and potential form of an Lpt bridge. The reconstitution uses two different types of proteoliposome: the first represents the IM, with LPS and the LptB/F/G/C protein complex incorporated into the membrane, while the second represents the OM, with the LptD/E protein complex incorporated into that membrane. When mixed with LptA, the system includes all of the predicted components

of the Lpt pathway, and movement of LPS from the IM to the OM can be monitored by site-specific photocrosslinking. By incorporating the artificial acid pBPA via amber-codon suppression, LPS can be crosslinked *in vivo* at the sites for LptC, LptA, and the N-terminus of LptD within the hydrophobic groove[94,124]. These crosslinks are all repeatable in the reconstitution, but only in the presence of ATP and of all of the preceding proteins in the pathway[95]; this shows that LPS transport can be reconstituted from one liposome into a protein embedded in another. The crosslink between LptD and LPS diminishes over time, suggesting that LPS eventually leaves LptD and finds its way from LptD into the OM-simulating liposomal membrane: thus, we conclude that that the system reconstitutes all of LPS transport. Without a clear picture of how the liposomes have arranged themselves, interpreting this reconstitution remains challenging.

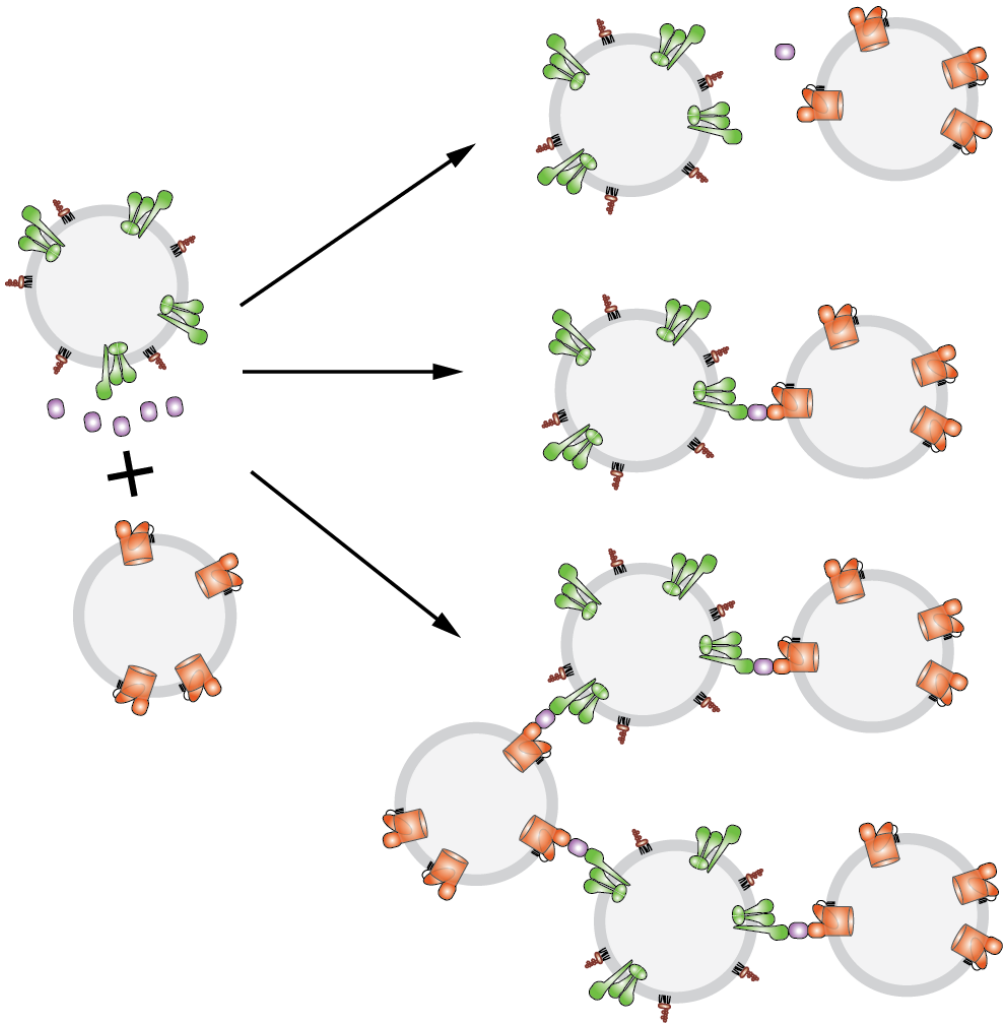

Figure 4.1: Possible arrangements of the reconstitution of LPS transport. Proteoliposomes (left) representing the IM (green) and OM (orange) are mixed with LptA (purple). It is unknown if this reconstitutes LPS transport via a shuttle mechanism (right, top), via bridged between heterodimers of liposomes (right, center), or via larger bridge-mediated liposomal aggregates (right, bottom).

Although neither of the protein components of the OM are transported via a bridge—β-barrel proteins and OM lipoproteins are both transported across the periplasm by chaperones[13,135]—the pull-downs and crosslinking described in chapter 1[92,93] suggests the presence of a periplasm-spanning bridge connecting the IM to the OM via a single protein complex. It is not clear, however, if the complete bridge is required for LPS transport, nor is it clear that the bridge is the default state of the Lpt proteins; it could represent only a small

fraction of the total population. The bridge model for LPS transport is suggested by the inability of LptA pre-loaded with LPS to hand off LPS to LptD without the IM proteoliposome and ATP[95]; if this model is accurate, the next question is the form the liposomal aggregates take (Figure 4.1): are they heterodimers or some larger oligomers? If the latter, what is the ratio of IM to OM proteoliposomes? To answer these questions, we turned to a variety of microscopic and cytometric techniques.

4.2: Results & Discussion

4.2.1: Cryo-TEM shows liposomal aggregates in the presence of LptA

Ran Xie and I first attempted transmission electron microscopy as a means of determining if the reconstitution of LPS transport displayed an LptA-dependent association between liposomes, in collaboration with Carolyn Marks of the Harvard Center for Nanoscale Systems. Negative staining of liposomes did not preserve liposome structure, but cryo-TEM preserved the liposomes for imaging. Proteoliposomes were prepared and mixed as if for the reconstitution, pipetted onto a carbon grid, flash-frozen in liquid ethane, and imaged on a cryo-TEM. We varied whether or not LptA was present. The resulting images showed spherical liposomes with a well-defined membrane and some variation in diameter. Without LptA, there was some liposome-liposomes overlap, though some of this was clearly out-of-plane projection, and adjacent liposomes did not distort each other (Figure 4.2, left). This could be due to a mix of non-specific liposome-liposome attraction and the high concentration of liposomes used in the reconstitution. In the presence of LptA, occasional liposomal aggregates could be seen (Figure 4.2, right). What distinguishes these from instances of liposomal overlap seen without LptA is that the liposomes are clearly interacting with each other as opposed to sitting in close proximity.

With LptA, the membranes of side-by-side liposomes do not extend past each other or overlap, they meet and deform around in each other. This LptA dependent close membrane-membrane interaction is not observed for dimers of liposomes, but only for larger aggregates. These images suggest that LptA induces liposome-liposome interactions, and hints that liposomes may be more likely to form larger oligomers rather than heterodimers.

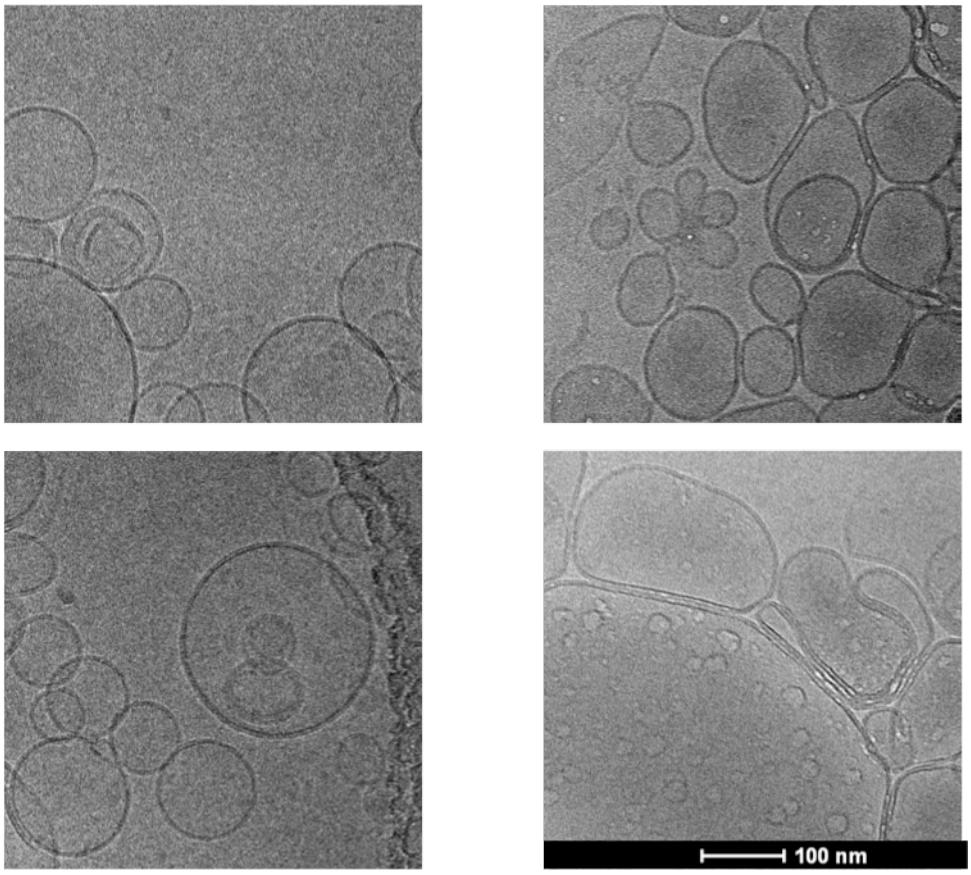

Figure 4.2: Cryo-TEM images of the Lpt pathway reconstitution. LptA-free conditions (left) show liposomal overlap, but no instances of proteoliposomes forming extended contact. Addition of LptA (right) leads to aggregates in which each liposome has extended contact with its neighbors, and the membranes of neighboring liposomes conform to each other.

Cryo-TEM does, however, have several traits that limited its further usefulness. It provides only a static image of the liposomes, providing no information about the dynamics of liposome-liposome aggregation, or the stability of any bridges holding liposomes together. It also

lacks the ability to distinguish between proteoliposomes containing the LptB/F/G/C complex and those containing the LptD/E complex, making it difficult to distinguish between false positive interactions between homogenous liposomes and the heteroliposomal associations we are searching for. A new technique will be needed to resolve these issues.

4.2.2: Confocal microscopy can discriminate between IM and OM proteoliposomes

Confocal microscopy presented itself as a solution to the above issues with Cryo-TEM, leading Ran Xie, Rebecca Taylor, and I to collaborate with Peter Foster of the Needleman laboratory. While magnification and resolution would be reduced, a confocal microscope could record samples continuously, allowing for potential observation of the formation and dissolution of liposomal aggregates and the study of their stability. In addition, it makes it comparatively easy to discriminate between different populations of proteoliposomes, as different fluorescently labeled lipids can be doped into proteoliposomes at the time of their preparation. Both variants of proteoliposomes were labeled by addition of fluorophore-tagged DPPE to the membrane at a final molar concentration of 1% of total lipid content. LptB/F/G/C proteoliposomes were labeled with Atto-565 and LptD/E proteoliposomes with Atto-488. Prior to imaging, the LPS transport functionality of the proteoliposomes was confirmed via the standard reconstitution and western blot. For imaging, the proteoliposomes were mixed, as for the reconstitution, with or without LptA. Movies recorded showed that individual liposomes could be resolved, and that the differently labeled liposomes could be readily distinguished. The liposomes tumble through solution, rapidly entering and exiting the plane of focus, making it impossible to track liposomes for periods of time long enough to measure distances between individual liposomes and identify

paired or aggregated liposomes, and necessitating a method of preventing liposomal drift out of the plane of focus.

4.2.3: Anchoring liposomes to the slide showed an LptA-dependent increase in liposome-liposome interactions

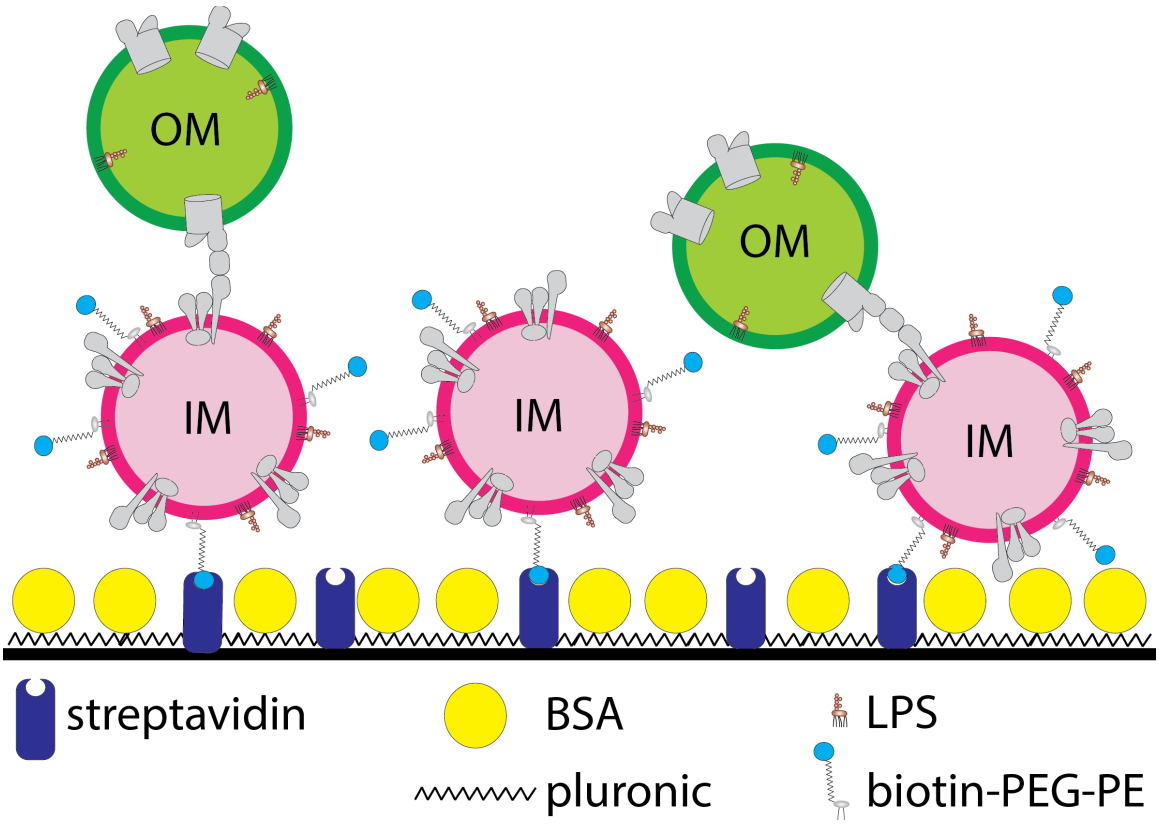

Figure 4.3: Immobilization of liposomes to the surface. A glass coverslip coated with streptavidin is passivated with a mix of bovine serum albumen (BSA) and the block copolymer Pluronic F-127. OM proteoliposomes, IM proteoliposomes, and LptA are pre-incubated and exposed to the surface. Biotinylated IM liposomes tether themselves to the surface via streptavidin-biotin binding, and any aggregated OM is co-localized to the surface.

In order to prevent liposomes from drifting in the Z-dimension, we selectively anchored them to the coverslip of the sample chamber (Figure 4.3). We added biotinylated lipid to the fluorescent LptB/F/G/C liposomes at a molar concentration of 1% of total lipid content, and

confirmed that these remained functional for both ATPase activity and LPS transport activity. The coverslip was silanized to make it hydrophobic, and was treated with streptavidin, and passivated with a mixture of the non-ionic triblock copolymer Pluronic F-127 and bovine serum albumen (BSA). The sample chambers were washed with reaction buffer, and the liposome mixture was introduced. The biotinylated IM proteoliposomes would anchor to the surface, but attempts to pass OM proteoliposomes, with or without LptA, over the captive IM proteoliposomes failed to show the OM attaching to the surface in either circumstance, suggesting that liposome-liposome associations could not form in sufficient quantity once the IM proteoliposomes were tethered to the coverslip surface.

To facilitate capture of any potential proteoliposome aggregates, we attempted to generate the aggregates prior to introduction to the sample chamber. We pre-mixed the IM and OM proteoliposomes in reaction conditions and incubated on ice for 15 minutes, as is done in the reconstitution of LPS transport, then introduced the whole mixture to the sample chamber, allowing it to incubate at room temperature for 15 minutes before rinsing out any untethered proteoliposomes with a wash of reaction buffer. Far more OM proteoliposomes were visible and anchored in place when LptA was included than in LptA-free conditions (Figure 4.4A-B). More OM proteoliposomes were anchored in the full reconstitution conditions than when OM proteoliposomes (with or without LptA) were imaged without IM proteoliposomes (Figure 4.4C-D), indicating that the LptA-dependent difference is due to interactions between the IM and OM proteoliposomes, not due to interactions between the OM proteoliposomes and the coverslip surface. In addition, some spots could be seen where there was clearly signal in both the 488 nm and 565 nm channels, indicating the presence of both IM and OM proteoliposomes in the same spot.

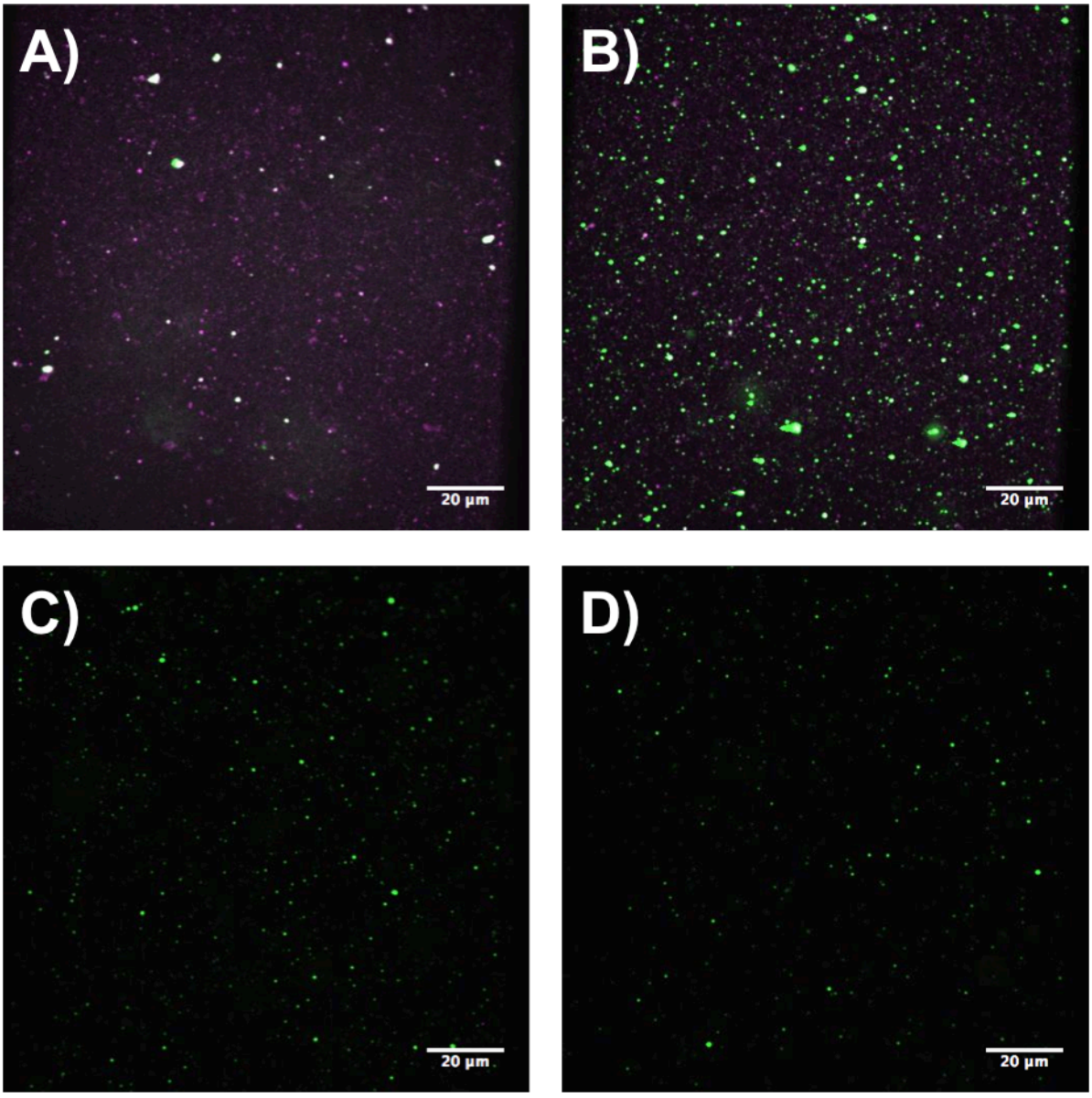

Figure 4.4: LptA induces OM proteoliposome (green) binding by the anchored IM proteoliposomes (pink). A) IM and OM proteoliposomes are pre-incubated prior to incubation with the streptavidinylated surface, leading to much IM and minimal OM anchoring. B) Addition of LptA leads to many more OM proteoliposomes anchoring to the surface. C) OM proteoliposomes alone bind the surface, but less than with the complete reconstitution. D) OM proteoliposomes with LptA do not anchor with any greater frequency than without LptA if IM proteoliposomes are not present.

All of this indicated that confocal microscopy would allow us to observe IM-OM proteoliposome interactions, to determine under what conditions they formed, and to see if they

took the form of heterodimers or larger aggregates. The current technique needed to first be refined in several ways. First, the above conditions led to too high a density of IM proteoliposomes to distinguish individual liposomes, preventing any quantification of individual interactions between IM and OM proteoliposomes. Second, the pluronic and BSA passivation proved inconsistent, making it difficult to repeat the process. Finally, the quantity of non-specific surface binding of OM proteoliposomes, while lower than specific binding in the presence of all of the reconstitution components, was high enough to cause difficulties for future quantification.

4.2.4: Development of conditions that allow for quantification

The pluronic and BSA passivation was optimized for work with protein systems, as opposed to proteoliposomes, so we adopted techniques developed for the imaging of liposomes. The most common of these is to coat the glass in a lipid bilayer. Plasma treatment of the glass renders it hydrophilic, and incubation with empty liposomes made of phosphatidylcholine leads to a lipid bilayer covering the glass[136-138]. We included a dilute quantity of the same biotinylated lipid in the surface liposomes, then used streptavidin as a bridge between biotinylated proteoliposomes and the surface (Fig. 4.5). Trial and error established that diluting the liposome mixture 1:100 immediately before addition to the sample chamber led to a density of liposomes such that individual liposomes could be distinguished. In addition, we tried both biotinylating the IM but not the OM proteoliposomes, as we had done previously, and biotinylating only the OM proteoliposomes, and found that non-biotinylated IM proteoliposomes exhibited much less non-specific binding to the surface than non-biotinylated OM proteoliposomes. All further liposomal preparations used had the OM, rather than the IM, proteoliposomes biotinylated.

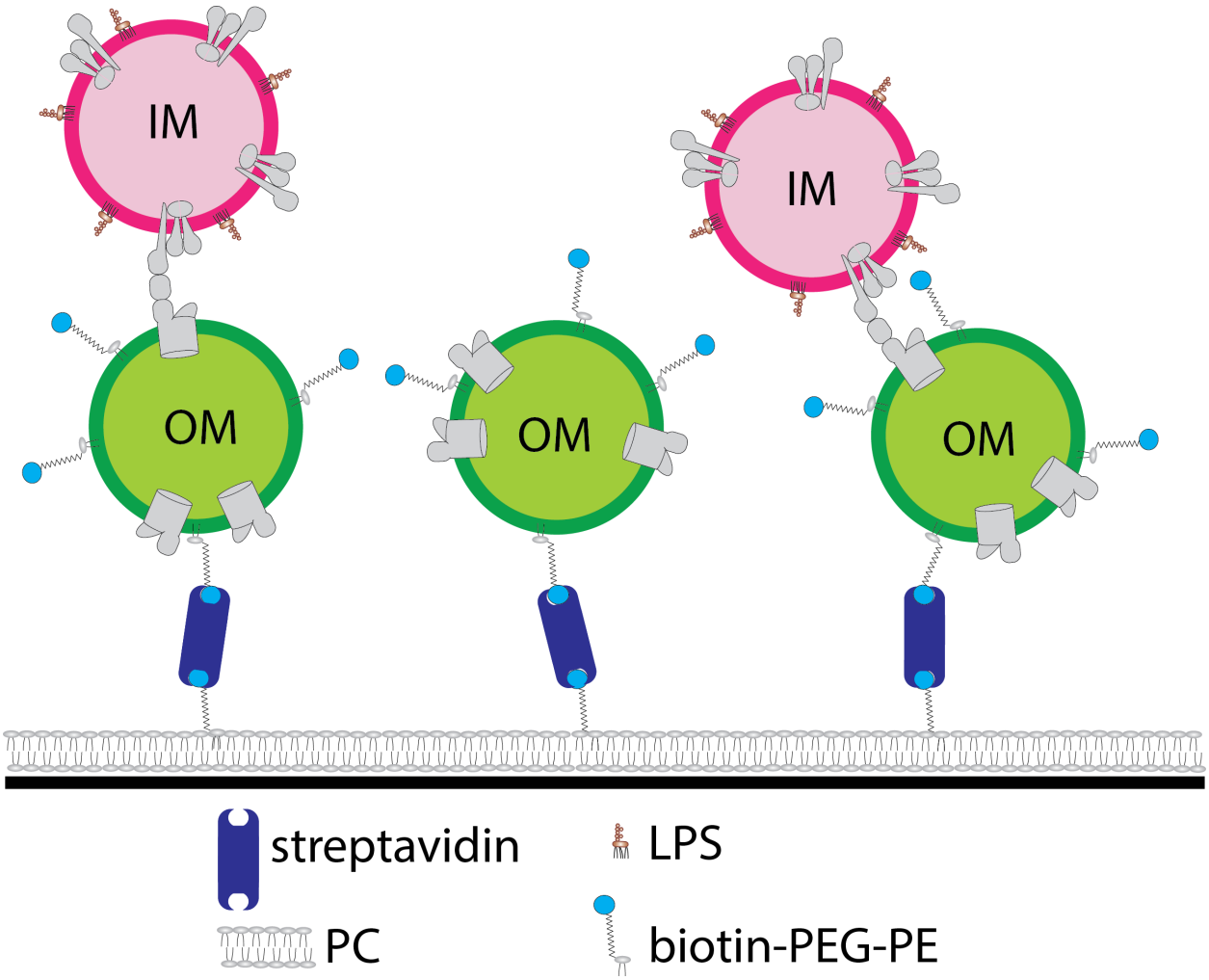

Figure 4.5: Passivation of the coverslip surface with a lipid bilayer. Egg-PC liposomes are placed on a plasma-treated coverslip and incubated at 37° C to induce bilayer formation. The bilayer contains 0.008% (by molarity) biotinylated lipid, to allow for tethering of the proteoliposomes via a streptavidin bridge.

These conditions allowed for deployment of quantification tools. Based on established particle-tracking software [139], Peter Foster wrote Matlab code to quantify the number of paired liposomes present in any given field of view. In each fluorescent channel, corresponding to either IM or OM proteoliposomes, individual liposomes were identified via thresholding relative to the background signal, and tracked from frame to frame. Liposomes that did not move relative to any stage drift were counted as immobile. For each immobile OM proteoliposomes, its position was checked against that of each immobile IM proteoliposome, and any that were within a short boundary were defined as paired (Figure 4.6). This allowed for counting of both the total number

of both kinds of proteoliposomes, and for counting of the number of paired IM and OM liposomes.

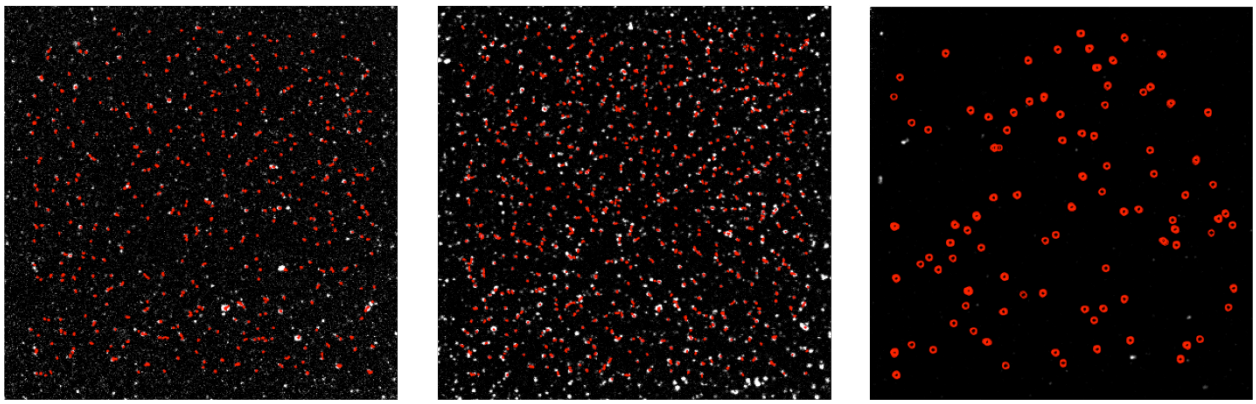

Figure 4.6: Tracking and quantification of liposomes. Trajectories (red) of individual liposomes (white) are first determined for both IM (left) and OM (center) proteoliposomes, and mobile liposomes are excluded. Each immobile liposome is then checked for proximity again all of the other variety of liposomes to identify pairs (right).

These new techniques allowed us to quantify the difference induced by adding LptA to the system. With two sets each of functional IM and OM liposomes, each of four possible pairings was prepared and imaged with and without LptA. Two different mixes of each condition were prepared and imaged, and each slide had movies recorded for two fields of view, before all data were quantified using the code described above. The results (Figure 4.7) show a visible to the eye increase both in the quantity of anchored IM proteoliposomes and the frequency of colocalized OM and IM proteoliposomes in the presence of LptA. IM liposomes stick to the surface only minimally, with or without LptA, if OM liposomes are not present (Figure 4.8), indicating that the LptA-induced anchoring is mediated by OM liposomes and is not directly to

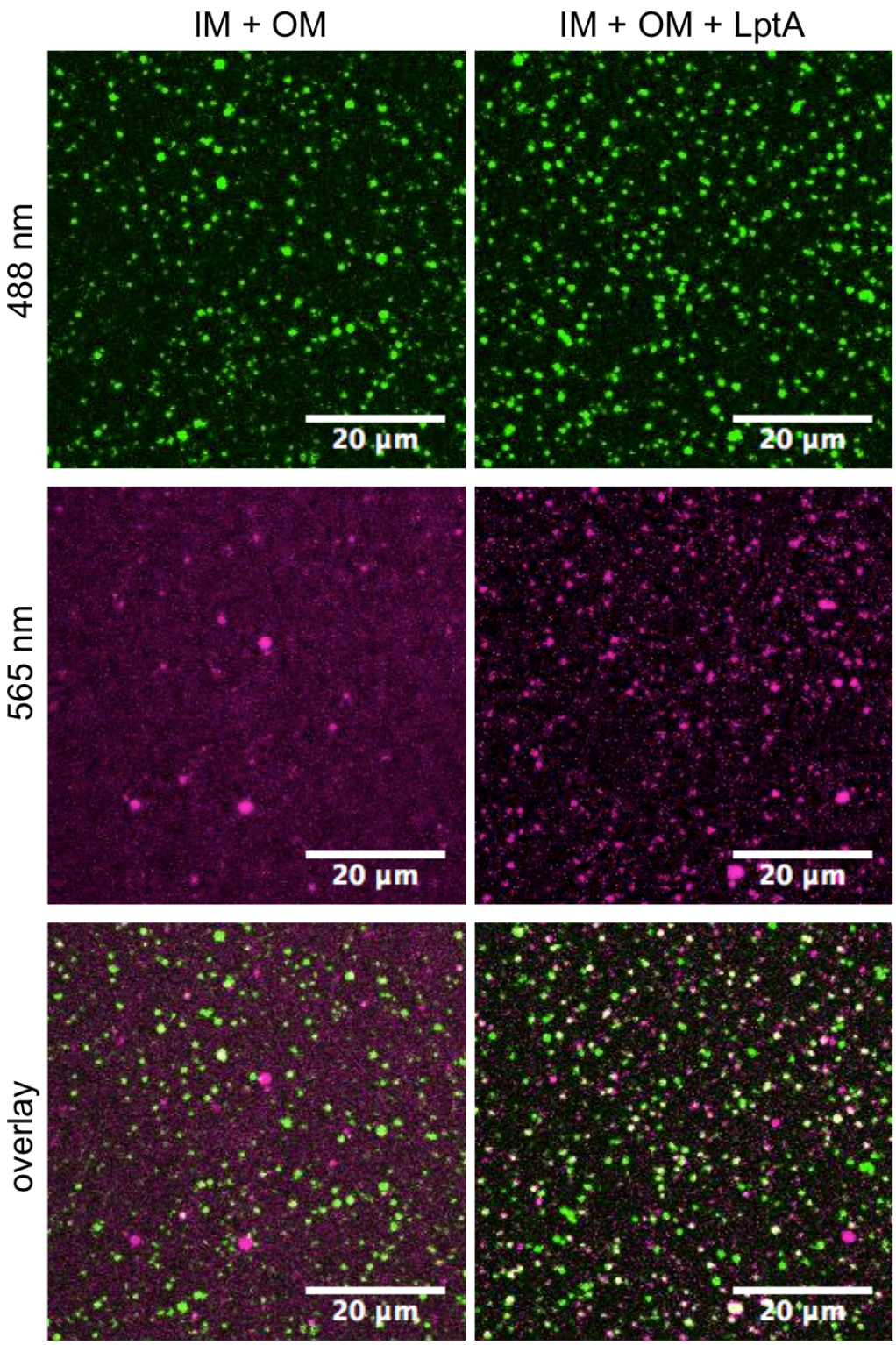

Figure 4.7: LptA leads to increased colocalization of IM and OM proteoliposomes. Including LptA leads to both more IM liposomes being anchored in total (565 nm channel, center), and leads to more overlapping signal in the overlaid image of both channels (overlay, bottom).

OM batch	IM batch	LptA	# OM Liposomes	# IM liposomes	IM/OM	# Pairs	% OM Paired
1	1	-	472	96	0.20	4	0.85
1	1	-	481	122	0.25	4	0.83
1	1	-	564	289	0.51	12	2.13
1	1	-	552	206	0.37	9	1.63
1	1	+	727	817	1.12	46	6.33
1	1	+	635	586	0.92	46	7.24
1	1	+	818	494	0.60	100	12.22
1	1	+	762	414	0.54	84	11.02
1	2	-	501	114	0.23	11	2.20
1	2	-	480	113	0.24	5	1.04
1	2	-	698	173	0.25	26	3.72
1	2	-	693	180	0.26	33	4.76
1	2	+	880	553	0.63	120	13.64
1	2	+	887	490	0.55	121	13.64
1	2	+	650	355	0.55	76	11.69
1	2	+	635	392	0.62	86	13.54
2	1	-	623	153	0.25	26	4.17
2	1	-	575	167	0.29	35	6.09
2	1	-	521	141	0.27	4	0.77
2	1	-	438	111	0.25	9	2.05
2	1	+	906	585	0.65	66	7.28
2	1	+	876	609	0.70	75	8.56
2	1	+	720	377	0.52	30	4.17
2	1	+	675	372	0.55	37	5.48
2	2	-	807	393	0.49	81	10.04
2	2	-	798	413	0.52	110	13.78
2	2	-	896	464	0.52	58	6.47
2	2	-	866	471	0.54	52	6.00
2	2	+	893	665	0.74	214	23.96
2	2	+	870	756	0.87	274	31.49
2	2	+	791	911	1.15	132	16.69
2	2	+	774	927	1.20	154	19.90
-	1	-	-	24	-	-	-
-	1	-	-	71	-	-	-
-	1	+	-	7	-	-	-
-	1	+	-	6	-	-	-
-	1	+	-	21	-	-	-
-	1	+	-	15	-	-	-

Table 4.1: Quantification of images collected using lipid-passivated coverslips.

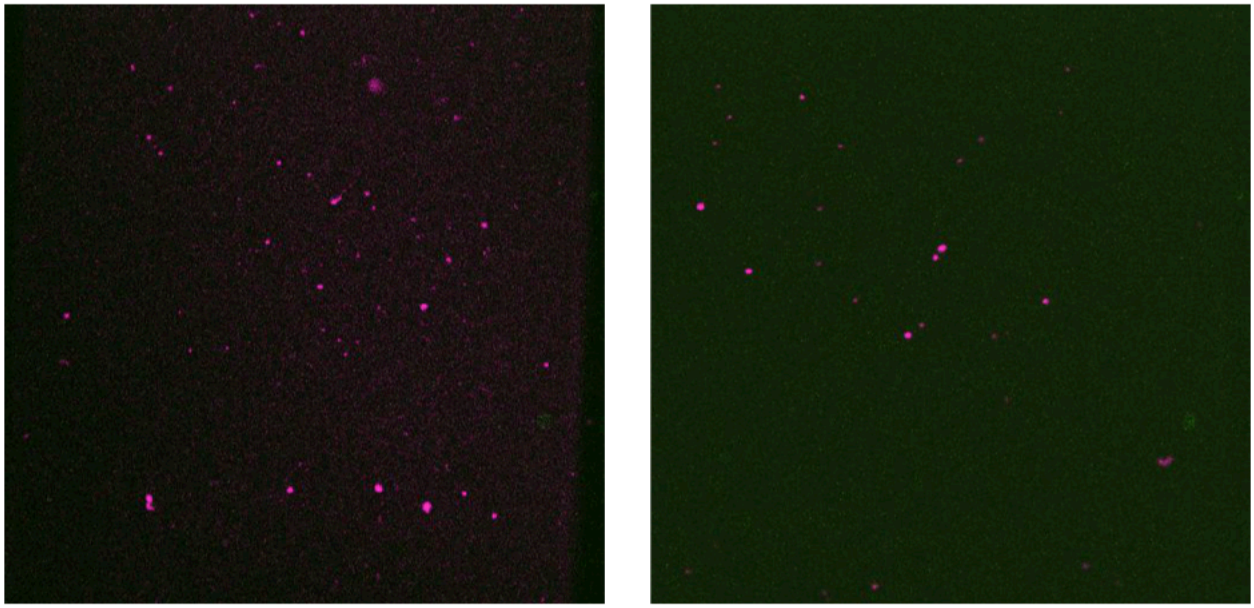

Figure 4.8: IM proteoliposomes stick to the surface only minimally without OM liposomes, without (left) or with (right) LptA present.

the surface. Quantification bears this out. The number of IM liposomes anchored without OM liposomes present is always lower than any instance when OM liposomes were included. For any given pair of preparations of IM and OM proteoliposome, the absolute number of IM anchored in a given field of view increased in the presence of LptA, as did the ratio of countable IM to OM proteoliposomes (Table 4.1). More importantly, the percentage of OM proteoliposomes with a colocalized IM proteoliposome increased in each case by at least two-fold, and as high as six-fold, with an average of a 3.93-fold increase in the presence of LptA (Table 4.2).

This LptA-dependent increase in liposome-liposome pairings is consistent with the bridge model of LPS transport, and indicates that we have reconstituted LPS transport through an LptA bridge, and confirms that we can quantify this difference. In contrast to the images obtained with TEM, liposome-liposome interactions appear as heterodimers, rather than as larger aggregates. Though this could be an artifact of our protocol, with sheer forces washing away larger aggregates, it seems more likely that this is a more accurate picture of liposomal association, as

the larger aggregates seen in TEM were seen only rarely. There is high variability from sample to sample, both in absolute number of liposomes (both IM and OM) anchored, and in the fraction in heterodimers, but the LptA-induced increase in heterodimer formation is always at least two-fold, indicating that while the degree may vary, there is a real LptA-dependent effect.

OM Batch	IM Batch	% OM paired w/o LptA	% OM Paired w/ LptA	Fold change with LptA
1	1	1.36 ± 0.63	9.21 ± 2.86	6.77
1	2	2.93 ± 1.64	13.1 ± 0.96	4.48
2	1	3.27 ± 2.34	6.37 ± 1.94	1.95
2	2	9.07 ± 3.62	23 ± 6.39	2.54
			Average	3.93 ± 2.18

Table 4.2: LptA consistently raises the fraction of paired OM liposomes, though with high variance. For percentage of OM liposomes paired, average is shown +/- standard deviation.

4.2.5: Issues with the passivating lipid bilayer limit its utility

While we were able to quantify liposomal aggregation using this technique, several problems arose preventing us from developing it further. The first was that several different negative controls failed, in that they led to an increase of nonspecific binding of the IM to the surface. Nus-his-LptA's large N-terminal Nus-tag is likely to prevent it from interacting with LptC, so it should prevent bridge formation. When Nus-his-LptA was used in an OM-free system, IM proteoliposomes were tethered to the surface more than when no LptA or nus-free LptA were used (Figure 4.9A). This suggests that Nus-his-LptA mediates non-specific binding of the IM proteoliposomes to the lipid bilayer on the coverslip surface in a way that nus-free LptA does not. Even more IM liposomes were tethered to the surface when combined with both Nus-

his-LptA and OM proteoliposomes, further suggesting that it interacts with the IM liposome via some mechanism that induces aggregation with other available lipid membranes (Figure 4.9B-C). These results shows Nus-his-LptA is not a negative control, and cast some doubt on the specificity of the LptA-dependent liposome-liposome interactions recorded earlier.

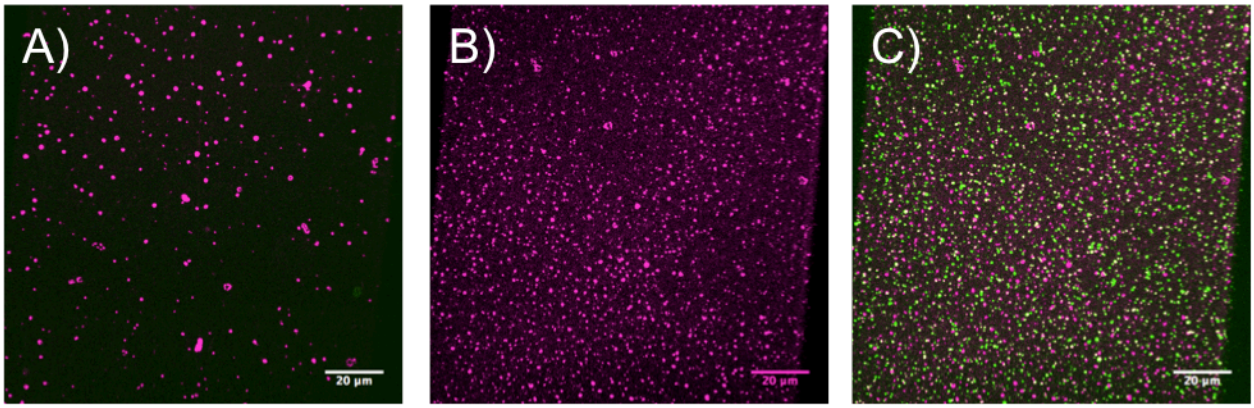

Figure 4.9: A) Nus-his-LptA induces surface binding of IM proteoliposomes without OM proteoliposomes. B) 565 nm channel for IM and OM proteoliposomes with Nus-his-LptA. IM binds more in the presence of OM than without. C) Dual-channel image for same sample as B.

We then tried liposomes that had been prepared without either LptB/F/G/C (in the case of the IM) or LptD/E (in the case of the OM) as negative controls. As these lacked the protein needed to form the bridge, they should show no LptA dependent difference in their interactions with the IM proteoliposomes. The empty IM liposomes stuck to the surface in great quantity, regardless of if LptA was present (Figure 4.10), suggesting that the LptB/F/G/C complex was actually preventing non-specific interactions. This was further supported by how IM was bound when both IM and OM liposomes lacked protein (Figure 4.11), implicating lipid-lipid interactions as a potential source of our problems. Most troublingly, we found that a great deal of colocalization between normal IM proteoliposomes and empty OM proteoliposomes could be seen, and was LptA dependent (Figure 4.12). This suggests that LptA is inducing liposome-

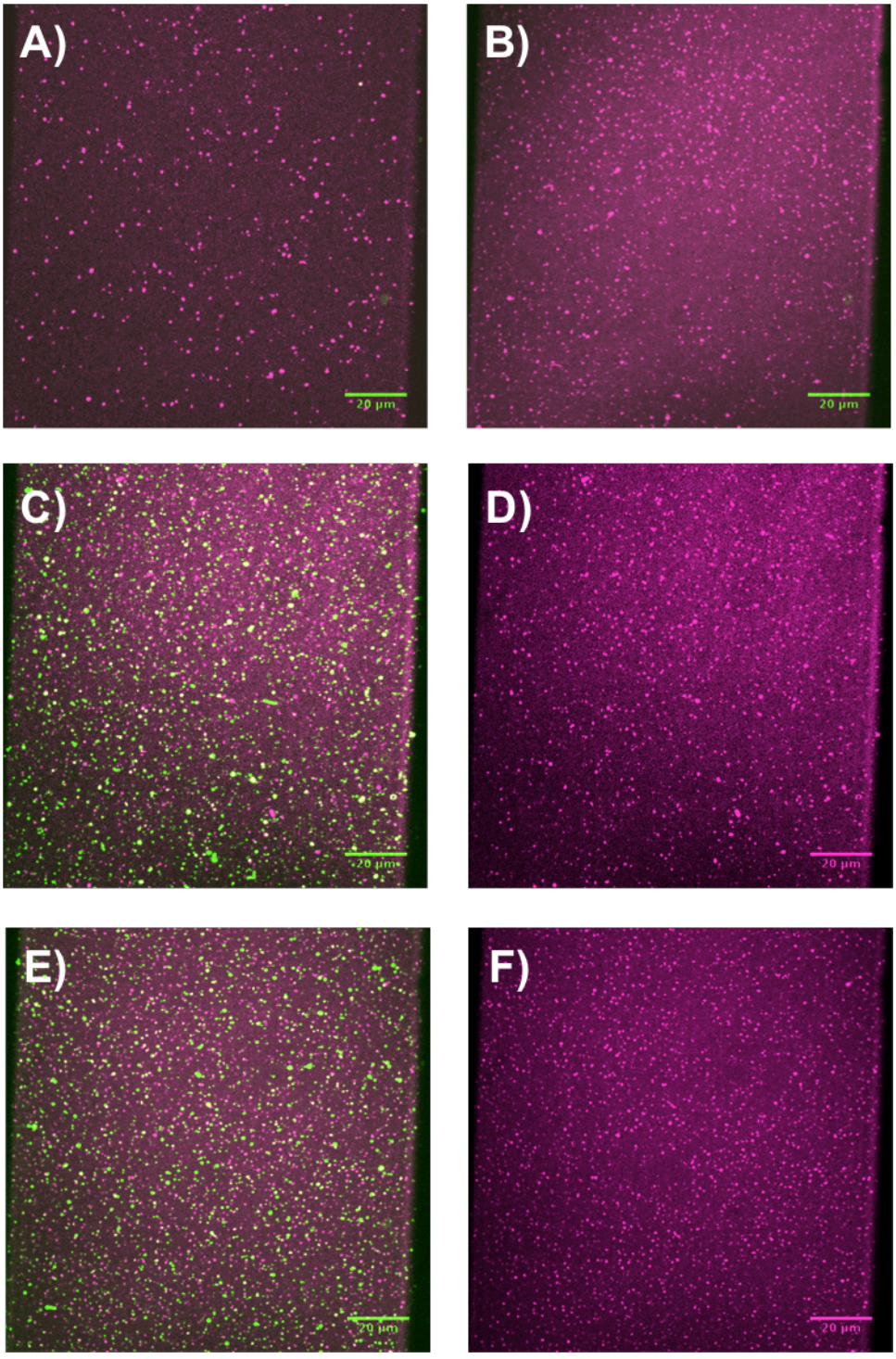

Figure 4.10: Surface binding of protein-free IM liposomes A) with neither LptA nor OM liposomes. B) With LptA. C) With OM liposomes. D) C, showing only the 565 nm channel for clarity. E) With OM liposomes and LptA. E) E, showing only the 565 nm channel for clarity.

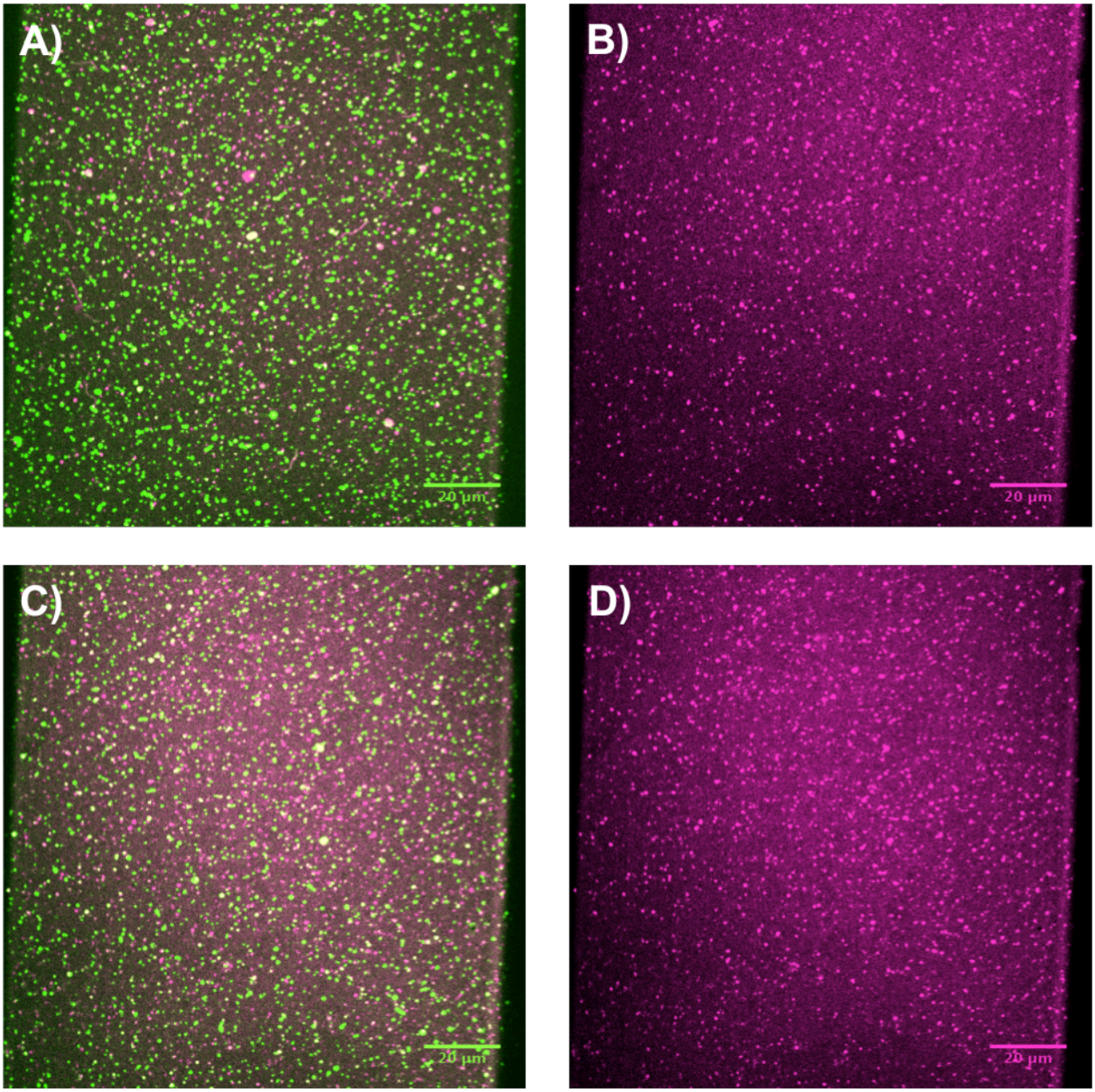

Figure 4.11: A) Empty IM and empty OM liposomes. B) A showing only the 565 nm channel for clarity. C) Empty IM and empty OM liposomes with LptA. D) C showing only the 565 nm channel for clarity.

liposome interactions without a need to form a bridge, and casts doubt on our earlier data. In addition, when collecting these data, it became apparent that the background signal, not associated with specific liposomes, was photobleaching, suggesting that liposomes are fusing to the surface bilayer. The presence of a bright band of fluorescence at the edges of the frame in

many images further suggested membrane fusion, as it is suggests that fluorescent lipids are diffusing in from out of frame and quickly photobleaching. We observed recovery of fluorescence after photobleaching, further supporting this model. This implicated our surface preparation in some of the problems with our failed negative controls. As multiple surface preparations attempted had led to their own unique problems, we sought out a means of quantifying liposomal interactions that did not rely on complicated surface preparations that might act on liposomes independent of the biotin-streptavidin anchor.

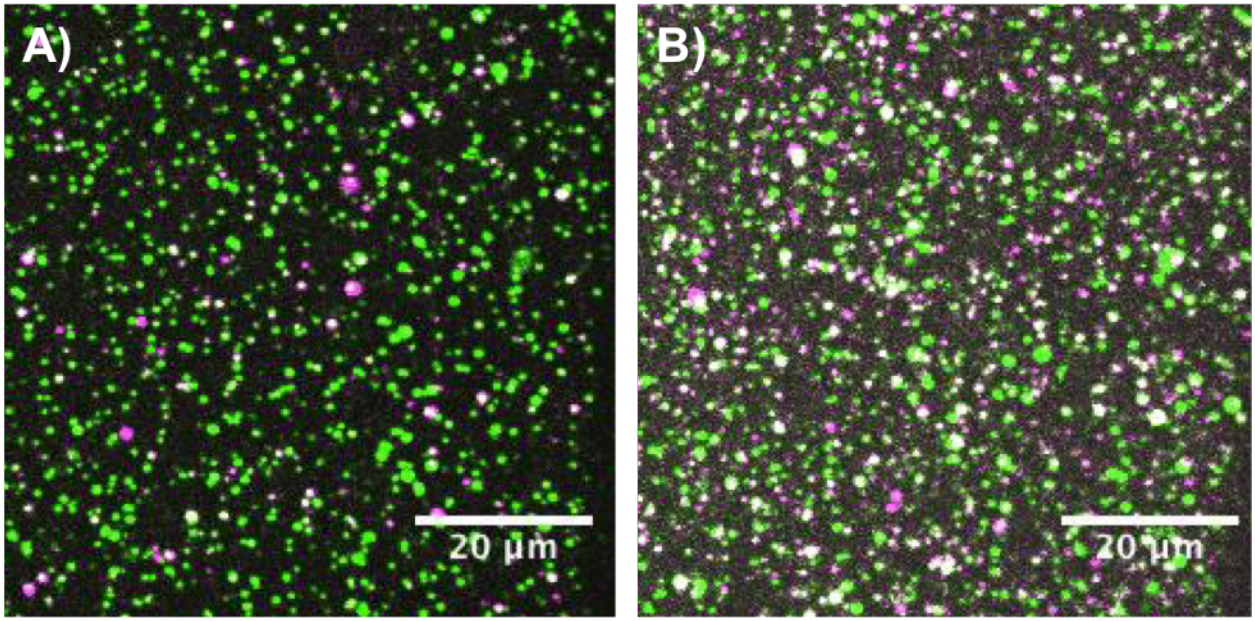

Figure 4.12: Empty OM leads to LptA dependent colocalization of OM and IM liposomes. A) Empty OM liposomes with normal IM liposomes. B) Empty OM liposomes with normal IM liposomes and LptA.

4.2.6: Flow cytometry shows an LptA-dependent shift in liposomal behavior, with functional negative controls.

To quantify liposomal interactions without troublesome surface preparations, we turned to fluorescent flow cytometry. Flow cytometry has previously been used to study liposomes [140], and does not require and specific surface chemistry. Rather than anchor the liposomes to count

them, microfluidic control allows each liposome to be counted individually as it passes by a laser. The same fluorescent labeling scheme used in microscopy can be deployed again, with signal in the 565 nm channel allowing us to count a particle as an IM proteoliposome and signal in the 488 nm channel indicating a particle is an OM proteoliposome. Signal in both channels would, in theory, thus represent an aggregate form of liposomes. As an initial test, IM and OM proteoliposomes were analyzed with a cytometer separately, confirming that they register as distinct, identifiable populations based on their fluorescent signals (Figure 4.13), allowing us to move forward with quantification of the reconstituted Lpt pathway.

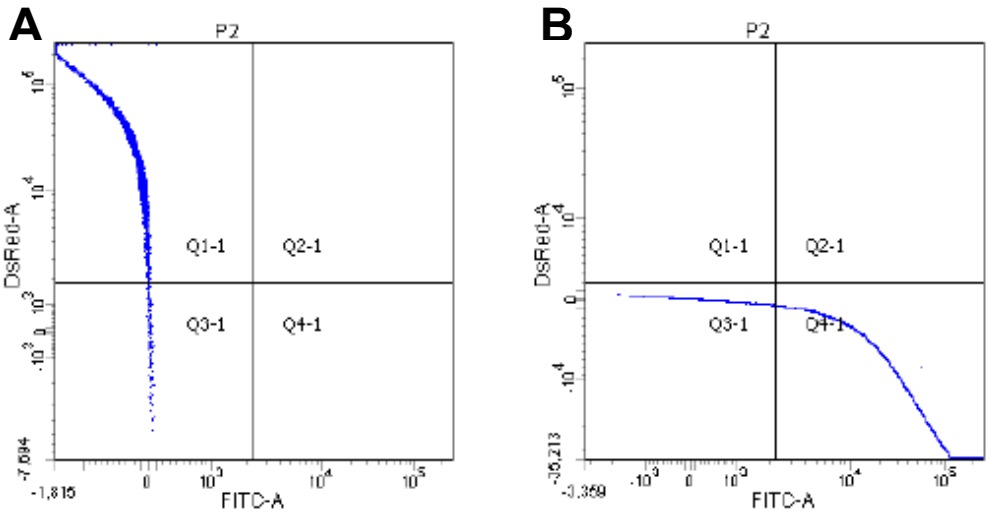

Figure 4.13: Flow cytometry can distinguish IM liposomes (A) from OM liposomes (B). IM shows signal exclusively in the DsRed channel, and OM shows signal exclusively in the FITC channel.

To determine if our issues with negative controls had been due to the surface or due to a deeper flaw in our reconstitution, we then used flow cytometry to analyze the whole reconstitution. In addition to analyzing the IM/OM proteoliposome mixture with and without LptA, we also looked at several negative controls: substituting Nus-his-LptA for unlabeled LptA, use of protein-free OM liposomes instead of those containing LptD/E, and use of OM liposomes

containing wild type LptE but mutant LptD without the N-terminal periplasmic domain leaving only the C-terminal β-barrel (cLptD/E) in lieu of wild type LptD. All of these except for the cLptD/E condition were tested with and without ATP, to see if aggregation was dependent on active LPS transport.

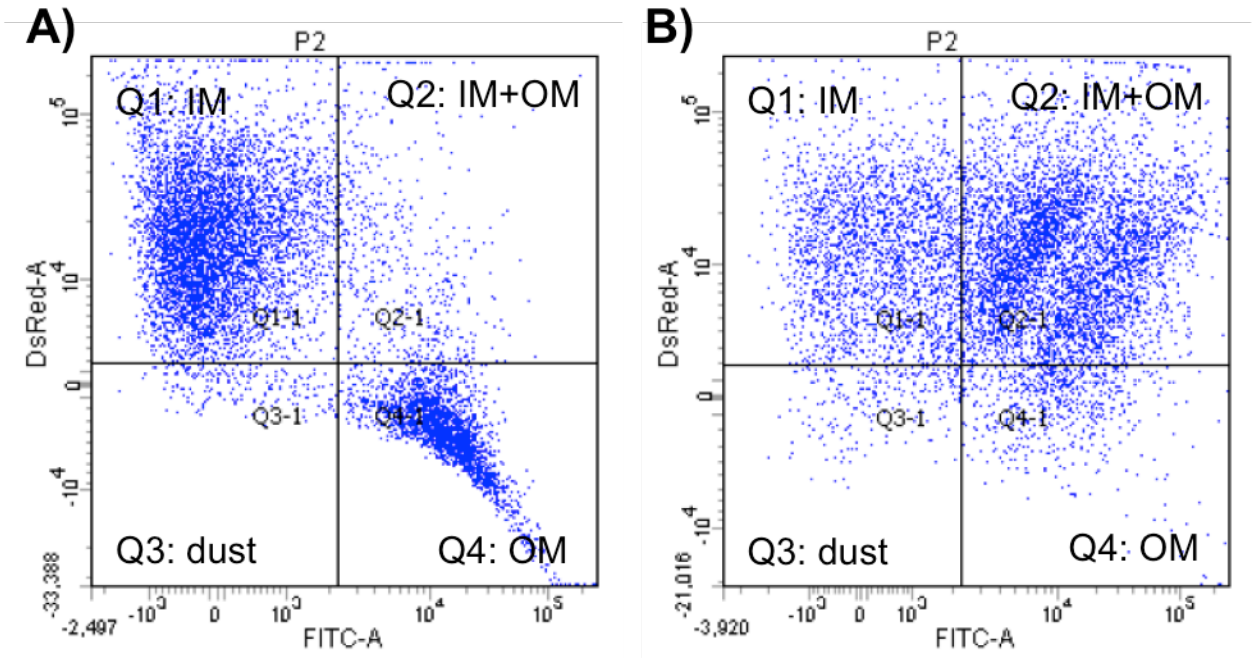

Figure 4.14: A) Without LptA, IM and OM sort as distinct populations. B) Addition of LptA leads to many particles showing fluorescent signal in both channels, indicating colocalization of IM and OM proteoliposomes.

None of the conditions save for the complete reconstitution showed a large population containing both (Figures 4.14-15, Table 4.3). In the complete reconstitution, there is a clear depletion of lone IM proteoliposomes, and very few lone OM proteoliposomes, while the quadrant representing both fluorophore signals is readily identified as the most populated. This is not seen in any other conditions, although there does appear to be a mild shift of sample into the dual-signal quadrant in the presence of Nus-his-LptA. The data show that there is no increase in aggregation induced by the presence of ATP under any conditions, indicating aggregation between liposomes is not dependent on the Lpt machinery actively transporting LPS.

Quantification shows that the complete reconstitution leads to 54-62% of particles containing both IM and OM proteoliposomes. In the other samples, only the Nus-his-LptA containing sample showed as much as 19% of particles to contain both proteoliposomes, with the rest containing less than 12%. If one assumes that each particle containing both fluorophores represents at least one IM and one OM proteoliposome, one can establish a lower bound for the percentage of the liposomes that are paired. No less than 81% of the OM liposomes and 65% of the IM liposomes are in some aggregate form in the complete reconstitution, numbers much higher than for any of the negative controls. This represents at least five to seven fold increase in aggregated IM proteoliposomes and a three to four fold increase in aggregated OM proteoliposomes relative to the condition lacking LptA, providing further evidence that LptA induces heteroliposomal aggregation. The negative controls, other than the Nus-his-LptA condition, show a similar lack of aggregation. The Nus-his-LptA condition shows at least 38-45% of OM liposomes and 22-26% of IM liposomes in aggregates, indicating that while it leads to aggregation, it leads to less than wild type LptA. This could be due either to Nus-his-LptA inducing non-specific interactions, of the alternate LptA construct could be forming interactions with LptC at a reduced efficiency relative to wild type.

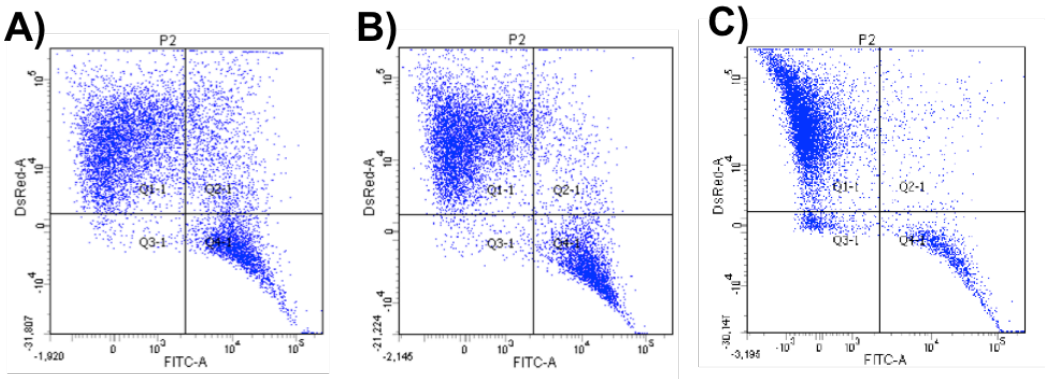

Figure 4.15 A) IM and OM proteoliposomes mixed with Nus-his-LptA show reduced presence of dual-signal particles relative to wild type LptA. B) IM proteoliposomes mixed with LptA and cDE-OM liposomes do not show a dual signal population. C) IM proteoliposomes mixed with empty OM liposomes and LptA do not show a dual signal population.

IM	OM	LptA	ATP	IM as % of total	OM as % of total	Aggregates as % of total	% of IM in aggregates	% of OM in aggregates
+	+	-	+	62.5 ± 2.7	26.3 ± 1.9	8.7 ± 0.6	12.2 ± 1.2	24.8 ± 0.9
+	+	-	-	62.8 ± 2.5	28.4 ± 1.3	6.7 ± 0.7	9.6 ± 1.2	19.0 ± 1.1
+	+	+	+	29.1 ± 1.3	12.1 ± 1.0	54.4 ± 0.9	65.2 ± 1.3	81.8 ± 1.2
+	+	+	-	27.8 ± 0.5	7.3 ± 0.5	62.4 ± 0.9	69.2 ± 0.7	89.6 ± 0.7
+	+	Nus-LptA	+	56.1 ± 2.3	26.1 ± 1.2	16.2 ± 0.7	22.4 ± 1.5	38.3 ± 0.1
+	+	Nus-LptA	-	55.1 ± 3.8	23.2 ± 2.4	19.0 ± 0.6	25.7 ± 1.9	45.2 ± 1.8
+	cDE	+	+	60.5 ± 2.2	30.4 ± 1.7	6.7 ± 0.1	10.0 ± 0.4	18.2 ± 0.9
+	cDE	+	-	61.7 ± 1.0	25.9 ± 0.9	9.9 ± 0.2	13.8 ± 0.0	27.6 ± 1.0
+	Empty	+	+	77.8 ± 4.1	10.1 ± 0.8	2.6 ± 0.6	3.2 ± 0.6	20.3 ± 2.4

Table 4.3: Quantification of preliminary flow cytometry analysis of the reconstitution indicates that LptA induced association between liposomes, and that this requires all Lpt proteins to be present in their wild type forms. Some increase in association is seen with Nus-LptA, indicating that it is either partially competent in bridge formation, or it induces non-specific associations.

All of the above data suggest that LptA leads to interactions between IM and OM proteoliposomes, and thus that we have reconstituted LPS transport via a bridge between liposomes. Removal of bridge components, be they LptA, LptD/E, or even the bridge-forming domain of LptD, all lead to a lack of aggregation, and a hobbled form of LptA is less capable of inducing aggregates, indicating that it is the LptC/A/D bridge that is needed for association. The lack of non-specific binding in the negative controls indicates that the issues faced in earlier microscopy experiments were due to issues with the liposomes interactions with the various surface preparations, rather than due to non-specific interactions inherent to the system. We have established flow cytometry as a tool for quantifying liposomal associations that lacks the problems associated with microscopy.

4.2.6: Imaging of sorted liposomal populations

Imaging of sorted populations of liposomes allowed us to overcome the limitations of both microscopy and flow cytometry. While flow cytometry quantifies the degree of aggregation more readily than microscopy, it remains unclear what form the heteroliposomal aggregates take.

We can infer the rough ratio of OM to IM liposomes in all of the aggregates counted, but we cannot tell how many liposomes are involved in a given aggregate particle. Furthermore, cytometry does not distinguish between association and fusion of liposomes. To address these issues, and to confirm that the particles showing signal in both fluorescent channels are indeed aggregates including both IM and OM liposomes, we combined microscopy with flow cytometry, imaging liposomes after they have been sorted into different populations.

While there have been troubles with microscopy in the past, using it in combination with flow cytometry should alleviate many of these. We no longer need the microscopy to be quantitative, as quantification is now provided by flow cytometry. What microscopy can provide is direct visualization of the different populations of proteoliposomes after they have been sorted and isolated by the flow cytometer. In addition, we no longer need to rely on complicated surface chemistries to simultaneously isolate paired liposomes while minimizing binding of unpaired liposomes. The isolation of aggregated liposomes will already have happened; the goal is to confirm aggregation in populations showing both signals, and to confirm lack of contamination in populations showing only one signal. Instead of complicated sample chambers, we can use the simpler, more traditional technique of squashes. To prepare squashes, a small volume (4 μL) of sample is deposited on a slide, and a coverslip is gently dropped directly onto the sample. Both coverslip and slide are untreated. Liposomes stick to bare glass, and there is too little total volume of sample for there to be significant free-floating liposomes.

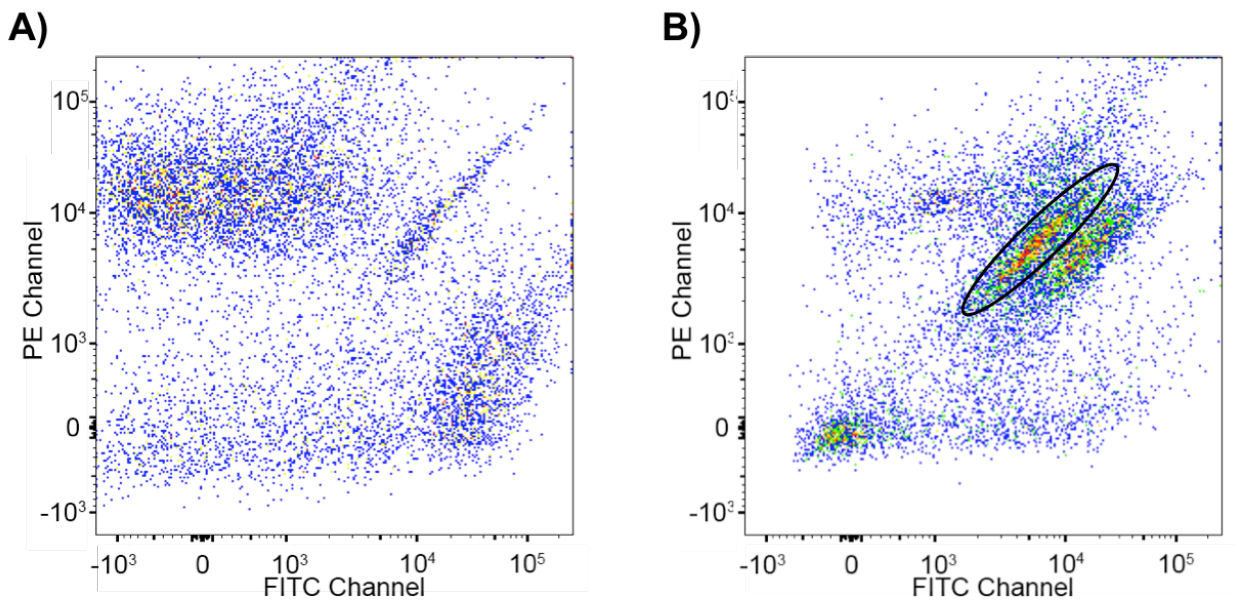

Figure 4.16: Sorting larger populations confirms LptA-induced association, and reveals two different associated populations. A) IM and OM liposomes without LptA generate only a small population of particles with both fluorophores. B) Mixing IM and OM liposomes with LptA leads to mostly particles with signals for both fluorophores. A new second population (circled) is readily identifiable among particles containing both fluorophores, close to where the small population dual-signal particles in the –LptA sample.

Improved flow cytometry revealed the existence of a new population of colocalized liposomes. Our flow cytometry protocol needed adapting to be able to generate sufficiently large populations for imaging. We switched from a cell analyzer, incapable of retaining liposomes analyzed, to a cell sorter, capable of isolating droplets that contained specific liposomes, and increased the volume of the reconstitution analyzed. In addition, as cytometry had provided us with measurement of the relative concentration, by number, of each liposome, we were able to adjust our concentrations to have equal numbers of IM and OM liposomes. The sorted colocalized population, when sorted by the cytometer a second time, continued to present as one population showing signal in both channels, indicating the stability of any association. In these new conditions, it became apparent that there were two populations of liposomes showing both fluorophore signals with the addition of LptA (Figure 4.16B). This could be either sets of liposomes that had aggregated at a different ratio of IM:OM liposomes, or one could perhaps be

a set of liposomes non-specifically aggregated via a means other than the Lpt bridge. This last possibility is supported by the presence of a smaller population of dual-signal particles in the LptA-free condition (Figure 4.16A).

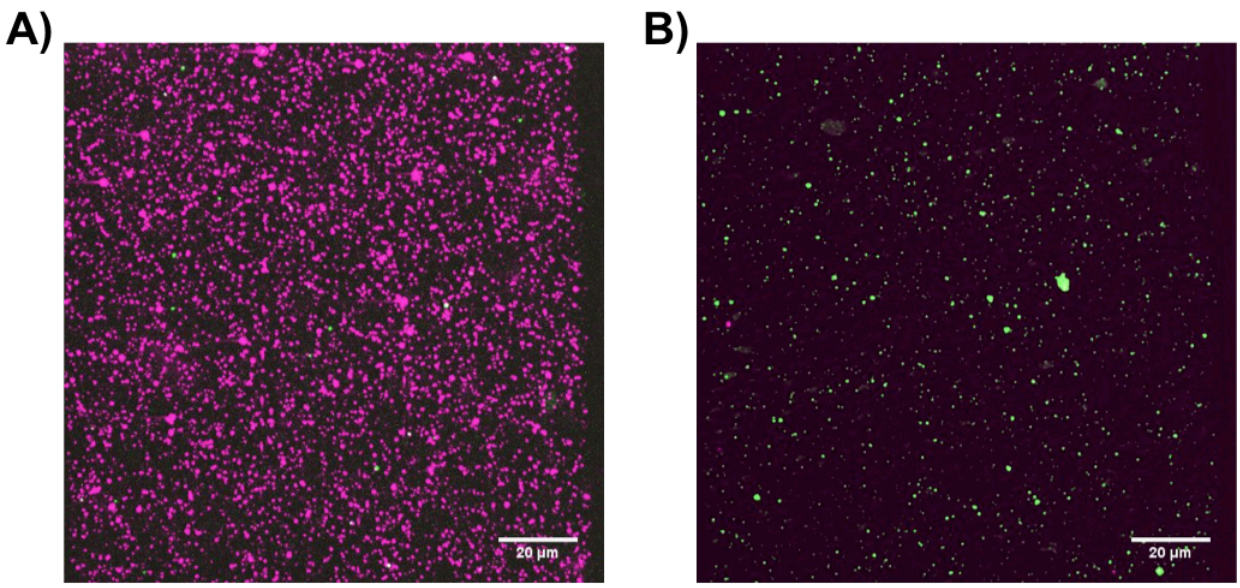

Figure 4.17: Populations of particles showing signal for only one fluorophore show little contamination. A) The sorted IM population shows only a few green OM liposomes. B) The sorted OM population shows only a few pink IM liposomes.

Microscopy confirmed that we had isolated pairs of IM and OM proteoliposomes, showed that the second dual-signal population was less stably associated. The populations showing significant signal in only a single channel, when imaged via squash samples, proved to be composed of almost entirely the IM or OM proteoliposomes expected, with little contamination (Figure 4.17), confirming that flow cytometry sorts liposomes accurately. Both of the populations showing signal in both channels showed both IM and OM liposomes as squash samples, but were otherwise very different. The population with slightly less FITC signal showed both IM and OM liposomes, but no significant colocalization (Figure 4.18, left), indicating that any liposome-liposome association formed in this population was fleeting. The

population with slightly more FITC signal showed both IM and OM populations at greater density, and showed an astonishing degree of colocalization between IM and OM proteoliposomes (Figure 4.18, right), indicating that the population sorted via flow cytometry consists of stably associated IM and OM proteoliposomes.

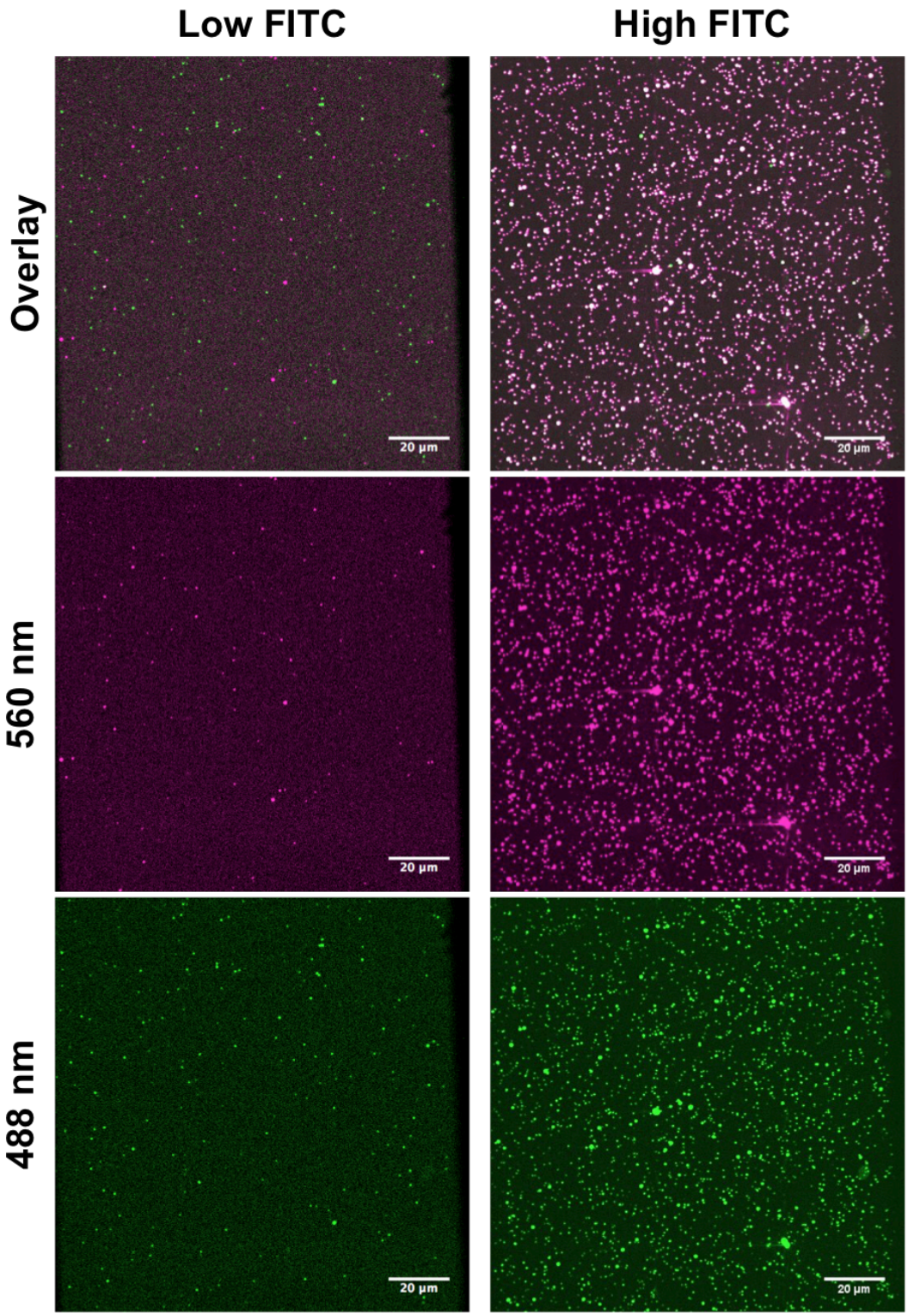

Figure 4.18: Microscopy reveals the difference between the two populations containing both liposomes. Both populations contain both IM and OM liposomes, but overlay (top) of the 560 nm (IM) channel (middle) and the 488 nm (OM) channel (bottom) reveals that the population showing a higher FITC signal according to the cytometer both has more liposomes, and a much greater incidence of colocalization between IM and OM liposomes.

4.2.7: Discussion and future work

As we have shown, the association between IM and OM liposomes— which can be quantified via fluorescent flow cytometry and confirmed visually via confocal microscopy—is both LptA-dependent and dependent on protein-protein interactions of the Lpt pathway. Removing LptA prevents this association entirely, while removing the N-terminus of LptD or adding a large Nus-tag to the LptC-interacting site of LptA also prevents or hinders this association. Preliminary quantification suggests that absent LptA, very few liposomes are associated but in the presence of LptA, the vast majority of liposomes are associated; this is consistent with a bridge model for LPS transport but not with a periplasmic shuttle model. Acting as a soluble periplasmic shuttle, LptA might bring liposomes into brief association; because it would only interact with LptC and LptD in sequence, it is hard to see how this would lead to association rates as high as we have observed. In addition, liposome-liposome associations identified via flow cytometry are stable, surviving multiple rounds of sorting in the cytometer as well as sheer forces in preparation for squash analysis, we can therefore conclude that the reconstitution of LPS transport requires conditions that lead to LptA-mediated, stable liposome-liposome associations; this is consistent with the Lpt bridge model and confirms that LPS transport does indeed proceed via a bridge. Because the bridge could transduce energy from the hydrolysis of ATP by LptB to the LptD/E translocon in the OM, it is thus possible that the final steps of LPS transport are energy dependent. The data do suggest the presence of non-bridge interactions between liposomes as well, consistent with the non-specific interactions seen in earlier microscopic studies; without LptA, a smaller population of liposomes associate in an unstable form, as judged by the lack of colocalization seen with it under the microscope.

The reconstitution is not yet truly complete. The recent flow cytometry and microscopy data are a step forward, but it must be repeated with additional sets of liposomes; in addition, the controls used for cytometry have yet to be imaged.

We also require confirmation that the liposomal associates we have seen are separate liposomes rather than IM and OM liposomes that have fused. We see two experimental strategies to addressing this issue: first, if an excess of non-fluorescent liposomes were be added to a mixture IM and OM liposomes and LptA that had been allowed to associate, a fall-off in association would demonstrate that the associations in the original mixture were reversible via competition, as would be impossible for fused liposomes; second, if traditional fluorophore dilution assays, in which one liposome is doped with lipids containing a FRET pair of fluorophores, were used, fused liposomes would lead to an increase in the average distance between the FRET donor and acceptor, observable by a decrease in FRET signal and an increase in unquenched fluorescent signal from the donor [141] [142].

Finally, we lack a readout of LPS being integrated into leaflet on the inside of the OM liposomes. Ran Xie, a fellow researcher in the Kahne lab, is developing a fluorescent probe, based on polymyxin, for this purpose. Once the cytometry controls have been imaged and the fluorescent probe has been incorporated into the OM liposomes, the reconstitution will allow us to monitor the comparative LPS transport efficiencies of different Lpt pathway mutants, such as the LptE R91D K136D mutant described in chapter 2. It will also allow us to measure how LPS transport efficiency is altered by changes to the LPS molecule.

To date, all our work has been done with Ra-LPS produced by a *K-12* strain of *E. coli*, which lacks the O-antigen and lipid A modifications. In addition to working toward the complete reconstitution, Kahne lab researcher Becca Taylor is studying mutations to Lpt proteins that we

believe correspond to changes in LPS modification; with the complete reconstitution, she will be better able to decipher the interplay between modifications of LPS and mutations to Lpt proteins in how they affect LPS transport.

The research detailed here has brought us a step closer to a complete reconstitution of LPS transport; with these data strongly suggesting an LptA-dependent bridge model, future researchers in the Kahne lab and elsewhere are poised to look ever more closely into LPS transports and changes to LPS.

4.3: Materials and Methods

Preparation and assessment of liposomes

Proteins and proteoliposomes were prepared as per the protocols of Sherman and Okuda[95], with a few exceptions noted below. In brief, purified LptB/F/G/C or purified LptD-Y112Am/LptE were incorporated into liposomes via the rapid detergent dilution method[143]. IM liposomes always contained 1% Ra-LPS (Sigma) by molar lipid content. ATPase activity of IM liposomes was confirmed via phosphate release assay, with empty liposomes used to make the standard curves[68 144 145]. LPS transport activity was confirmed by mixing IM and OM proteoliposomes in the presence of excess LptA and 0.1 mM ATP; samples were incubated at 30° C for 45 minutes, and placed on ice under a UV lamp for five minutes before quenching with Anzergent 3-14 (Anatrace) and TCA precipitating the samples. The LptD-LPS crosslink was confirmed via western blot.

For confocal microscopy and flow cytometry, all proteoliposomes were prepared with fluorescent DPPE (Atto-tec) as 1% of total lipid content, with IM proteoliposomes being labeled with Atto-565 and OM proteoliposomes being labeled with Atto-488. In cases where liposomes

were tethered to a surface, 1% of total lipid content was 18:0 PE with biotin attached to the headgroup via a PEG-2000 linker (Avanti).

Cryo-TEM

Liposomes were mixed as for the LPS transport activity assay, but without ATP, pipetted onto a carbon grid, and flash frozen in liquid ethane under the guidance of Harvard CNS staff. This was done with and without LptA. Samples were imaged on an FEI Tecnai Arctica CryoTEM.

Imaging of free-floating liposomes

Sample chambers were prepared by two pieces of double-sided tape of a glass slide to create a channel approximately 2mm wide, and placing a glass coverslip. Samples were prepared as for LPS crosslinking, and added to the chamber, which was then sealed at each end with candlewax. Samples were imaged on the Needleman lab's inverted confocal spinning disk microscope (Hamamatsu, Nikon) using μManager software (Open Imaging)[146]. Samples were kept at 30° C during imaging. Images were analyzed using ImageJ software (NIH)[147].

Imaging of surface-tethered liposomes

Pluronic passivated chambers were prepared according to Dixit and Ross[148]. Lipid-passivated coverslips were prepared in the following roundabout manner: prior to assembly of sample chambers, coverslips were sonicated for 30 minutes in 3M KOH, washed extensively with ultrapure water, sonicated for 30 minutes in ethanol, washed extensively with ultrapure

water, and sonicated for 10 minutes in ultrapure water, before being dried under a nitrogen stream and left in a 70° C drying oven until use. Immediately prior to sample chamber assembly, coverslips were treated with a plasma wand for 10 minutes. Empty liposomes consisting of 10 mg/ml Egg-PC (Avanti) with 0.008% (by molarity) biotin-PEG2000-18:0-PE in lipid buffer (10 mM Tris-HCl pH = 7.8, 100 mM NaCl) were prepared by sonication, and stored at -80° C until use. These liposomes were diluted to 0.5 mg/ml in lipid buffer immediately before injection into the sample chamber, and were incubated in the chamber for 30 minutes at 37° C. Excess lipids were washed out with 1X PBS pH = 7.4, and 0.1 mg/ml streptavidin (Life Technologies) in 1X PBS was added, and incubated at room temperature for 15 minutes before being washed out with reaction buffer. Liposome samples were prepared as for the reconstitution, but without ATP, and incubated at reconstitution concentrations for 15 minutes on ice. Immediately before addition to the samples chamber, samples were diluted 1:100 in reaction buffer using a broad-mouthed pipet tip and mixed only by gentle inversion. Samples incubated in the samples chambers for 15 minutes at room temperature, before unbound liposomes were washed out with 20 μl of reaction buffer. Chambers were then sealed with candle wax to prevent evaporation. Samples were imaged as in 4.3.3, and processed using Matlab (Mathworks)

Flow Cytometry and imaging of squash samples

The reconstitution was prepared as per usual. Quantitative analysis was performed on a BD LSRII (BD Biosciences). Cell sorting was performed on a BD FACS Aria Cell Sorter (BD Biosciences). All cytometry was done with the assistance of the Bauer core staff. 4 μl of sorted liposomes were pipetted onto a glass slide, and a glass coverslip was gently dropped directly onto the sample. Samples were imaged as above.

References

1. Silhavy, T. J., Kahne, D. & Walker, S. The bacterial cell envelope. *Cold Spring Harbor Perspectives in Biology* **2,** a000414–a000414 (2010).

2. H Nikaido, M. V. Molecular basis of bacterial outer membrane permeability. *Microbiological Reviews* **49,** 1 (1985).

3. Nikaido, H. Molecular basis of bacterial outer membrane permeability revisited. *Microbiol. Mol. Biol. Rev.* **67,** 593–656 (2003).

4. Raetz, C. R. H. & Whitfield, C. Lipopolysaccharide endotoxins. *Annu. Rev. Biochem.* **71,** 635–700 (2002).

5. Ruiz, N., Kahne, D. & Silhavy, T. J. Transport of lipopolysaccharide across the cell envelope: the long road of discovery. *Nat Rev Micro* **7,** 677–683 (2009).

6. Okuda, S., Sherman, D. J., Silhavy, T. J., Ruiz, N. & Kahne, D. Lipopolysaccharide transport and assembly at the outer membrane: the PEZ model. *Nat Rev Micro* **14,** 337–345 (2016).

7. Simpson, B. W., May, J. M., Sherman, D. J., Kahne, D. & Ruiz, N. Lipopolysaccharide transport to the cell surface: biosynthesis and extraction from the inner membrane. *Philos. Trans. R. Soc. Lond., B, Biol. Sci.* **370,** 20150029 (2015).

8. May, J. M., Sherman, D. J., Simpson, B. W., Ruiz, N. & Kahne, D. Lipopolysaccharide transport to the cell surface: periplasmic transport and assembly into the outer membrane. *Philos. Trans. R. Soc. Lond., B, Biol. Sci.* **370,** 20150027 (2015).

9. Graham, L. L., Harris, R., Villiger, W. & Beveridge, T. J. Freeze-substitution of gram-negative eubacteria: general cell morphology and envelope profiles. *Journal of Bacteriology* **173,** 1623–1633 (1991).

10. Wülfing, C. & Plückthun, A. Protein folding in the periplasm of Escherichia coli. *Molecular Microbiology* **12,** 685–692 (1994).

11. Malinverni, J. C. & Silhavy, T. J. An ABC transport system that maintains lipid asymmetry in the Gram-negative outer membrane. *Proc. Natl. Acad. Sci.* **106**, 8009-8014 (2009).

12. Whitfield, C. & Trent, M. S. Biosynthesis and export of bacterial lipopolysaccharides. *Annu. Rev. Biochem.* **83,** 99–128 (2014).

13. Okuda, S. & Tokuda, H. Lipoprotein Sorting in Bacteria. *Annu. Rev. Microbiol.* **65,** 239–259 (2011).

14. Hagan, C. L., Silhavy, T. J. & Kahne, D. β-Barrel Membrane Protein Assembly by the Bam Complex. *Annu. Rev. Biochem.* **80,** 189–210 (2011).

15. Nikaido, H. Multidrug resistance in bacteria. *Annu. Rev. Biochem.* **78,** 119–146 (2009).

16. Boucher, H. W. *et al.* Bad bugs, no drugs: no ESKAPE! An update from the Infectious Diseases Society of America. *Clin. Infect. Dis.* **48,** 1–12 (2009).

17. Services, U. D. O. H. A. H. *Antibiotic Resistance Threats in the United States, 2013*. (Atlanta: CDC, 2013).

18. Carpenter, C. F. & Chambers, H. F. Daptomycin: another novel agent for treating infections due to drug-resistant gram-positive pathogens. *Clin. Infect. Dis.* **38,** 994–1000 (2004).

19. Fowler, V. G. *et al.* Daptomycin versus standard therapy for bacteremia and endocarditis caused by Staphylococcus aureus. *N Engl J Med* **355,** 653–665 (2006).

20. Lesher, G. Y., Froelich, E. J. & Gruett, M. D. 1, 8-Naphthyridine derivatives. A new class of chemotherapeutic agents. *J. Med. Chem.* **5,** 1063–1065 (1962).

21. Mauldin, P. D., Salgado, C. D., Hansen, I. S., Durup, D. T. & Bosso, J. A. Attributable hospital cost and length of stay associated with health care-associated infections caused by antibiotic-resistant gram-negative bacteria. *Antimicrob. Agents Chemother.* **54,** 109–115 (2010).

22. Peleg, A. Y. & Hooper, D. C. Hospital-Acquired Infections Due to Gram-Negative Bacteria. *N Engl J Med* **362,** 1804–1813 (2010).

23. Li, J. *et al.* Colistin: the re-emerging antibiotic for multidrug-resistant Gram-negative bacterial infections. *Lancet Infect Dis* **6,** 589–601 (2006).

24. Cai, Y., Chai, D., Wang, R., Liang, B. & Bai, N. Colistin resistance of Acinetobacter baumannii: clinical reports, mechanisms and antimicrobial strategies. *J. Antimicrobial Chemotherapy* **67**, 1607-1615 (2012).

25. Liu, Y.-Y. *et al.* Emergence of plasmid-mediated colistin resistance mechanism MCR-1 in animals and human beings in China: a microbiological and molecular biological study. *Lancet Infect Dis* **16,** 161–168 (2016).

26. Du, H., Chen, L., Tang, Y.-W. & Kreiswirth, B. N. Emergence of the mcr-1 colistin resistance gene in carbapenem-resistant Enterobacteriaceae. *Lancet Infect Dis* **16,**

287–288 (2016).

27. Muhlradt, P. F. & Golecki, J. R. Asymmetrical Distribution and Artifactual Reorientation of Lipopolysaccharide in the Outer Membrane Bilayer of Salmonella typhimurium. *Eur J Biochem* **51,** 343–352 (1975).

28. Kamio, Y. & Nikaido, H. Outer membrane of Salmonella typhimurium: accessibility of phospholipid head groups to phospholipase C and cyanogen bromide activated dextran in the external medium. *Biochemistry* **15,** 2561–2570 (1976).

29. Funahara, Y. & Nikaido, H. Asymmetric localization of lipopolysaccharides on the outer membrane of Salmonella typhimurium. *Journal of Bacteriology* **141,** 1463–1465 (1980).

30. Stevenson, G. *et al.* Structure of the O antigen of Escherichia coli K-12 and the sequence of its rfb gene cluster. *Journal of Bacteriology* **176,** 4144–4156 (1994).

31. Plesiat, P. & Nikaido, H. Outer membranes of gram-negative bacteria are permeable to steroid probes. *Molecular Microbiology* **6,** 1323–1333 (1992).

32. Plesiat, P., Aires, J. R., Godard, C. & Köhler, T. Use of steroids to monitor alterations in the outer membrane of Pseudomonas aeruginosa. *Journal of Bacteriology* **179,** 7004–7010 (1997).

33. Plesiat, P. & Vaara, M. Outer membrane permeability of the antibiotic-supersusceptible lipid A mutants of Escherichia coli to hydrophobic steroid probes. *Journal of Antimicrobial Chemotherapy* **43,** 608–610 (1999).

34. Vaara, M. Antibiotic-supersusceptible mutants of Escherichia coli and Salmonella typhimurium. *Antimicrob. Agents Chemother.* **37,** 2255–2260 (1993).

35. de Cock, H., Brandenburg, K., Wiese, A., Holst, O. & Seydel, U. Non-lamellar structure and negative charges of lipopolysaccharides required for efficient folding of outer membrane protein PhoE of Escherichia coli. *J. Biol. Chem.* **274,** 5114–5119 (1999).

36. Sen, K. & Nikaido, H. Lipopolysaccharide structure required for in vitro trimerization of Escherichia coli OmpF porin. *Journal of Bacteriology* **173,** 926–928 (1991).

37. Takeuchi, Y. & Nikaido, H. Persistence of segregated phospholipid domains in phospholipid--lipopolysaccharide mixed bilayers: studies with spin-labeled phospholipids. *Biochemistry* **20,** 523–529 (1981).

38. Coughlin, R. T., Tonsager, S. & McGroarty, E. J. Quantitation of metal cations bound to membranes and extracted lipopolysaccharide of Escherichia coli.

Biochemistry **22,** 2002–2007 (1983).

39. Galanos, C. & Lüderitz, O. Electrodialysis of lipopolysaccharides and their conversion to uniform salt forms. *Eur J Biochem* **54,** 603–610 (1975).

40. Kotra, L. P., Golemi, D., Amro, N. A., Liu, G.-Y. & Mobashery, S. Dynamics of the Lipopolysaccharide Assembly on the Surface of Escherichiacoli. *Biochemistry* **121,** 8707–8711 (1999).

41. Raetz, C. R. H., Reynolds, C. M., Trent, M. S. & Bishop, R. E. Lipid A Modification Systems in Gram-Negative Bacteria. *Annu. Rev. Biochem.* **76,** 295–329 (2007).

42. Osborn, M. J., Gander, J. E. & Parisi, E. Mechanism of assembly of the outer membrane of Salmonella typhimurium. Site of synthesis of lipopolysaccharide. *J. Biol. Chem.* **247,** 3973–3986 (1972).

43. Raetz, C. R. H. *et al.* Discovery of new biosynthetic pathways: the lipid A story. *The Journal of Lipid Research* **50,** S103–S108 (2008).

44. Meredith, T. C., Aggarwal, P., Mamat, U., Lindner, B. & Woodard, R. W. Redefining the requisite lipopolysaccharide structure in Escherichia coli. *ACS Chem. Biol.* **1,** 33–42 (2006).

45. Lee, H., Hsu, F.-F., Turk, J. & Groisman, E. A. The PmrA-regulated pmrC gene mediates phosphoethanolamine modification of lipid A and polymyxin resistance in Salmonella enterica. *Journal of Bacteriology* **186,** 4124–4133 (2004).

46. Arroyo, L. A. *et al.* The pmrCAB operon mediates polymyxin resistance in Acinetobacter baumannii ATCC 17978 and clinical isolates through phosphoethanolamine modification of lipid A. *Antimicrob. Agents Chemother.* **55,** 3743–3751 (2011).

47. Werneburg, M. *et al.* Inhibition of lipopolysaccharide transport to the outer membrane in Pseudomonas aeruginosa by peptidomimetic antibiotics. *ChemBioChem* **13,** 1767–1775 (2012).

48. Guo, L. *et al.* Regulation of Lipid A Modifications by *Salmonella typhimurium* Virulence Genes *phoP-phoQ*. *Science* **276,** 250–253 (1997).

49. Guo, L. *et al.* Lipid A Acylation and Bacterial Resistance against Vertebrate Antimicrobial Peptides. *Cell* **95,** 189–198 (1998).

50. Miura, T. & Mizushima, S. Separation by density gradient centrifugation of two types of membranes from spheroplast membrane of Escherichia coli K12. *Biochim. Biophys. Acta* **150,** 159–161 (1968).

51. Osborn, M. J., Gander, J. E., Parisi, E. & Carson, J. Mechanism of assembly of the outer membrane of Salmonella typhimurium. Isolation and characterization of cytoplasmic and outer membrane. *J. Biol. Chem.* **247,** 3962–3972 (1972).

52. Polissi, A. & Georgopoulos, C. Mutational analysis and properties of the msbA gene of Escherichia coli, coding for an essential ABC family transporter. *Molecular Microbiology* **20,** 1221–1233 (1996).

53. Doerrler, W. T. MsbA-dependent Translocation of Lipids across the Inner Membrane of Escherichia coli. *J. Biol. Chem.* **279,** 45102–45109 (2004).

54. Serina, S. *et al.* Scanning the Escherichia coli chromosome by random transposon mutagenesis and multiple phenotypic screening. *Res. Microbiol.* **155,** 692–701 (2004).

55. Sperandeo, P. *et al.* Characterization of lptA and lptB, Two Essential Genes Implicated in Lipopolysaccharide Transport to the Outer Membrane of Escherichia coli. *Journal of Bacteriology* **189,** 244–253 (2006).

56. Sperandeo, P. *et al.* Functional Analysis of the Protein Machinery Required for Transport of Lipopolysaccharide to the Outer Membrane of Escherichia coli. *Journal of Bacteriology* **190,** 4460–4469 (2008).

57. Ruiz, N., Gronenberg, L. S., Kahne, D. & Silhavy, T. J. Identification of two inner-membrane proteins required for the transport of lipopolysaccharide to the outer membrane of Escherichia coli. *Proc. Natl. Acad. Sci. U.S.A.* **105,** 5537–5542 (2008).

58. Sampson, B. A., Misra, R. & Benson, S. A. Identification and characterization of a new gene of Escherichia coli K-12 involved in outer membrane permeability. *Genetics* **122,** 491–501 (1989).

59. Aono, R., Negishi, T., Aibe, K., Inoue, A. & Horikoshi, K. Mapping of organic solvent tolerance gene ostA in Escherichia coli K-12. *Biosci. Biotechnol. Biochem.* **58,** 1231–1235 (1994).

60. Braun, M. & Silhavy, T. J. Imp/OstA is required for cell envelope biogenesis in Escherichia coli. *Molecular Microbiology* **45,** 1289–1302 (2002).

61. Steeghs, L. *et al.* Meningitis bacterium is viable without endotoxin. *Nature* **392,** 449–449 (1998).

62. Zhang, G., Meredith, T. C. & Kahne, D. On the essentiality of lipopolysaccharide to Gram-negative bacteria. *Current Opinion in Microbiology* **16,** 779–785 (2013).

63. Bos, M. P., Tefsen, B., Geurtsen, J. & Tommassen, J. Identification of an outer

membrane protein required for the transport of lipopolysaccharide to the bacterial cell surface. *Proc. Natl. Acad. Sci. U.S.A.* **101,** 9417–9422 (2004).

64. Wu, T. Identification of a protein complex that assembles lipopolysaccharide in the outer membrane of Escherichia coli. *Proc. Natl. Acad. Sci. U.S.A.* **103,** 11754–11759 (2006).

65. Jia, W. *et al.* Lipid Trafficking Controls Endotoxin Acylation in Outer Membranes of Escherichia coli. *J. Biol. Chem.* **279,** 44966–44975 (2004).

66. Narita, S.-I. & Tokuda, H. Biochemical characterization of an ABC transporter LptBFGC complex required for the outer membrane sorting of lipopolysaccharides. *FEBS Letters* **583,** 2160–2164 (2009).

67. Gronenberg, L. S. & Kahne, D. Development of an Activity Assay for Discovery of Inhibitors of Lipopolysaccharide Transport. *J. Am. Chem. Soc.* **132,** 2518–2519 (2010).

68. Sherman, D. J. *et al.* Decoupling catalytic activity from biological function of the ATPase that powers lipopolysaccharide transport. *Proceedings of the National Academy of Sciences* **111,** 4982–4987 (2014).

69. Chng, S. S., Ruiz, N., Chimalakonda, G., Silhavy, T. J. & Kahne, D. Characterization of the two-protein complex in Escherichia coli responsible for lipopolysaccharide assembly at the outer membrane. *Proc. Natl. Acad. Sci. U.S.A.* **107,** 5363–5368 (2010).

70. Bos, M. & Robert, V. Biogenesis of the Gram-Negative Bacterial Outer Membrane. *Annu. Rev. Microbiol.* **61,** 191-214 (2007).

71. Hu, K. Y. & Saier, M. H. Bioinformatic analyses of Gram-negative bacterial OstA outer membrane assembly homologues. *Current Genomics* **7**, 447-461 (2006).

72. Liu, C. C. & Schultz, P. G. Adding New Chemistries to the Genetic Code. *Annu. Rev. Biochem.* **79,** 413–444 (2010).

73. Ryu, Y. & Schultz, P. G. Efficient incorporation of unnatural amino acids into proteins in Escherichia coli. *Nature Methods* **3,** 263–265 (2006).

74. Chin, J. W. Addition of a photocrosslinking amino acid to the genetic code of Escherichiacoli. *Proceedings of the National Academy of Sciences* **99,** 11020–11024 (2002).

75. Freinkman, E., Chng, S.-S. & Kahne, D. The complex that inserts lipopolysaccharide into the bacterial outer membrane forms a two-protein plug-and-barrel. *Proc. Natl. Acad. Sci. U.S.A.* **108,** 2486–2491 (2011).

76. Papanikou, E., Karamanou, S. & Economou, A. Bacterial protein secretion through the translocase nanomachine. *Nat Rev Micro* **5,** 839–851 (2007).

77. Ruiz, N., Falcone, B., Kahne, D. & Silhavy, T. J. Chemical conditionality: a genetic strategy to probe organelle assembly. *Cell* **121,** 307–317 (2005).

78. Wu, T. *et al.* Identification of a Multicomponent Complex Required for Outer Membrane Biogenesis in Escherichia coli. *Cell* **121,** 235–245 (2005).

79. Ruiz, N., Chng, S.-S., Hiniker, A., Kahne, D. & Silhavy, T. J. Nonconsecutive disulfide bond formation in an essential integral outer membrane protein. *Proceedings of the National Academy of Sciences* **107,** 12245–12250 (2010).

80. Chimalakonda, G. *et al.* Lipoprotein LptE is required for the assembly of LptD by the beta-barrel assembly machine in the outer membrane of Escherichia coli. *Proceedings of the National Academy of Sciences* **108,** 2492–2497 (2011).

81. Chng, S. S. *et al.* Disulfide Rearrangement Triggered by Translocon Assembly Controls Lipopolysaccharide Export. *Science* **337,** 1665–1668 (2012).

82. Lee, J. *et al.* Characterization of a stalled complex on the β-barrel assembly machine. *Proc. Natl. Acad. Sci. U.S.A.* **113,** 8717–8722 (2016).

83. Matsuyama, S., Tajima, T. & Tokuda, H. A novel periplasmic carrier protein involved in the sorting and transport of Escherichia coli lipoproteins destined for the outer membrane. *EMBO J* **14,** 3365–3372 (1995).

84. Okuda, S. & Tokuda, H. Model of mouth-to-mouth transfer of bacterial lipoproteins through inner membrane LolC, periplasmic LolA, and outer membrane LolB. *Proc. Natl. Acad. Sci. U.S.A.* **106,** 5877–5882 (2009).

85. Tefsen, B., Geurtsen, J., Beckers, F., Tommassen, J. & de Cock, H. Lipopolysaccharide transport to the bacterial outer membrane in spheroplasts. *J. Biol. Chem.* **280,** 4504–4509 (2005).

86. Suits, M. D. L., Sperandeo, P., Dehò, G., Polissi, A. & Jia, Z. Novel structure of the conserved gram-negative lipopolysaccharide transport protein A and mutagenesis analysis. *J. Mol. Biol.* **380,** 476–488 (2008).

87. Tran, A. X., Dong, C. & Whitfield, C. Structure and Functional Analysis of LptC, a Conserved Membrane Protein Involved in the Lipopolysaccharide Export Pathway in Escherichia coli. *J. Biol. Chem.* **285,** 33529–33539 (2010).

88. Qiao, S., Luo, Q., Zhao, Y., Zhang, X. C. & Huang, Y. Structural basis for lipopolysaccharide insertion in the bacterial outer membrane. *Nature* **511,** 108–111

(2014).

89. Tran, A. X., Trent, M. S. & Whitfield, C. The LptA Protein of Escherichia coli Is a Periplasmic Lipid A-binding Protein Involved in the Lipopolysaccharide Export Pathway. *J. Biol. Chem.* **283,** 20342–20349 (2008).

90. Merten, J. A., Schultz, K. M. & Klug, C. S. Concentration-dependent oligomerization and oligomeric arrangement of LptA. *Protein Sci.* **21,** 211–218 (2012).

91. Ishidate, K. *et al.* Isolation of differentiated membrane domains from Escherichia coli and Salmonella typhimurium, including a fraction containing attachment sites between the inner and outer membranes and the murein skeleton of the cell envelope. *J. Biol. Chem.* **261**, 428-443 (1986).

92. Chng, S.-S., Gronenberg, L. S. & Kahne, D. Proteins Required for Lipopolysaccharide Assembly in Escherichia coliForm a Transenvelope Complex. *Biochemistry* **49,** 4565–4567 (2010).

93. Freinkman, E., Okuda, S., Ruiz, N. & Kahne, D. Regulated Assembly of the Transenvelope Protein Complex Required for Lipopolysaccharide Export. *Biochemistry* **51,** 4800–4806 (2012).

94. Okuda, S., Freinkman, E. & Kahne, D. Cytoplasmic ATP hydrolysis powers transport of lipopolysaccharide across the periplasm in E. coli. *Science* **338,** 1214–1217 (2012).

95. Sherman, D. J. Reconstitution of bacterial lipopolysaccharide transport from purified components. Doctoral dissertation, Harvard University (2015).

96. Uxa, O. & Haas, E. Pocket article dispensing container. US Patent #2,620,061 (1952).

97. Malojčić, G. *et al.* LptE binds to and alters the physical state of LPS to catalyze its assembly at the cell surface. *Proceedings of the National Academy of Sciences* **111,** 9467–9472 (2014).

98. Dong, H. *et al.* Structural basis for outer membrane lipopolysaccharide insertion. *Nature* **511,** 52–56 (2014).

99. Bos, M. P. & Tommassen, J. The LptD Chaperone LptE Is Not Directly Involved in Lipopolysaccharide Transport in Neisseria meningitidis. *J. Biol. Chem.* **286,** 28688–28696 (2011).

100. Evans, D. G., Evans, D. J., Moulds, J. J. & Graham, D. Y. N-acetylneuraminyllactose-binding fibrillar hemagglutinin of Campylobacter pylori: a

putative colonization factor antigen. *Infect. Immun.* **56,** 2896–2906 (1988).

101. Moran, A. P., Prendergast, M. M. & Appelmelk, B. J. Molecular mimicry of host structures by bacterial lipopolysaccharides and its contribution to disease. *FEMS Immunol. Med. Microbiol.* **16,** 105–115 (1996).

102. A Hoess, S. W. G. R. S. R. L. Crystal structure of an endotoxin-neutralizing protein from the horseshoe crab, Limulus anti-LPS factor, at 1.5 A resolution. *EMBO J* **12,** 3351 (1993).

103. Morita, T. *et al.* Isolation and Biological Activities of Limulus Anticoagulant (AntiLPS Factor) which Interacts with Lipopolysaccharide (LPS). *J Biochem (Tokyo)* **97,** 1611–1620 (1985).

104. Nachum, R., Watson, S. W., Sullivan, J. D., Jr. & Siegel, S. E. Antimicrobial defense mechanisms in the horseshoe crab, Limulus polyphemus: Preliminary observations with heat-derived extracts of Limulus amoebocyte lysate. *Journal of Invertebrate Pathology* **33,** 290–299 (1979).

105. D Ferguson, A. *et al.* A conserved structural motif for lipopolysaccharide recognition by procaryotic and eucaryotic proteins. *Structure* **8,** 585–592 (2000).

106. Ried, C. *et al.* High affinity endotoxin-binding and neutralizing peptides based on the crystal structure of recombinant Limulus anti-lipopolysaccharide factor. *J. Biol. Chem.* **271,** 28120–28127 (1996).

107. Ruiz, N., Wu, T., Kahne, D. & Silhavy, T. J. Probing the Barrier Function of the Outer Membrane with Chemical Conditionality. *ACS Chem. Biol.* **1,** 385–395 (2006).

108. Richter, W. *et al.* Morphology, size distribution, and aggregate structure of lipopolysaccharide and lipid A dispersions from enterobacterial origin. *Innate Immunity* **17,** 427–438 (2010).

109. Andra, J. *et al.* Surface Acoustic Wave Biosensor as a Tool to Study the Interaction of Antimicrobial Peptides with Phospholipid and Lipopolysaccharide Model Membranes. *Langmuir* **24,** 9148–9153 (2008).

110. Andres, D. *et al.* Tail morphology controls DNA release in two Salmonella phages with one lipopolysaccharide receptor recognition system. *Molecular Microbiology* **83,** 1244–1253 (2012).

111. Danner, R. L. *et al.* Purification, toxicity, and antiendotoxin activity of polymyxin B nonapeptide. *Antimicrob. Agents Chemother.* **33,** 1428–1434 (1989).

112. Andra, J. *et al.* Biophysical characterization of the interaction of Limulus

polyphemus endotoxin neutralizing protein with lipopolysaccharide. *Eur J Biochem* **271,** 2037–2046 (2004).

113. Devleeschouwer, M. J., Cornil, M. F. & Dony, J. Studies on the sensitivity and specificity of the Limulus amebocyte lysate test and rabbit pyrogen assays. *Appl. Environ. Microbiol.* **50,** 1509–1511 (1985).

114. BAYER, M. Zones of membrane adhesion in the cryofixed envelope of Escherichia coli. *Journal of Structural Biology* **107,** 268–280 (1991).

115. Gutsmann, T. *et al.* Lipid-mediated resistance of Gram-negative bacteria against various pore-forming antimicrobial peptides. *Journal of Endotoxin Research* **11,** 167–173 (2016).

116. Gutsmann, T. *et al.* Lipopolysaccharide-binding protein-mediated interaction of lipid A from different origin with phospholipid membranes. *Phys. Chem. Chem. Phys.* **2,** 4521–4528 (2000).

117. Ferguson, A. D. Siderophore-Mediated Iron Transport: Crystal Structure of FhuA with Bound Lipopolysaccharide. *Science* **282,** 2215–2220 (1998).

118. Beamer, L. J., Carroll, S. F. & Eisenberg, D. Crystal Structure of Human BPI and Two Bound Phospholipids at 2.4 Angstrom Resolution. *Science* **276,** 1861–1864 (1997).

119. Eckert, J. K. *et al.* The Crystal Structure of Lipopolysaccharide Binding Protein Reveals the Location of a Frequent Mutation that Impairs Innate Immunity. *Immunity* **39,** 647–660 (2013).

120. Weiss, J. Bactericidal/permeability-increasing protein (BPI) and lipopolysaccharide-binding protein (LBP): structure, function and regulation in host defence against Gram-negative bacteria. *Biochemical Society Transactions* **31,** 785–790 (2003).

121. Schromm, A. B. *et al.* Lipopolysaccharide-binding protein mediates CD14-independent intercalation of lipopolysaccharide into phospholipid membranes. *FEBS Letters* **399,** 267–271 (1996).

122. Ohvo-Rekilä, H. & Mattjus, P. Monitoring glycolipid transfer protein activity and membrane interaction with the surface plasmon resonance technique. *Biochimica et Biophysica Acta (BBA) - Biomembranes* **1808,** 47–54 (2011).

123. Sugiki, T., Takahashi, H., Nagasu, M., Hanada, K. & Shimada, I. Real-time assay method of lipid extraction activity. *Anal. Biochem.* **399,** 162–167 (2010).

124. Li, X., Gu, Y., Dong, H., Wang, W. & Dong, C. Trapped lipopolysaccharide and LptD intermediates reveal lipopolysaccharide translocation steps across the

Escherichia coli outer membrane. *Sci Rep* **5,** 11883 (2015).

125. Jerala, R. Structural biology of the LPS recognition. *International Journal of Medical Microbiology* **297,** 353–363 (2007).

126. Park, B. S. *et al.* The structural basis of lipopolysaccharide recognition by the TLR4–MD-2 complex. *Nature* **458,** 1191–1195 (2009).

127. Lamping, N. *et al.* Effects of site-directed mutagenesis of basic residues (Arg 94, Lys 95, Lys 99) of lipopolysaccharide (LPS)-binding protein on binding and transfer of LPS and subsequent immune cell activation. *The Journal of Immunology* **157,** 4648–4656 (1996).

128. Warren, H. S. *et al.* Binding and neutralization of endotoxin by Limulus antilipopolysaccharide factor. *Infect. Immun.* **60,** 2506–2513 (1992).

129. Kim, H. M. *et al.* Crystal Structure of the TLR4-MD-2 Complex with Bound Endotoxin Antagonist Eritoran. *Cell* **130,** 906–917 (2007).

130. Doering, C. Binding specifity of E.coli lipopolysaccharide transporter protein LptC . 1–32 (2013).

131. Reynolds, C. M. & Raetz, C. R. H. Replacement of Lipopolysaccharide with Free Lipid A Molecules in Escherichia coliMutants Lacking All Core Sugars. *Biochemistry* **48,** 9627–9640 (2009).

132. Gu, Y. *et al.* Lipopolysaccharide is Inserted into the Outer Membrane through An Intramembrane Hole, A?Lumen Gate, and the Lateral Opening of LptD. *Structure* **23,** 496–504 (2015).

133. Moison, E. *et al.* A Fluorescent Probe Distinguishes between Inhibition of Early and Late Steps of Lipopolysaccharide Biogenesis in Whole Cells. *ACS Chem. Biol.* **12,** 928–932 (2017).

134. Grabowicz, M., Yeh, J. & Silhavy, T. J. A dominant-negative lptE mutation that supports a role for LptE as a plug in the LptD barrel. *Journal of Bacteriology* **195**, 1327-1334 (2013).

135. Hagan, C. L., Westwood, D. B. & Kahne, D. Bam lipoproteins assemble BamA in vitro. *Biochemistry* **52**, 6108-6113(2013).

136. Piwonski, H. M., Goomanovsky, M., Bensimon, D., Horovitz, A. & Haran, G. Allosteric inhibition of individual enzyme molecules trapped in lipid vesicles. *Proc. Natl. Acad. Sci. U.S.A.* **109,** E1437–E1443 (2012).

137. Boukobza, E., Sonnenfeld, A. & Haran, G. Immobilization in Surface-Tethered

Lipid Vesicles as a New Tool for Single Biomolecule Spectroscopy. *J. Phys. Chem. B* **105,** 12165–12170 (2001).

138. Bally, M. *et al.* Liposome and lipid bilayer arrays towards biosensing applications. *Small* **6,** 2481–2497 (2010).

139. Blair, D. & Dufresne, E. The matlab particle tracking code repository. http://site.physics.georgetown.edu/matlab/ (2013).

140. Vorauer Uhl, K., Wagner, A., Borth, N. & Katinger, H. Determination of liposome size distribution by flow cytometry. *Cytometry Part A* **39,** 166–171 (2000).

141. Hoekstra, D., de Boer, T., Klappe, K. & Wilschut, J. Fluorescence method for measuring the kinetics of fusion between biological membranes. *Biochemistry* **23,** 5675–5681 (1984).

142. Struck, D. K., Hoekstra, D. & Pagano, R. E. Use of resonance energy transfer to monitor membrane fusion. *Biochemistry* **20,** 4093–4099 (1981).

143. van der Does, C., de Keyzer, J., van der Laan, M. & Driessen, A. J. Reconstitution of purified bacterial preprotein translocase in liposomes. *Meth. Enzymol.* **372,** 86–98 (2003).

144. Sherman, D. J., Okuda, S., Denny, W. A. & Kahne, D. Validation of inhibitors of an ABC transporter required to transport lipopolysaccharide to the cell surface in Escherichia coli. *Bioorganic & Medicinal Chemistry* **21,** 4846–4851 (2013).

145. Chifflet, S., Torriglia, A., Chiesa, R. & Tolosa, S. A method for the determination of inorganic phosphate in the presence of labile organic phosphate and high concentrations of protein: Application to lens ATPases. *Anal. Biochem.* **168,** 1–4 (1988).

146. Edelstein, A., Amodaj, N. & Hoover, K. Computer control of microscopes using μManager. *Current protocols in …* (2010). doi:10.1002/0471142727.mb1420s92

147. Schneider, C. A., Rasband, W. S. & Eliceiri, K. W. NIH Image to ImageJ: 25 years of image analysis. *Nature Methods* **9,** 671–675 (2012).

148. Dixit, R. & Ross, J. L. Studying plus-end tracking at single molecule resolution using TIRF microscopy. *Methods in cell biology* (2010). doi:10.1016/S0091-679X(10)95027-9